

Multiwavelength Studies of Accretion Disks Around Compact Objects

by

Zhongxiang Wang

B.S. Optical Engineering, Changchun Institute of Optics and Fine Mechanics, China, 1990

M.S. Astrophysics, Nanjing University, China, 1997

M.S. Physics, Georgia State University, 1999

Submitted to the Department of Physics
in partial fulfillment of the requirements for the degree of

Doctor of Philosophy

at the

MASSACHUSETTS INSTITUTE OF TECHNOLOGY

September 2004

©2004 Zhongxiang Wang. All rights reserved.

The author hereby grants to MIT
permission to reproduce and to
distribute publicly paper and
electronic copies of this thesis
document in whole or in part

Author *Zhongxiang Wang*

Department of Physics

August 30, 2004

Certified by *Deepto Chakrabarty*

Deepto Chakrabarty

Associate Professor of Physics

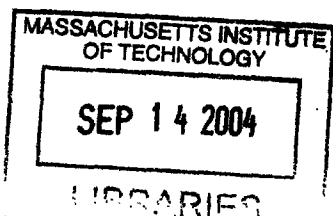
Thesis Supervisor

Accepted by *Thomas J. Greytak*

Thomas J. Greytak

Professor of Physics

Associate Department Head for Education



ARCHIVES



Multiwavelength Studies of Accretion Disks Around Compact Objects

by

Zhongxiang Wang

Submitted to the Department of Physics
on August 30, 2004, in partial fulfillment of the
requirements for the degree of
Doctor of Philosophy

Abstract

In this thesis, I present multiwavelength studies of phenomena related to accretion disks around compact objects. The observations were made mainly with ground-based telescopes and the *Hubble Space Telescope*. I observed several known and candidate ultracompact low-mass X-ray binaries (LMXBs) and found that their optical spectra all show a lack of hydrogen emission lines, supporting the theoretical prediction that mass donors in ultracompact LMXBs must be H-depleted. Time-resolved photometry of the candidate source 4U 1543–624 revealed an 18 minute orbital periodicity, verifying the ultracompact nature of this binary. These studies strongly support the identification of several candidate systems with similar X-ray spectral features as ultracompact binaries. In the ultracompact binary 4U 1820–30, which has the shortest orbital period (685 s) among the known LMXBs, I discovered a 692-s periodicity from its far-ultraviolet (FUV) time series data. I interpret this longer-period FUV signal as a superhump oscillation, arising from a tidal resonance in the accretion disk of an extreme-mass-ratio binary.

I also present multiband imaging of the fields surrounding five newly discovered X-ray millisecond pulsars (MSPs) in an effort to identify and study their optical/IR counterparts. For the MSP SAX J1808.4–3658, the optical light curve taken during its 1998 X-ray outburst shows an exponential decay in intensity, roughly following the X-ray light curve early in the outburst. An optical counterpart of XTE J1814–338 was also detected.

Finally, optical/IR observations of anomalous X-ray pulsars (AXPs) and X-ray point sources (XPSs) in young supernova remnants (SNRs) identified the IR counterpart to the AXP 1E 1048.1–5937 and a likely IR counterpart to the XPS in SNR RCW 103. The multiple IR band measurements of 1E 1048.1–5937 provide marginal evidence for spectral flattening, and cannot rule out an accretion disk scenario for AXPs.

Thesis Supervisor: Deepto Chakrabarty
Title: Associate Professor of Physics

Acknowledgments

I am grateful to many people who have helped me during the years of studying and completing this thesis. Among them, the first person I would like to thank is my supervisor Deepto Chakrabarty. Not only has he worked closely with me on all research projects which result in this thesis, but also aided me greatly through his valuable advice and suggestions. During these years, I have learned a lot from him, especially the advanced skills of how to find the best approaches to different problems and present research results clearly and effectively.

I have been fortunate to work, yet shortly, with my thesis committee members Saul Rappaport and Paul Schechter. Their sharp physical intuition and excellent technical skills have made a deep impression on me. They have also monitored my work and provided constructive comments on my thesis research during the past two years.

Our weekly group meeting has been a great place to share exciting science news and particular working experience in various research fields, and seek insightful suggestions. Here I thank Dimitrios Psaltis, Duncan Galloway, Jennifer Sokoloski, Michael Muno, Sebastian Heinz, Adrienne Juett, Jacob Hartman, and Miriam Krauss for their help. It has been a pleasure talking with them every week about research and all kinds of news.

I would also like to thank Paul Wiita and Douglas Gies at Georgia State University. They greatly helped me during my first two years of studying in the United States. Without their encouragement, I would never have come to MIT.

Finally, I am deeply indebted to my family. They have supported me unconditionally in my career decisions and this journey into studying astrophysics.

Contents

1	Introduction	15
1.1	Accretion Disks in LMXBs	17
1.2	Ultracompact LMXBs and X-ray MSPs	20
1.2.1	Ultracompact LMXBs	21
1.2.2	X-ray Millisecond pulsars	22
1.3	Fallback disk model for Anomalous X-ray Pulsars and X-ray Point Sources	24
1.4	Thesis Organization	26
2	Telescopes and Instruments	29
2.1	Ground-based Observations	29
2.1.1	Optical Observations	29
2.1.2	Infrared Observations	32
2.2	<i>Hubble Space Telescope</i> Observations	33
2.2.1	<i>Hubble Space Telescope</i> and Space Telescope Imaging Spectrograph	33
2.2.2	Data Reduction	35
3	UV/Optical Spectroscopy of the Ultracompact X-ray Binary 4U 1626-67	37
3.1	Introduction	37
3.2	Observations and Data Reduction	38
3.2.1	HST/STIS Data	38

3.2.2	Ground-based Data	40
3.3	Results	40
3.3.1	HST/STIS Spectrum	40
3.3.2	Ground-based Spectra	45
3.4	Discussion	47
3.4.1	X-ray heated accretion disk	47
3.4.2	Spectral Features	52
4	Optical Survey of Known and Suspected Ultracompact X-Ray Binaries	55
4.1	Introduction	55
4.2	Spectroscopy of 4U 0614+091, 4U 1543–624, and 4U 1916–05	57
4.2.1	Observations and Data Reduction	57
4.2.2	Common Spectral features	58
4.2.3	Discussion	62
4.3	Time-resolved Optical Photometry of the LMXB 4U 1543–624 and 4U 1822–000	64
4.3.1	Observations and Data Reduction	64
4.3.2	Results	65
4.3.3	Discussion	67
5	The Ultracompact X-ray Binary 4U 1820–30: Superhumper or Hierarchical Triple?	71
5.1	Introduction	71
5.2	Observations and Data Reduction	73
5.3	Period Determination	74
5.4	Discussion	76
6	The Optical Counterpart of the Accreting Millisecond Pulsar SAX J1808.4–3658 in Outburst	81
6.1	Introduction	81

6.2	Observations	82
6.3	Results	82
6.4	Discussion	86
7	Search for Optical/IR Counterparts to X-ray Millisecond Pulsars	89
7.1	Introduction	89
7.2	Observations	90
7.3	Results	91
7.3.1	The Optical Counterpart to SAX J1808.4–3658 in Quiescence	91
7.3.2	XTE J1751–305	91
7.3.3	XTE 0929–314	92
7.3.4	XTE J1807–294	93
7.3.5	XTE J1814–338	93
7.4	Summary	95
8	The possible Near-Infrared Counterpart to the Bursting X-Ray Pulsar GRO J1744–28	97
8.1	Introduction	97
8.2	Observation	98
8.3	X-ray position and Astrometry	99
8.4	Results and Discussion	100
9	The likely Near-Infrared Counterpart to the Anomalous X-Ray Pulsar 1E 1048.1–5937	103
9.1	Introduction	103
9.2	Optical/Infrared Observations	104
9.3	X-Ray Position and Astrometry	105
9.4	Results	108
9.5	Summary	110
10	Search for IR Counterparts of the Central X-ray Point Sources in Young Supernova Remnants	113

10.1	Introduction	113
10.2	Optical and Infrared Observations	114
10.3	Astrometry	117
10.4	Results	119
10.4.1	RCW 103 (1E 1614–5055)	119
10.4.2	PKS 1209–52 (1E 1207–5209)	123
10.4.3	RX J0822–4300 and RX J0852–4617	124
10.5	Discussion	124
11	Summary and Future Work	127
11.1	Ultracompact LMXBs	127
11.2	X-ray MSPs	129
11.3	Searching For Fallback Disks	129
A	FUV spectrum of the Ultracompact LMXB 4U 1820-30	131

List of Figures

1-1	Edge-on view of a steady, thin accretion disk around a neutron star.	16
1-2	Illustration of an low-mass X-ray binary	18
2-1	Magellan Telescopes	30
2-2	The <i>Hubble Space Telescope</i>	34
3-1	The composite <i>HST</i> /STIS spectrum of 4U 1626–67	39
3-2	HST/STIS FUV spectrum of the ultracompact LMXB 4U 1626–67	41
3-3	Reconstruction of Ly α λ 1216 absorption line toward 4U 1626–67	42
3-4	Optical spectrum between 2150-4150 Å of 4U 1626–67	44
3-5	Ground-based optical spectra of 4U 1626–67	46
3-6	The binned spectrum of 4U 1626–67	50
3-7	Allowed values of r_i and \dot{M}	51
4-1	Spectra of ultracompact low-mass X-ray binaries	59
4-2	LDSS-2 spectrum of the LMXB EXO 0748–676	61
4-3	Dereddened and corrected spectra	62
4-4	Sloan r' -band images of the fields	64
4-5	Light curves of 4U 1543–624 and 4U 1822–000	66
4-6	The r' band photometric data for 4U 1543–624	67
4-7	Mass-radius constraints for the companion star	69
5-1	FUV light curve of 4U 1820–30	74
5-2	Result of χ^2 folded period searching	75
5-3	A 10 times overresolved power spectrum	76

5-4	Folded light curves with the FUV period 692.50 s	77
6-1	X-ray (3–150 keV) and optical flux histories	85
6-2	Broadband optical/IR spectra of SAX J1808.4–3658	87
7-1	Sloan r' image of the SAX J1808.4–3658 field	91
7-2	K_s image of the XTE J1751–305 field	92
7-3	Optical spectrum of XTE J0929–314	93
7-4	Sloan r' image of the XTE J0929–314 field	94
7-5	Sloan i' image of the XTE J1807–294	95
8-1	Near-infrared image of the region around GRO J1744–28	98
8-2	Color-magnitudes and color-color diagrams	102
9-1	Optical and near-infrared images of the 1E 1048.1–5937	107
9-2	Color-color diagrams for the objects	109
9-3	Dereddened flux from object <i>X1</i>	111
10-1	Optical and near-infrared images	116
10-2	J -band image of the PKS 1209–52	117
10-3	Classicam K_s image of the RX J0852-4617 field	118
10-4	Sloan i' and IR K_s images of the Puppis A	120
10-5	Color-magnitude and color-color diagrams	121
10-6	Color-magnitude diagram of the objects	123
10-7	Unabsorbed energy spectra	125
11-1	Resolved $\lambda\lambda 4640$ – 4650 C III/N III feature.	128
11-2	Dereddened fluxes and flux limits of RCW103 and PKS1209–52 . . .	130
A-1	<i>HST</i> /STIS FUV spectrum	132
A-2	Reconstruction of $\text{Ly}\alpha$ $\lambda 1216$ absorption line	132

List of Tables

1.1	Currently known X-ray MSPs	23
1.2	Properties of Anomalous X-ray Pulsars and X-ray Point Sources . . .	25
1.3	Summary of the results of our studies of X-ray sources	28
2.1	Standard grating setups of B&C Spectrograph	31
2.2	Grisms of the LDSS-2	31
2.3	STIS spectroscopic capabilities	34
3.1	Equivalent width upper limits (\AA) on Bowen O III lines	43
4.1	Log of Magellan Observations of Ultracompact X-ray Binaries	58
4.2	Equivalent width measurements and 2σ upper limits (\AA) on H and He emission lines	60
4.3	Parameters of Gaussian fits to the $\lambda 4650$ feature	60
6.1	Optical/IR Photometry of SAX J1808.4–3658 ^a	83
7.1	Log of the Magellan imaging observations of the X-ray MSPs.	90
9.1	Astrometry and Photometry of Candidate Counterparts	112
10.1	Optical/IR photometry of XPSs	122

Chapter 1

Introduction

Accretion disks have been discovered in various astrophysical systems, and proved to play an important role in the appearances and evolutions of these systems. Generally, for point-like astrophysical objects, especially those compact objects, such as white dwarfs, neutron stars, and black holes, with relatively strong gravitational fields. the gravitational capture of a large amount of mass from either nearby objects or local environment may occur. When the captured material has sufficiently high specific angular momentum to prevent direct infall onto such a point object, the material will settle down and form a disk around the object due to interactions between streams of material. In most cases, the disk matter will be gradually accreted onto the central object.

Accretion disks are essential for the creation of planetary systems, formation of young stars, mass-transfer in binary systems, and fueling of the central engines in active galactic nuclei (AGN), even though their scales can differ by several orders of magnitude in these systems, such as from millions of km in binaries, AU scale (1.5×10^8 km) around protostars, to parsec scale (3×10^{13} km) in AGN. In addition, jet/outflow-like phenomena in binary systems, protostars, and AGN are also believed to be associated with accretion disks.

In this thesis, we concentrate on accretion disks around neutron stars. These neutron stars are located in our Galaxy, either in a binary system or isolated. They are strong X-ray emitters with their X-ray luminosities in the range of 10^{30} - 10^{38}

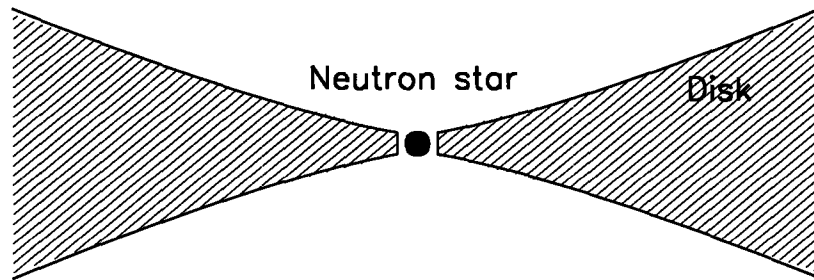


Figure 1-1 Edge-on view of a steady, thin accretion disk around a neutron star.

ergs s^{-1} . The strong X-ray emission is produced by either mass accretion onto, or intrinsic thermal emission ($kT \sim 0.5$ keV) from the neutron stars,

For our objects, the associated accretion disks can be well described by a steady thin disk model (Figure 1-1; Frank et al. 1992) with disk matter being assumed to have Keplerian angular velocity throughout the disk. The kinematic viscosity of the disk material causes an outward transfer of angular momentum and inflow of the material, and heats the disk. The flux densities from such a disk are proportional to its inflow mass accretion rate.

However, required by a few pieces of observational evidence revealed during the past ten years, modifications have been developed on the basis of the thin disk model. For example, X-ray flux emitted from a neutron star will illuminate the surface/corona of an accretion disk around it, producing observable optical, ultraviolet (UV), and X-ray emission lines (see, e.g., Raymond 1993; Ko & Kallman 1994). Since an accretion disk has a concave shape (Figure 1-1), a fraction of the X-ray flux is intercepted by the disk, and it is often strong enough to have important effects on the temperature profile and geometrical structure of the disk, triggering off instabilities that may be responsible for warping of accretion disks (see, e.g., Wijers & Pringle 1999; Ogilvie &

Dubus 2001). Long-term periods (“superorbital” periods), typically on a time scale of several tens of days, have been detected from several X-ray sources, and are probably due to the precession of warped disks (see, e.g., Clarkson et al. 2002). In addition, accretion disks in binaries with extreme mass ratios between accreting primary stars and mass donors may develop an elliptical shape due to a tidal resonance, resulting in a “superhump” phenomenon (Haswell et al. 2001). In a superhump binary source, a period, about several percent longer than its binary orbital period, is present.

In this thesis, we present multiwavelength studies of accretion disks in ultracompact low-mass X-ray binaries (LMXBs), in newly discovered X-ray millisecond pulsars (MSPs), and around young neutron stars with strong X-ray emission. Below, we first introduce the X-ray heated, thin disk model in LMXBs, and then give a brief overview of the stellar objects studied in this thesis.

1.1 Accretion Disks in LMXBs

A low-mass X-ray binary (LMXB) contains an accreting primary, either a neutron star or a black hole, and a low mass secondary star (generally with mass below $2 M_{\odot}$; White, Nagase, & Parmar 1995). As the secondary star overfills its Roche-lobe, the gravitational potential lobe, mass transfer from the secondary to the primary occurs via an accretion disk around the primary, and mass accretion onto the primary powers this binary to a luminous X-ray source (see Figure 2). Roughly, the X-ray luminosity of a LMXB can be estimated from its accretion luminosity, defined as the gravitational potential energy of the accreted matter released at a stellar surface R_{\star} ,

$$L_{\text{X}} = \frac{GM\dot{M}}{R_{\star}} = 1.2 \times 10^{36} \left(\frac{M}{1.4 M_{\odot}} \right) \left(\frac{\dot{M}}{10^{-10} M_{\odot}\text{yr}^{-1}} \right) \left(\frac{R_{\star}}{10^6 \text{ cm}} \right)^{-1} \text{ erg s}^{-1}. \quad (1.1)$$

In illustrating the typical X-ray brightness of a LMXB, the quantities in equation 1.1 are normalized to their order of magnitude values for a neutron star accretor.

Accretion disks are an essential element of the LMXB systems, and can be described by the standard thin disk model (Shakura & Sunyaev, 1973). This standard

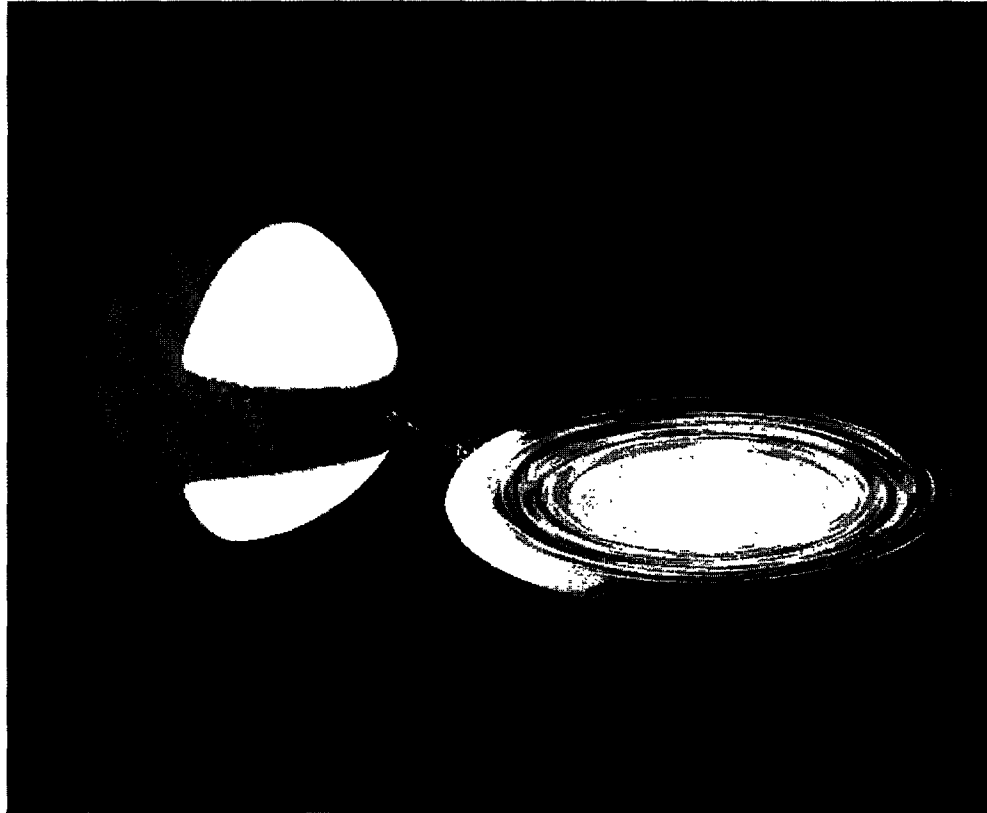


Figure 1-2 Illustration of an low-mass X-ray binary. This binary system, containing a $1.4 M_{\odot}$ neutron star accretor and a $0.4 M_{\odot}$ Roche-lobe filling low-mass companion, would have an orbital period of 4 hours. The figure is adapted from the binary visualization program `binsim`, written by R. Hynes (<http://obelix.as.utexas.edu/rih/binsim>).

model has two basic approximations. The accretion disks are *geometrically thin*, thus allowing for a treatment of the disk as a two-dimensional gas flow on the orbital plane of a binary system, and *optically thick*, implying that every part of a disk reaches a state of thermodynamic equilibrium at a local temperature. The temperature profile, $T_0(r)$, of a standard disk around a neutron star with mass M can be written as a function of mass accretion rate \dot{M} and its midplane radius r from the central neutron star,

$$T_0 = \left\{ \frac{3GM\dot{M}}{8\pi\sigma r^3} \left[1 - \left(\frac{r_i}{r} \right)^{1/2} \right] \right\}^{1/4} \approx 7100 M_{1.4}^{1/4} \dot{M}_{-10}^{1/4} r_{10}^{-3/4} \text{ K}, \quad (1.2)$$

where $\sigma = 5.67 \times 10^{-5} \text{ ergs cm}^{-2} \text{ K}^{-4} \text{ s}^{-1}$ is the Stefan-Boltzmann constant, $M_{1.4}$ represents the neutron star mass in units of $1.4 M_\odot$, \dot{M}_{-10} is the mass accretion rate in units of 10^{-10} solar mass per year, r_{10} is the radius in units of 10^{10} cm, and r_i is the inner radius of an accretion disk.

Assuming values for the r_i and outer radius, r_o , of such an accretion disk are known, it is straightforward to derive the flux densities from the disk. However, it has been realized that a fraction of X-ray flux emitted by a central source is intercepted by a disk and, in most cases, the X-ray flux is strong enough to have important effects on the structure of the disk.

First, X-ray photons can heat the disk and modify a disk temperature profile. This can be estimated by adding an additional X-ray temperature T_X (see, e.g., Cunningham, 1976),

$$T_X = \left[\frac{L_X(1 - \eta_d)}{4\pi\sigma r^2} \cos \psi \right]^{1/4} \approx \left[\frac{L_X(1 - \eta_d)}{4\pi\sigma r^2} \left(\frac{dH}{dr} - \frac{H}{r} \right) \right]^{1/4}, \quad (1.3)$$

where L_X is the X-ray luminosity, η_d is the X-ray albedo of the disk indicating η_d fraction of X-ray photons being reflected, ψ is the angle between the normal to the disk surface and the vector from the central star, and H is the scale-height of the disk. For a standard thin disk, H can be estimated as (Shakura & Sunyaev, 1973; Frank, King, & Raine, 1992)

$$H = 1.2 \times 10^8 \alpha^{-1/10} \mu^{-3/8} M_{1.4}^{-3/8} \dot{M}_{-10}^{3/20} r_{10}^{9/8} \text{ cm}, \quad (1.4)$$

where α is an order unity dimensionless parameter for constructing the standard disk model and μ is the mean molecular weight in units of the hydrogen atomic mass. This allows us to find

$$T_X = 1.2 \times 10^4 \alpha^{-1/40} \mu^{-3/32} (1 - \eta_d)^{1/4} M_{1.4}^{5/32} \dot{M}_{-10}^{23/80} r_{10}^{-15/32} \text{ K} . \quad (1.5)$$

The total temperature profile of an X-ray heated disk is thus modified as

$$T_d = (T_0^4 + T_X^4)^{1/4} . \quad (1.6)$$

Secondly, when $T_X^4 > \tau T_0^4$ (Spruit, 1995), where τ is the disk's optical depth, $\tau = 34\alpha^{-4/5} \mu^{1/4} \dot{M}_{-10}^{1/5}$, X-ray heating dominates over internal viscous heating of a disk. This condition indicates that, generally, disk regions with radii exceeding 3×10^{10} cm are dominated by the X-ray heating. Moreover, the scale height will not obey the relation given by the equation 1.4, but instead can be shown to have an $H \propto r^{9/7}$ power law (Cunningham, 1976; Vrtilik et al., 1990). Then this disk temperature profile is

$$T_d = 1.4 \times 10^4 \mu^{-1/7} (1 - \eta_d)^{2/7} M_{1.4}^{1/7} \dot{M}_{-10}^{2/7} r_{10}^{-3/7} \text{ K} . \quad (1.7)$$

With either of the above disk temperature profiles, the flux at frequency ν from an X-ray irradiated disk to an observer at a distance D is

$$F_\nu = \frac{4\pi h\nu^3 \cos i}{c^2 D^2} \int_{r_i}^{r_o} \frac{r dr}{\exp[h\nu/kT_d(r)] - 1} , \quad (1.8)$$

where h is Planck's constant, c is light speed, and i is binary inclination.

1.2 Ultracompact LMXBs and X-ray MSPs

Currently there are about 150 identified LMXBs (Liu, van Paradijs, & van den Heuvel 2001). These sources, along with high-mass X-ray binaries (HMXBs; the companion in a HMXB is an O or B star with mass above $2 M_\odot$), are a major class of stellar objects in X-ray Astrophysics and have been extensively studied by X-ray

observatories over the past four decades. In addition, these LMXBs have also been studied at wavelengths from the ultraviolet, and optical to the infrared. Low-mass companion stars and accretion disks are bright in these wavelength ranges. The studies provide direct information about companion stars, such as their masses and spectral types, and accretion process, such as mass accretion rates and structures of accretion disks, helping establish our understanding of these X-ray binaries. The general properties and optical/ultraviolet observations of these X-ray sources have been reviewed by White et al. (1995) and van Paradijs & McClintock (1995) respectively.

The LMXBs are often divided into subgroups based on their characteristic features. In this thesis, we present studies of sources in two subgroups, the ultracompact LMXBs and X-ray MSPs.

1.2.1 Ultracompact LMXBs

Binaries containing compact primaries and ordinary, hydrogen-rich mass donors have a minimum orbital period around 80 minutes. This was first realized for cataclysmic variables (CVs), binary systems with white dwarfs as primary accretors, that there is a cut-off at ~ 80 minutes in their orbital period distribution (Warner 1995). The minimum period can be well explained by evolutionary studies (e.g., Paczyński, 1981; Paczyński & Sienkiewicz, 1981; Rappaport et al., 1982). Considering such a binary with a hydrogen-rich companion, it will evolve along the track of decreasing angular momentum (and orbital period) due to either gravitational radiation (Paczyński, 1967) or magnetic braking (Verbunt & Zwaan 1981; Rappaport, Verbunt, & Joss 1983). At a point when the hydrogen-burning companion star becomes degenerate, the binary approaches its minimum orbital period. However, a few exceptional systems exhibit ultra-short (far below 80 minutes) orbital periods. They are AM CVn systems (Warner, 1995) among CVs and ultracompact LMXBs. For example, the X-ray binary 4U 1820–30 has an orbital period of 685 seconds (Stella et al., 1987), the shortest among known LMXBs. Evolutionary calculations suggest that, in order to have shorter orbital periods than 80 min, the mass donors must be hydrogen-depleted (Nelson, Rappaport, & Joss 1986). This has been proved in

AM CVn systems, as their optical spectra are featured with helium lines and lack of any hydrogen lines (see, e.g., Groot et al. 2001 and references therein), implying that the donors are low mass helium stars, either degenerate (Faulkner, Flannery, & Warner 1972; Joss, Avni, & Rappaport 1978; Rappaport et al. 1987) or evolved and semi-degenerate (Iben & Tutukov 1991).

Among the X-ray binaries, there are 7 known ultracompact systems. They are 2 globular cluster sources (4U 1820–30, Stella, Friedhorsky, & White 1987; 4U 1850–087, Homer et al. 1996), 3 newly discovered millisecond X-ray pulsars (see Chapter 1.2.2), X-ray pulsar 4U 1626–67 (Middleditch et al. 1981; Chakrabarty 1998), and X-ray dipper 4U 1916–053 (Walter et al. 1982; White & Swank 1982). These systems, along with the AM CVn systems, represent an extreme and exotic endpoint of binary and stellar evolution (see, e.g., Podsiadlowski, Rappaport, Pfahl 2002; Podsiadlowski, Han, & Rappaport 2003).

1.2.2 X-ray Millisecond pulsars

The X-ray millisecond X-ray pulsars (MSPs) are highly evolved X-ray binaries with their neutron star primaries spun up to millisecond spin periods by the mass flow accreted from the companion stars. The first X-ray millisecond pulsar, SAX J1808.4–3658, was discovered in 1996 September by the *BeppoSAX* Wide Field Cameras during a ~ 20 day transient outburst (in't Zand et al. 1998). A second source outburst was detected with the *RXTE* in 1998 April (Marshall 1998). Timing analysis of the 2–30 keV *RXTE* data revealed the presence of a 401 Hz pulsar in a 2-hr binary with a low-mass companion (Wijnands & van der Klis 1998; Chakrabarty & Morgan 1998). Since 2002, a monitoring program of the Galactic bulge region (Swank & Markwardt 2001), using the *RXTE* Proportional Counter Array (PCA), has been successful in discovering new X-ray MSPs. To date, five X-ray MSPs have been discovered (see Table 1.1). These discoveries not only provide firm evidence supporting the theory that accreting neutron stars in LMXBs are progenitors of radio MSPs (Bhattacharya & van den Heuvel, 1991), but also show intriguing features: (1) they are all X-ray transients (see, e.g., Tanaka & Shibazaki 1996); (2) 3 of 5 are ultracompact

binaries with uniform orbital periods around 40 minutes; (3) they have very low mass companions. A detailed observational review of these MSPs was presented by Wijnands (2004).

Table 1.1 Currently known X-ray MSPs

Source	Spin frequency (Hz)	Orbital period (min)	Mass Function (M_{\odot})	References
SAX J1808.4–3658	401	120.8	3.8×10^{-5}	1, 2
XTE J1751–305	435	42.4	1.3×10^{-6}	3
XTE J0929–314	185	43.6	2.7×10^{-7}	4
XTE J1807–294	191	40.1	—	5
XTE J1814–338	314	256.5	2.0×10^{-3}	6

References. – (1) Wijnands & van der Klis 1998. (2) Chakrabarty & Morgan 1998. (3) Markwardt et al. 2002. (4) Galloway et al. 2002. (5) Markwardt et al. 2003. (6) Markwardt & Swank 2003.

Theoretically, two evolutionary scenarios have been developed for the ultracompact X-ray MSPs, indicating that they result from the evolution of either an evolved main-sequence star and neutron star binary (Podsiadlowski et al., 2002; ?) or a white dwarf and neutron star binary (Yungelson et al., 2002). One distinct feature between the two scenarios is in the first one a companion star may contain detectable hydrogen. Optical/IR observations of the X-ray MSPs, especially the identification of their counterparts, would certainly help our understanding of the possible evolutionary paths. In addition, the neutron stars in these binaries may have accreted a substantial amount of matter over the course of being spun up to milliseconds periods. Identifications of optical counterparts would allow us to further obtain radial velocity curve of the companions through spectroscopy and thus the masses of the neutron stars. One exception of a high mass neutron star would challenge many proposed equation of state of neutron star matter (van Paradijs & McClintock 1995).

1.3 Fallback disk model for Anomalous X-ray Pulsars and X-ray Point Sources

Accretion disks may also exist around isolated young neutron stars, as a small amount of mass can fall back onto a neutron star after its birth in a core-collapse supernova. Much of the fallback material will have sufficient angular momentum to form a disk while it cools. In many ways, a fallback disk resembles a standard thin accretion disk (Perna et al., 2000), like one in a low-mass X-ray binary. As in a neutron star binary, the inner edge of the disk would presumably be truncated by the magnetosphere of the neutron star. However, at least three significant differences exist: (1) fallback disk accretion needs not necessarily to power the central X-ray source; (2) the lack of a binary companion leaves the outer disk untruncated; (3) the high metal content of a fallback disk might lead to different stability regimes.

Recently, it has been realized that, besides classical radio pulsars like the one in the Crab supernova remnant (SNR), there are two other types of young neutron stars: the anomalous X-ray pulsars (AXPs) and the X-ray point sources (XPSs). The AXPs are a small group of neutron stars with spin periods falling in a narrow range (6–12 s) and no evidence of binary companions (e.g., Mereghetti et al., 2002). Their X-ray luminosities greatly exceed the power available from spin-down of the pulsars. Having many X-ray similarities with the AXPs, the XPSs is a group of “radio-quiet” neutron stars that are found at the center of several very young SNRs (e.g., Pavlov et al., 2002a). In Table 1.2 the properties of currently known AXPs and XPSs are given.

Fallback disks can play a significant role in these objects (Chatterjee et al. 2000; Alpar 2001). Because these objects are not contaminated by strong non-thermal emission from a radio pulsar and its synchrotron nebula (plerion), they offer an attractive target for detecting fallback disks. Perna et al. (2001) have also shown that the combination of an untruncated outer edge (in contrast to a binary accretion disk) and irradiation by the central X-ray source should lead to strong emission in the IR/submm bands. The strength of the optical/UV emission depends sensitively on

Table 1.2. Properties of Anomalous X-ray Pulsars and X-ray Point Sources

Source	SNR	d (kpc)	Age (10^3 yr)	$\log L_x$ (ergs s $^{-1}$)	P_{spin} (s)	Refs
AXPs						
4U 0142+61	...	1.0	63	34.5	8.69	1, 2
1E 1048.1–5937	...	3.0	5.0	34.4	6.45	3, 4
RXS J1708–40	...	10.0	10	35.8	11.0	5, 6
1E 1841–045	Kes 73	7.0	2.0	35.4	11.8	6, 7
1E 2259+586	CTB 109	4.0	10	35.0	6.98	8, 9
XPSs						
CXO J2323+5848	Cas A	3.4	0.3	33.8	...	10
1E 0820–4247	Pup A	2.0	3.7	33.6	...	11–13
RX J0852–4622	G266.1–1.2	1.0	2.0	32.5	...	14
1E 1207–5209	PKS 1209–52	1.5	7	33.1	0.424	15–17
1E 1614–5055	RCW 103	3.3	1-3	33.9	...	18–20

References. — (1) Israel et al. 1996. (2) Juett et al. 2002. (3) Seward et al. 1986. (4) Tiengo et al. 2002. (5) Sugizaki et al. 1997. (6) Mereghetti et al. 2002. (7) Vasisht & Gotthelf 1997. (8) Fahlman & Gregory 1981. (9) Patel et al. 2001. (10) Chakrabarty et al. 2001. (11) Petre et al. 1982. (12) Petre, Becker, & Winkler 1996. (13) Pavlov et al. 1999. (14) Pavlov et al. 2001. (15) Helfand & Becker 1984. (16) Mereghetti, Bignami, & Caraveo 1996. (17) Zavlin et al. 2000. (18) Tuohy & Garmire 1980. (19) Gotthelf, Petre, & Hwang 1997. (20) Becker & Aschenbach 2002.

the inner radius of the disk, presumably set by magnetic truncation by the neutron star. The overall normalization of the disk spectrum is set by the mass of the fallback disk.

1.4 Thesis Organization

In Chapter 2, capabilities of the telescopes and instruments used for our observations are described. In addition, the data reduction procedures are also briefly given in this chapter.

Chapter 3 and 4 present the spectroscopic and photometric studies of the known and candidate ultracompact LMXBs. In Chapter 3, a composite spectrum (1150-9000 Å) of the ultracompact LMXB 4U 1626–67 taken with the *HST* and optical spectra taken with the Magellan telescopes are shown. Several spectral features were identified: (1) Ly α λ 1216 absorption line, from which I derived the hydrogen column density to the source, (2) the absence of hydrogen lines, (3) the absence of He II λ 4686 emission line, and (4) a strong C III/N III λ 4640 blend. In Chapter 4, optical spectra of one known ultracompact LMXB, 4U 1916–05, and two candidate ultracompact systems, 4U 0614+09 and 4U 1543–62, are shown. There clearly are similarities between the optical spectra of these three sources and 4U 1626–67. The spectra are flat and can be approximately fitted by a power-law curve, consistent with emission from an X-ray heated disk model. The common spectral features are the same as those of the optical spectra of 4U 1626–67. The absence of hydrogen lines again probably implies that the low-mass donors are hydrogen-depleted and supports the suggestion that the candidate systems are ultracompact. Furthermore, the discovery of an 18 min periodicity from the time-resolved photometry of 4U 1543–62 is presented. The periodicity is probably orbital in origin, confirming the ultracompact nature of the binary.

Chapter 5 presents the discovery of a 692-s periodicity in the FUV light curve of the ultracompact LMXB 4U 1820–30. The FUV time series data from this source were recorded with *HST*/STIS, and indicated a period of 692.5 s which is approximately

1% longer than the X-ray period 685 s. This FUV period is consistent with a triple system model proposed for this globular cluster X-ray source. However, we find that the longer-period FUV signal can also be interpreted as a “superhump oscillation”, arising from a tidal resonance in the accretion disk of an extreme-mass-ratio binary. The 1 percent period excess implies a neutron-star/white-dwarf mass ratio around 20.

Chapter 6 and 7 report our optical/IR observations of the newly discovered X-ray MSPs. In Chapter 6, the optical/IR observations of the X-ray MSP SAX J1808.4–3658 during its 1998 X-ray outburst. Multiband optical/IR photometry at several epochs was taken. The optical light curve of this source roughly followed its X-ray light curve during the outburst. In Chapter 6, optical/IR search and identifications of counterparts to the other four MSPs are presented.

In Chapter 8, our identification of IR counterpart to the Bursting X-Ray Pulsar GRO J1744–28 is reported. Using *Chandra* imaging observations, we derived an astrometric solution for this source and thus found one IR object within the X-ray error circle. Based on its colors and magnitudes, this source could be a K giant. In order to further verify our identification, spectroscopy is needed.

Chapter 9, 10, and 11 report our search for optical/IR counterparts of anomalous X-ray pulsars and X-ray point sources in young supernova remnants. Identification of the IR counterpart to the AXP 1E 1048.1–5937 is presented in Chapter 9. This is the first AXP counterpart detected in multiple infrared bands with marginal evidence for spectral flattening at longer wavelengths. In Chapter 10, the observations of the sources within or near the X-ray error regions of two XPSs, RCW 103 and PKS 1209–52, are shown. Our color-color and color-magnitude analyses indicate the likely IR counterpart to the XPS in RCW 103 and non-detection of the XPS in PKS 1209–52. In Chapter 11, we present our search for optical/IR counterpart to two XPSs, RX J0822–4300 in SNR Puppis A and J0852–4617 in SNR RX J0852.0–4622. Upper limits on the optical/IR flux for these two objects were derived from our observations.

Chapter 12 summarizes our studies of the three types of X-ray sources, and indi-

Table 1.3 Summary of the results of our studies of X-ray sources

Source	Class	Major new results
4U 1626–67	Ultracompact	Magnetic truncation Spectral features
4U 1916–05	Ultracompact	Spectral features
4U 0614+091	Suspected ultracompact	Spectral features
4U 1543–624	Suspected ultracompact	Spectral features
4U 1822–000	Suspected ultracompact	Discovery of 18.2 min period Discovery of 80 min modulation
4U 1820–30	Ultracompact	Discovery of a 692.5 s period
SAX J1808.4–3658	MSP	Ourburst optical light curve Identification of counterpart
XTE J1751–309	MSP	Upper limits of IR counterpart
XTE J0929–314	MSP	Spectroscopy during outburst
XTE J1807–294	MSP	Upper limits of optical counterpart
XTE J1814–338	MSP	Photometry of counterpart
1E 1048.1–5937	Neutron star	Identification of IR counterpart
RCW 103	Neutron star	Identification of IR counterpart
PKS 1209–52	Neutron star	Search for optical/IR counterpart
Puppis A	Neutron star	Search for optical/IR counterpart
RX J0852.0–4622	Neutron star	Search for optical/IR counterpart

cates our future work based on the studies. Here, since we have studied quite a few X-ray sources, we also summarize our major results in Table 1.3.

Chapter 2

Telescopes and Instruments

2.1 Ground-based Observations

2.1.1 Optical Observations

Magellan Telescopes and Instruments

The optical observations presented in this thesis were made mainly using the Magellan telescopes at Las Campanas Observatory (LCO), Chile. The Magellan telescopes, Walter Baade (Magellan I) Telescope and London Clay (Magellan II) Telescope, are the twin 6.5-m telescopes located 60 meters apart on Cerro Manqui peak at LCO (Figure 2-1). The Magellan project is a collaboration between the observatories of the Carnegie Institute of Washington (OCIW), University of Arizona, Harvard University, University of Michigan, and Massachusetts Institute of Technology (MIT). The Baade telescope started science operations on February, 2001. Its principal focus is $f/11$ at two Nasmyth locations. Currently, the Inamori Magellan Areal Camera and Spectrograph (IMACS) is mounted at its Nasmyth West port, and the Persson's Auxiliary Nasmyth Infrared Camera (PANIC) is available on the telescope. The Clay telescope started science operations on September 7, 2002. It has the Raymond and Beverly Sackerly Magellan Instant Camera (MagIC) mounted on its auxiliary folded port. In addition, the Boller and Chivens (B&C) spectrograph and the Low Dispersion Survey Spectrograph (LDSS-2) are also available on this telescope.

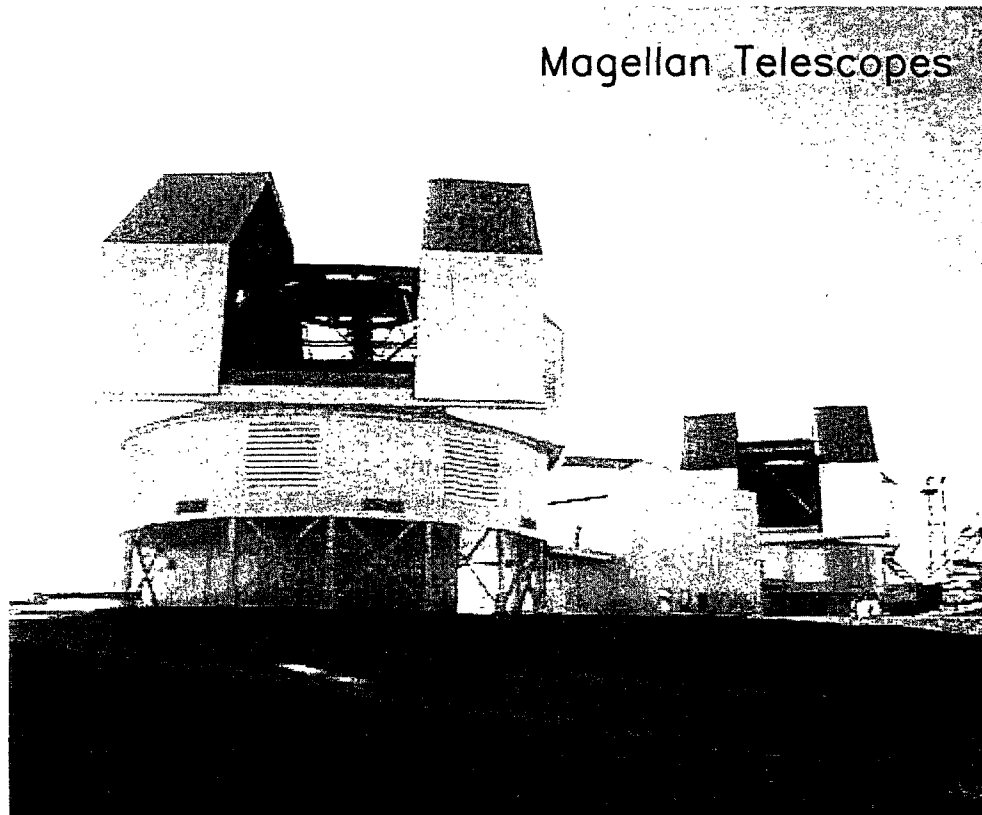


Figure 2-1 Magellan Baade & Clay 6.5-m Telescopes. This photo is copied from <http://www.ociw.edu/magellan>

Table 2.1 Standard grating setups of B&C Spectrograph

l/mm	Blaze (Å)	Dispersion (Å/pixel)	Wavelength coverage (Å)
300	5000	3.0	6230
600	5000	1.6	3210
1200	4000	0.80	1630

Table 2.2 Grisms of the LDSS-2

Grism name	Blaze (Å)	Central Wavelength (Å)	Dispersion (Å/pixel)
Low	5500	5500	11.3
Med/Blue	5000	5500	5.3
Med/Red	6000	5500	5.3
High	5000	4200	2.4

The instruments used for our observations on the Magellan telescopes are MagIC, B&C, and LDSS-2.

- **MagIC.** The MagIC is a 2048×2048 pixel CCD camera, providing a 0.069 arcsec/pixel plate scale and a 142 arcsec field of view at the f/11 focus of the telescope. Its CCD detector consists of four amplifiers, thus allowing a fast data readout of 20 seconds a frame.
- **B&C Spectrograph.** The B&C uses a Marconi 2048×515 pixel CCD with a spatial scale of 0.25 arcsec/pixel on the Magellan telescopes. Several diffraction gratings are available with this spectrograph. The characteristics for several standard grating setups are summarized in Table 2.1.
- **LDSS-2.** The LDSS-2 uses a SITe 2048×2048 pixel CCD detector with a scale of 0.378 arcsec/pixel. It has four grisms, providing different spectral resolutions. The wavelength coverage for all the grisms is approximately the same, 4000-8000 Å. The grisms are listed in Table 2.2. The LDSS-2 can also be used to give direct images over a 7.5 arcmin diameter field of view. The available broadband filters are the *BVR* Harris set; imaging in the *UI* bands is not feasible as the efficiencies at wavelengths blueward of 4000 Å and redward of 8000 Å are poor.

Data Reduction

The Image Reduction and Analysis Facility (IRAF) packages have always been used to reduce our data. Every image was first bias-subtracted with using each image's bias value, which was recorded at CCD detector's overscan region, usually a number of rows or columns that is added to and stored with each image frame. The second data reduction step is flat-fielding, which is done to remove pixel-to-pixel variations of any CCD detector. A flat field image was constructed by averaging a number of either dome-flats, images of an illuminated dome screen, or sky-flats, images of the dawn or dusk sky.

2.1.2 Infrared Observations

Telescopes and IR Imaging Cameras

Our infrared observations were made using both the Magellan telescopes and the Blanco telescope at Cerro Tololo Inter-American Observatory (CTIO), Chile. The instruments used are "Classic Cam" near-infrared imager (Classicam; Persson et al. 1992) and PANIC (Martini et al. 2004) on the Magellan telescopes and the Ohio State InfraRed Imager/Spectrometer (OSIRIS; Depoy et al. 1993) on the Blanco telescope.

The Classicam was an old infrared imager used on the Magellan telescopes and is not available any more. Its detector was a Rockwell NICMOS3 HgCdTe 256×256 array. The camera had a low-resolution mode, with a 0.112 arcsec/pixel plate scale and a 29 arcsec field of view.

The PANIC has replaced the Classicam since April 2003 as the infrared imager on the Magellan telescopes. Its detector is a Rockwell Hawaii HgCdTe 1024×1024 array, and it provides a 0.125 arcsec/pixel plate scale and a 2 arcmin field of view.

The Blanco 4-m telescope is a Ritchey-Chretien telescope, and was commissioned in 1974. It allows four focus positions. The OSIRIS was a standard instrument used at its Tip-tilt focus f/14.5. The detector in OSIRIS was a Rockwell HAWAII HgCdTe 1024×1024 array. When used with its f/7 camera, the OSIRIS had a 0.161 arcsec/pixel plate scale and a 93 arcsec field of view.

The filters used for these infrared cameras are the standard JHK_s set. The central wavelengths of J , H and K_s are 1.25, 1.65, and 2.16 microns respectively.

Data Reduction

Due to bright IR sky background and its variability on short time scales, several additional data reduction steps are required for IR imaging observations besides the bias-subtracting and flat-fielding given in section 2.1.1. The first one is linearity correction, as most IR detectors are nonlinear. This has been done by using IRAF scripts with given coefficient numbers, provided by the instrumentation groups of local observatories. Over the course of an IR observation of a target, the telescope is dithered a few arcseconds between exposures several times (often 5 or 9). This is to obtain several frames with the target measured at different positions of the CCD detector and then construct a sky image from these frames for the target by median filtering them. A final image of a targeted field is obtained by shifting and combining all the individual frames from which the sky image have been subtracted.

2.2 *Hubble Space Telescope* Observations

2.2.1 *Hubble Space Telescope* and Space Telescope Imaging Spectrograph

Part of our observations were made using the *Hubble Space Telescope* (*HST*) and one of its instruments, Space Telescope Imaging Spectrograph (STIS). *HST* is a 2.4-m reflecting telescope and started its operations on April 25, 1990. Because *HST*'s position is above the Earth's atmosphere, it provides the capability for observations in a wide spectral range from the far-ultraviolet (FUV; starting from 1150 Å) to the near-IR (ending at 25000 Å). It also provides a resolution of 0.1 arcsec, 10 times better than the general resolution of ground-based telescopes.

The STIS (Kim Quijano et al., 2003) was installed in *HST* on February 14, 1997, and provides the capability for both imaging and spectroscopic observations at ul-

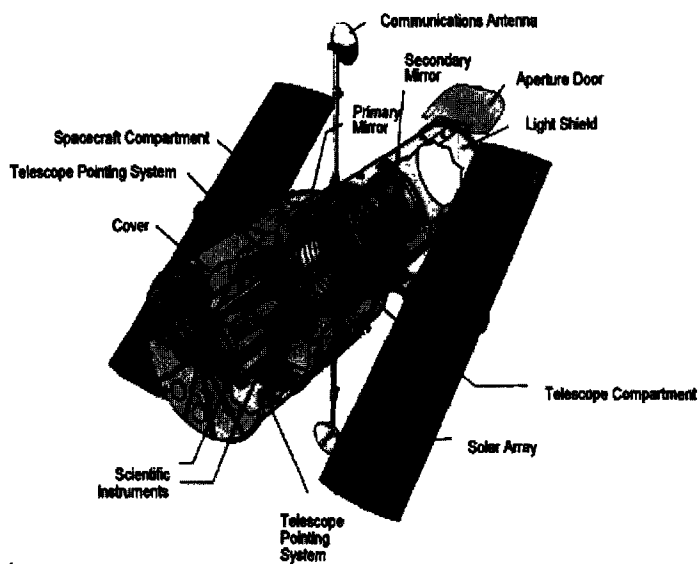


Figure 2-2 The *Hubble Space Telescope* (<http://oposite.stsci.edu/pubinfo/spacecraft>).

Table 2.3 STIS spectroscopic capabilities

Detector	Grating	Spectral Range (Å)	Spectral Scale (Å/pixel)
CCD	G750L	5240-11490	4.92
CCD	G430L	2900-5700	2.73
NUV-MAMA	G230L	1570-3180	1.58
FUV-MAMA	G140L	1150-1730	0.60

traviolet and visible wavelengths. It has three 1024×1024 pixel detectors, a Scientific Image Technologies (SITe) CCD (STIS/CCD), a Cs₂Te Multi-Anode Microchannel Array (MAMA) detector (STIS/NUV-MAMA), and a solar-blind CsI MAMA (STIS/FUV-MAMA), used to cover three different wavelength ranges. Table 2.3 gives STIS's typical spectroscopic capabilities when the detectors are used with several STIS's gratings. The STIS/FUV-MAMA and STIS/NUV-MAMA can also be operated in TIME-TAG mode, which allows to record the position and detection time of every photon with 125 microsecond time resolution.

2.2.2 Data Reduction

The HST/STIS data have been automatically processed through its standard calibration pipeline `calstis`. The detailed description of the STIS pipeline is given by Brown et al. (2002). The data through the pipeline can often be directly used for scientific analysis. However, two special data calibrations have been used for our observations. The first one is, sometimes, to remove hot pixels, which are caused by radiation damage of the detectors. For this case, “superdark” images were generated with using daily dark images obtained near our observation times. The task `daydark` in the IRAF STSDAS package was used to make the superdark images. The second is to correct time series data for the barycenter arrival times. This was done by obtaining the *HST* ephemeris file (ORX file) at the observation times and then using task `odelaytime` in the IRAF STSDAS package.

Chapter 3

UV/Optical Spectroscopy of the Ultracompact X-ray Binary 4U 1626-67

3.1 Introduction

The LMXB 4U 1626–67 contains an accreting X-ray pulsar with a spin period of 7.7 s (Rappaport et al. 1977) and a low mass Roche-lobe-filling companion, very likely the $0.02 M_{\odot}$ core of a C-O or O-Ne white dwarf (Schulz et al. 2001). It has an ultra-short orbital period of 42 min (Middleditch et al. 1981; Chakrabarty 1998), indicating that it is an ultracompact LMXB which must have a H-depleted mass donor (Nelson, Rappaport, & Joss 1986). The X-ray timing measurements have failed to detect periodic pulse arrival time delays due to a binary orbit, yielding an upper limit of $a_x < 10$ lt-ms for the projected radius of the neutron star orbit (Levine et al. 1988; Shinoda et al. 1990). This limit requires that the binary inclination must be $i < 33^{\circ}$ for a $0.02 M_{\odot}$ companion. The cyclotron resonance feature discovered in its X-ray spectrum implies that the neutron star has a magnetic field strength of $\sim 3.2 \times 10^{12}$ G (Orlandini et al. 1998).

The optical counterpart of 4U 1626–67 has a strong ultraviolet (UV) excess (Mc-

Clintock et al. 1977), and the measured flux densities can be well fitted by an X-ray heated accretion disk (Chakrabarty 1998). Its UV light curve showed 1000 s quasi-periodic oscillations, probably due to warping of the accretion disk in this system (Chakrabarty et al. 2001). The far-UV (FUV) spectroscopy, using the Space Telescope Imaging Spectrograph (STIS; Woodgate et al. 1998) on board the *HST*, detected strong, broad emission lines plausibly formed in the accretion disk (Homer et al. 2002). This is consistent with the results of *Chandra* X-ray observations (Schulz et al. 2001) and supports the suggestion that the companion is a C-O/O-Ne white dwarf. In the optical, previous spectroscopy showed only the C III/N III 4641-4651 Å blend and possible weak H β emission line (Cowly, Hutchings, & Crampton 1988). In this chapter, we report our UV/optical spectroscopic observations of 4U 1626–67 made with using *HST*/STIS as well as the ground-based telescope. Our observations provide supporting evidence for the scenario of this binary being a neutron star and a C-O/O-Ne white dwarf, and constraints on the structures of the accretion disk in this binary.

3.2 Observations and Data Reduction

3.2.1 HST/STIS Data

The *HST* observations were carried on 1998 April 23 during five spacecraft orbits using the STIS. Two orbits of data in each the FUV and Near-UV (NUV) and one orbit of data in the optical were obtained. All observations were made through a $52'' \times 0''.2$ long slit.

The FUV and NUV data were both taken in TIMETAG mode with using the solar-blind CsI multi-anode microchannel array (STIS/FUV-MAMA) and the Cs₂Te MAMA (STIS/NUV-MAMA) detector respectively. The low-resolution gratings G140L and G230L were used, respectively providing the wavelength ranges of 1150-1730 Å and 1570-3180 Å and spectral scales of 0.60 Å/pixel and 1.58 Å/pixel. The exposure time for each set of FUV/NUV data was about 45 min during each 96 min *HST* orbit.

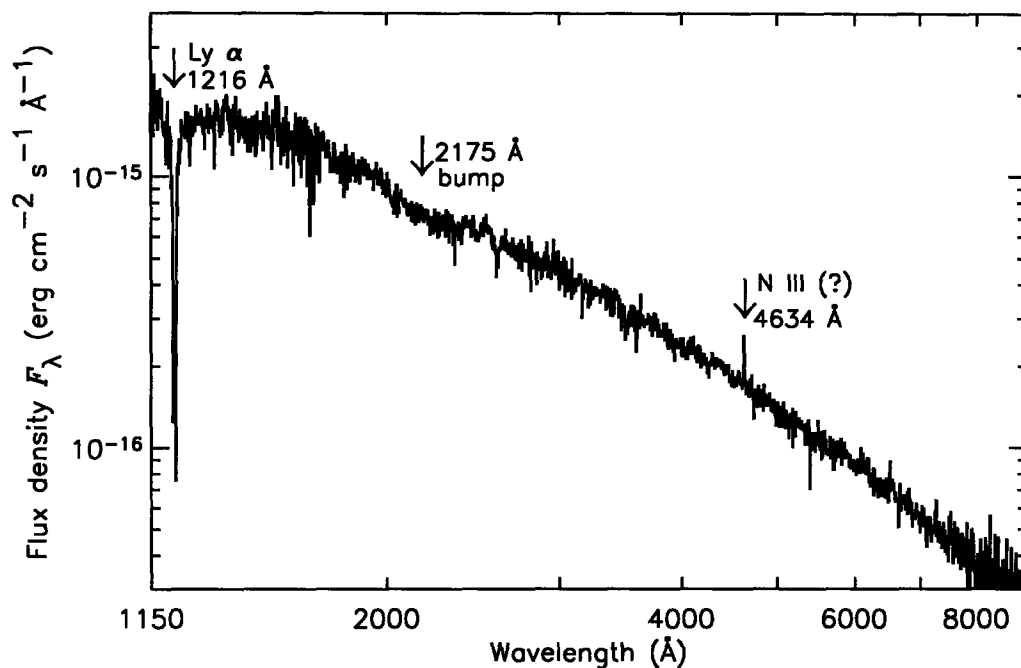


Figure 3-1 The composite *HST*/STIS spectrum of 4U 1626–67. The indicated features are Ly α λ 1216, 2175 Å interstellar bump, and N III λ 4634 emission line.

The optical data were taken in ACCUM mode with using the detector STIS/CCD. We obtained one optical/blue spectrum (2900-5700 Å) with the grating G430L and one optical/red spectrum (5240-10270 Å) with the grating G750L. The respective spectral scales are 2.73 Å/pixel in the optical/blue and 4.92 Å/pixel in the optical/red. The exposure times were 1200 s in the optical/blue and 810 s in the optical/red.

The FUV/NUV data were processed through the STIS calibration pipeline (*calstis*; Brown et al. 2002). The detailed description of the STIS pipeline is given by Brown et al. (2002).

In order to remove hot pixels in the CCD detector due to radiation damage, we recalibrated our STIS/CCD data. Daily dark images near our observations date were obtained from *HST* Archive and were used to generate a “superdark” image. The superdark image was made using the *daydark* task in the IRAF STSDAS package. The *iraf* version *calstis* task was then used in calibrating the CCD data with the best reference files.

3.2.2 Ground-based Data

On 2001 March 23, we obtained two optical spectra of 4U 1626–67 with the 6.5-meter Baade/Magellan-I telescope at Las Companas Observatory. The exposure time for each spectrum was 1800 s. We used a Boller & Chivens (B&C) slit spectrograph with a 600 lines mm^{-1} grating, giving a spectral scale of $2.75 \text{ \AA pixel}^{-1}$. The grating tilt was set at 11° , providing a wavelength coverage of 3900–6500 \AA . The slit width was $1''.3$. A WG360 Schott glass blocking filter was used to block the second order contamination.

We also obtained one optical spectrum of 4U 1626–67 on 2002 August 10 with the same telescope. A Low-Dispersion Survey Spectrograph (LDSS-2) with a high dispersion grism was used, providing a spectral scale of $2.4 \text{ \AA/pixel}^{-1}$ and a wavelength coverage of $\sim 3900\text{--}6800 \text{ \AA}$. A long slit with a width of $1''.0$ was used. The exposure time was 2100 s.

We used the IRAF packages to reduce the data. The spectral images were bias-subtracted and flat-fielded, and the IRAF package `twodspec` was used to extract the spectra. The spectra of white dwarf EG 274 were obtained and used to calibrate flux for both observations. A B&C spectrum was derived by averaging the two 1800 s spectra.

3.3 Results

3.3.1 HST/STIS Spectrum

The composite *HST*/STIS spectrum covering from the FUV, NUV, optical/blue, and optical/red wavelength range is shown in Figure 3-1. Since the spectral data longward of 9000 \AA have very low signal-to-noise (S/N) ratio ($S/N < 3$), the spectrum is only shown to 9000 \AA . We identified three prominent features for this spectrum: Ly α absorption line, 2175 \AA interstellar bump, and an emission line at $\lambda 4634$, probably N III. These features are indicated in Figure 3-1.

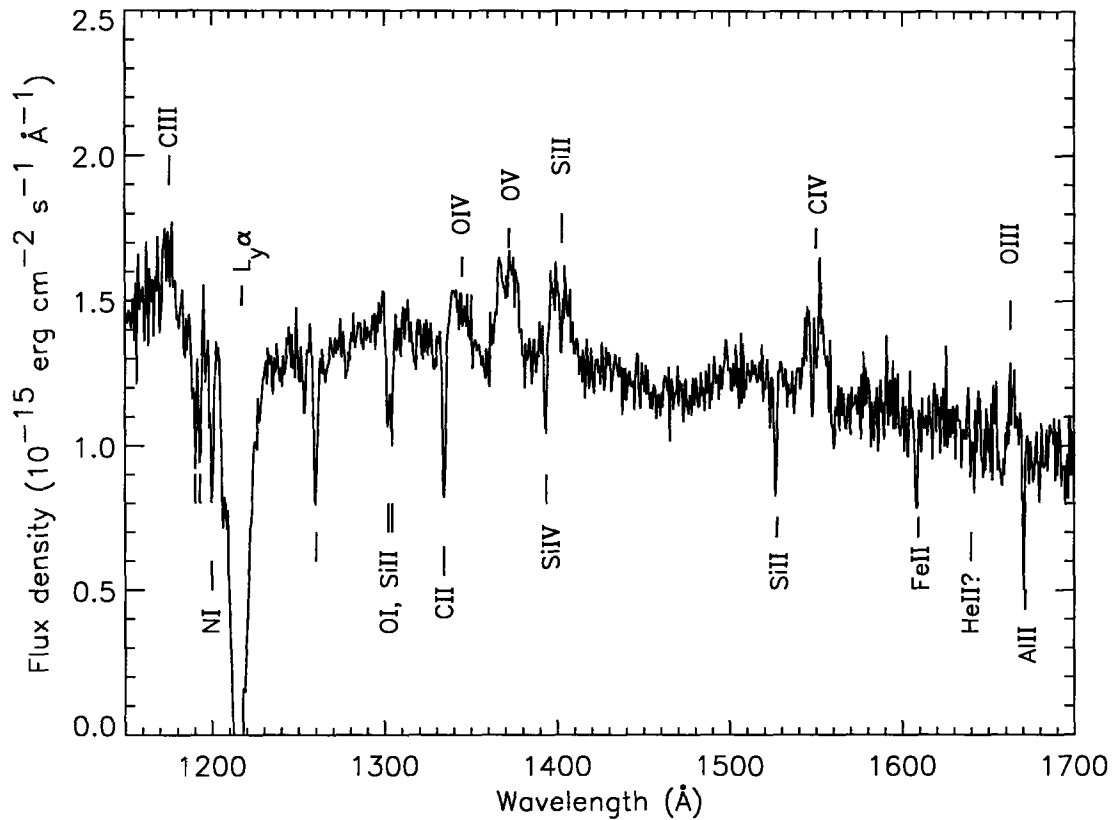


Figure 3-2 HST/STIS FUV spectrum of the ultracompact LMXB 4U 1626–67. The identified emission lines and interstellar absorption lines are indicated.

FUV Spectrum

In the FUV spectrum, a few lines were detected (see Figure 3-2). They are C III λ 1176, O IV λ 1340, O V λ 1371, Si III λ 1550, and O III λ 1663 emission lines and typical interstellar absorption lines (see, e.g., Bohlin et al. 1983). The emission lines were strong and broad, and showed double-peaked features, implying that they were likely formed in the accretion disk (see Homer et al. 2002 for the detailed study of these lines). We note that one emission line, He II λ 1640, which is a common feature in the FUV spectra of other LMXBs and is often as strong as those C, O, or Si emission lines, was not detected in the spectrum.

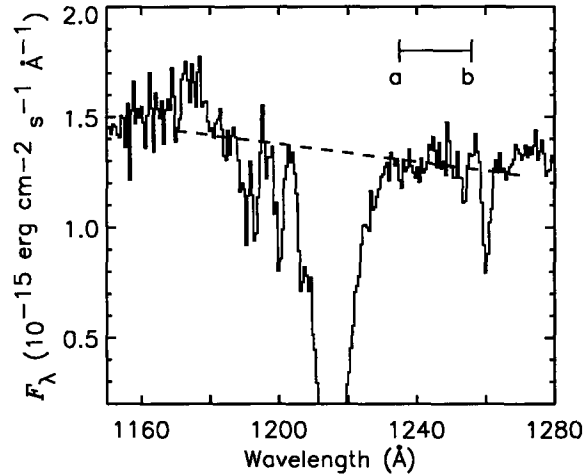


Figure 3-3 Reconstruction of $\text{Ly}\alpha$ $\lambda 1216$ absorption line toward 4U 1626–67. The dashed straight line is our estimated continuum over the $\text{Ly}\alpha$ line. Following the method of Diplás & Savage (1994a), the spectral region marked between a and b was used for deriving the noise level in the continuum. The $N(\text{H I})$ we obtained was $(6.4 \pm 1.0) \times 10^{20} \text{ cm}^{-2}$.

$\text{Ly}\alpha$ $\lambda 1216$ and Extinction

In the FUV, besides the emission and absorption lines, there is a broad $\text{Ly}\alpha$ $\lambda 1216$ absorption line, caused by the absorption of interstellar neutral H and can be fitted with a pure damping profile (Jenkins 1972; Bohlin 1975). Using the continuum reconstruction technique (Bohlin 1975), the H I column density $N(\text{H I})$ can be derived. We followed the procedure given by Diplás & Savage (1994a) to obtain $N(\text{H I})$ value. A continuum was constructed over $\text{Ly}\alpha$ line by linearly fitting the spectrum in the proximity of the $\text{Ly}\alpha$, and the noise level in the continuum was estimated by using a nearby region of the spectrum (see Figure 3-3). The $N(\text{H I})$ we obtained was $(6.4 \pm 1.0) \times 10^{20} \text{ cm}^{-2}$.

This value should be an upper limit of the total neutral hydrogen along the line of sight because it may contain the absorption local to the source 4U 1626–67. However, given that we did not detect any hydrogen lines, such as $\text{H}\alpha$ and $\text{H}\beta$, in the optical region of our spectrum and theoretical studies suggest that the donor in an ultracompact binary must be hydrogen-depleted (Nelson et al. 1986), we may take

Table 3.1. Equivalent width upper limits (\AA) on Bowen O III lines

	$\lambda 3044$	$\lambda 3133$	$\lambda 3407$	$\lambda 3444$
Upper limit (2σ)	$\lesssim 1.4$	$\lesssim 2.0$	$\lesssim 1.4$	$\lesssim 1.6$

it as the pure interstellar column density. Using the relation of the average ratio of neutral hydrogen to dust, $\langle N(\text{H I})/E(B-V) \rangle = 4.93 \times 10^{21} \text{ cm}^{-2} \text{ mag}^{-1}$ (Diplas & Savage 1994b), we obtained $E(B-V) \simeq 0.13$. This value is consistent with the Galactic reddening in the direction of 4U 1626–67 ($E(B-V) \approx 0.09$; Schlegel, Finkbeiner, & Davis 1998).

The interstellar extinction feature, 2175 \AA bump, also allows an independent measurement of extinction to a source (Fitzpatrick 1998). The bump in our spectrum is quite shallow, already indicating low extinction to 4U 1626–67. A detailed study of the whole UV/optical spectrum with using the empirical extinction law which includes this bump, given in Chapter 3.4, shows a consistently low extinction value. This provides additional support for the interstellar origin of the Ly α absorption line.

Searching for O III Emission Lines

In the NUV spectral range, a few interstellar absorption lines were detected and there were no strong emission features (Homer et al. 2002). However, the strong N III $\lambda 4634$, shown in the optical spectrum (see Figure 3-1), is generally considered to be produced by the Bowen Fluorescence (BF) mechanism (Bowen 1934, 1935; McClintock et al. 1975), and therefore we may expect BF O III emission lines in the NUV spectrum. We extracted the NUV archival data reported by Homer et al. (2002) and derived an averaged spectrum with the total exposure time of ~ 10.8 ks. The 3 pixel boxcar smoothed spectrum between 2150–3150 \AA is shown in Figure 3-4(a). In the figure, we indicate the positions of a couple of strong Bowen O III lines $\lambda 3044$ and $\lambda 3133$, which are predicated by theoretical studies (Kallman & McCray 1980; Deguchi 1985) and one of which, O III $\lambda 3133$, was detected in the spectra of the

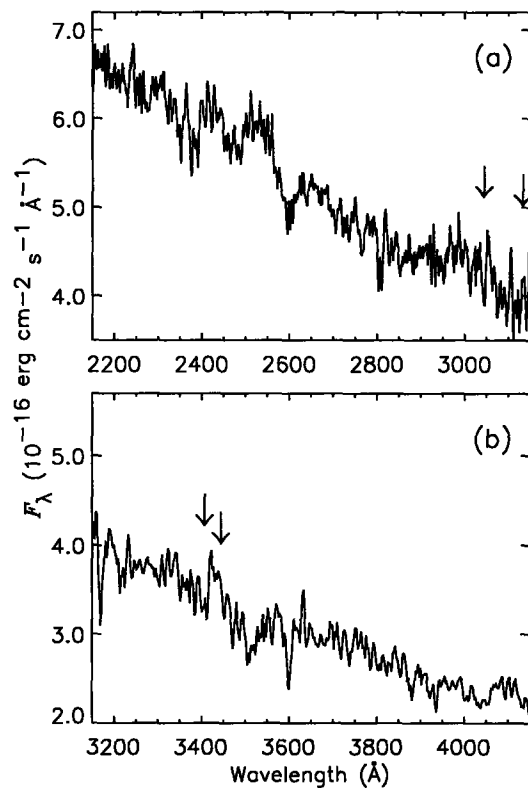


Figure 3-4 Optical spectrum between 2150-4150 Å of 4U 1626-67. (a) The NUV wavelength region between 2150-3150 Å. The positions of Bowen O III λ 3044 and λ 3133 are indicated with arrows. (b) The optical/blue region between 3150-4150 Å. The positions of two relatively strong O lines λ 3407, 3444 are indicated with arrows.

LMXB SCO X-1 (Schachter, Filippenko, & Kahn 1989). The figure illustrates the absence of O III emission lines, including other predicted weak lines in this region. It is interesting to note that the O III λ 3044 is produced through the O3 channel and may be enhanced by a rotating motion such as an accretion disk (Deguchi 1985).

Our *HST*/STIS optical/blue data cover the wavelength region between 3000-4000 Å, in which a few O III Bowen lines may exist. We did a search for these lines as well as other He and N emission lines reported in the spectrum of SCO X-1 (Schachter et al. 1989). However none of them was convincingly detected. In Figure 3-4(b), we show this region and mark the wavelength positions of a couple of relatively strong O III lines. The upper limits (2σ) on these relatively strong Bowen O III emission lines are given in Table 3.1.

3.3.2 Ground-based Spectra

Our ground-based spectra show broad, strong emission features between wavelength 4000-5000 Å, but no hydrogen lines, such as H α or H β line, were detected in any spectrum. In Figure 3-5, we present our both B&C and LDSS-2 spectra, with 3 pixel boxcar smoothing applied. By comparing the two spectra, we have identified emission features at two wavelength regions: 4288-4372 Å and 4615-4700 Å.

The first one between 4288-4372 Å has the central peak at 4320 Å. The region is so broad that it can coincide with many emission lines, such as O II, N III, and Fe II, (see, e.g., Baldwin et al. 2000), and H γ λ 4341. Given that we did not detect any other hydrogen line in our optical spectra, it is not likely that this broad feature contains H γ line. As the X-ray spectroscopic observations (Schulz et al. 2001) suggested a C-O/O-Ne white dwarf mass donor for 4U 1626–67, this feature is probably the O II λ 4320. We note that, although in general this O II line is rarely observed in spectra of LMXBs, similar but weak O lines and Fe lines were found in the spectra of LMXB 2S 0921–63 (Cowley, Crampton & Hutchings 1982) and 4U 1735–44 (Canizares, McClintock, & Grindlay 1979). The second one is the well known feature N III/C III $\lambda\lambda$ 4640-4650, one of the prominent emission features in the optical spectra of LMXBs (van Paradijs & McClintock 1995). In our spectra, especially the LDSS-2 one, it is

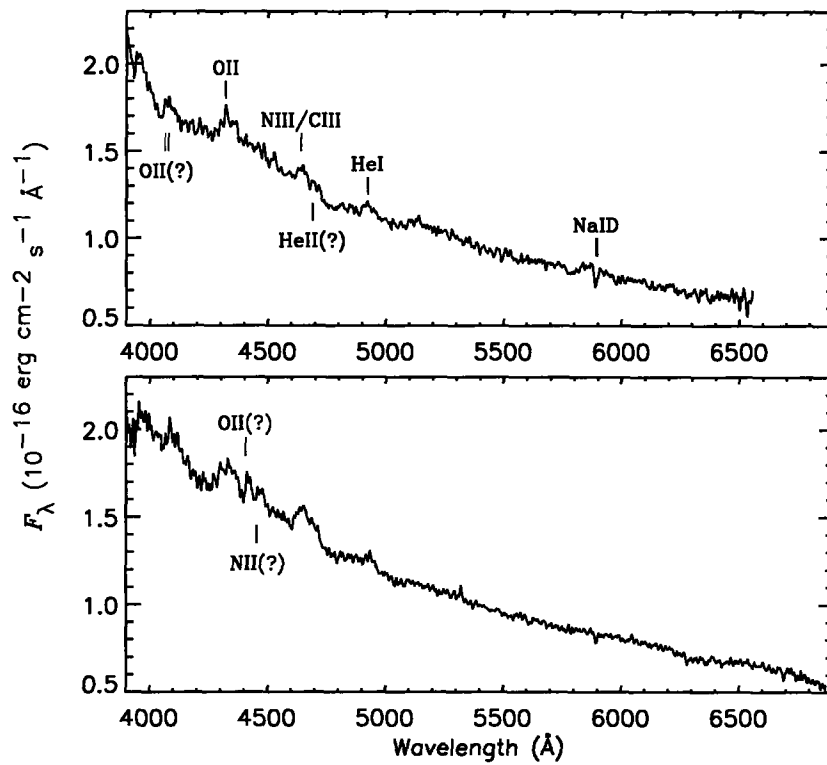


Figure 3-5 Ground-based optical spectra of 4U 1626-67. The top panel shows the B&C spectrum while the bottom one shows the LDSS-2 spectrum. The identified spectral features are indicated.

broad and strong with the central peak at C III $\lambda 4647$. The equivalent width (EW) of the $\lambda 4647$ line is estimated to be 3.6 Å.

In addition to these features, we also detected the likely emission feature at 4063 and 4079 Å, which are probably O II lines. In our LDSS-2 spectrum, two strong emission features are shown at about 4406 and 4453 Å, coinciding with O II and N II lines respectively. Further high-resolution observations are needed to identify these features.

3.4 Discussion

3.4.1 X-ray heated accretion disk

The optical emission from 4U 1626–67 can be well fitted by an X-ray heated accretion disk model (Chakrabarty 1998). Using the same model, we fitted our composite *HST*/STIS spectrum.

Spectral Data and X-ray Bolometric Flux

We first removed the broad Ly α absorption line from our spectral data. Then we binned our data into 424 points with roughly one data point per 10 Å between 1150–3100 Å, 20 Å between 3100–5700 Å, and 30 Å between 5700–9000 Å. The resultant binned spectrum is shown in Figure 3-6.

In order to estimate the simultaneous X-ray flux during the UV/optical observations, we used the following method. First, the simultaneous X-ray observations of 4U 1626–67 on 1998 April 23, which were carried out with the Proportional Counter Array on board the *RXTE* and were reported by Chakrabarty et al. (2001), gave the X-ray flux of 2.54×10^{-10} erg cm $^{-2}$ s $^{-1}$ between 2–30 keV. Second, we extracted one set of X-ray data of the source, which was carried on 1993 August 11 by the *Advanced Satellite for Cosmology and Astrophysics* (*ASCA*) and was reported by Angelini et al. (1995), from the *High Energy Astrophysics Science Archive Research Center* (*HEASARC*). The *ASCA* data provide the spectral coverage between 0.4–10 keV.

We found that, between 2-10 keV which was covered by both *ASCA* and *RXTE* observations, the two spectra were quite similar and the integrated fluxes were almost equal ($F_{\text{ASCA}} = 2.47 \times 10^{-10}$ ergs cm $^{-2}$ s $^{-1}$ and $F_{\text{RXTE}} = 2.53 \times 10^{-10}$ ergs cm $^{-2}$ s $^{-1}$). Thus for the flux between 0.4-2.0 keV, we used the value obtained from the *ASCA* data, $F(0.4 - 2.0 \text{ keV}) = 0.57 \times 10^{-10}$ ergs cm $^{-2}$ s $^{-1}$. Thirdly, for the X-ray flux above 30 keV, we used the power law, $F_E \propto E^{-5}$ (Chakrabarty et al. 1997). Combining these three parts of the X-ray emission, the bolometric X-ray flux between 0.4-60 keV was obtained as $F_X \approx 8.2 \times 10^{-10}$ ergs cm $^{-2}$ s $^{-1}$.

X-ray Heated Accretion Disk Model

In calculating the flux emitted from an X-ray heated, geometrically thin, and optically thick accretion disk in an ultracompact binary, we used the equations given in Chapter 1.3.

The whole shape of the composite spectrum provides strong constraints on the disk parameters as well as the interstellar extinction along the line of sight to the source. We took the inner disk radius r_i , outer disk radius r_o , and $A(V)$, the extinction in V band, as three parameters. The empirical extinction law is given by Cardelli, Clayton, & Mathis (1989). We used $R_V = A(V)/E(B-V) = 3.1$, the mean value of R_V .

Since the dominant part of the accretion energy of a LMXB is emitted in the X-ray band, we have $GM\dot{M}/R \approx 4\pi D^2 F_X$. For a given F_X , either \dot{M} or D is needed to be one parameter. However for 4U 1626–67, its X-ray flux has been decaying ever since its discovery. (Chakrabarty et al. 1997) while its optical flux has not exhibited any noticeable change (Chakrabarty 1998). We suspect that the observed F_X may not reflect \dot{M} in the accretion disk, and we thus took \dot{M} and D as two parameters. In addition, a low limit on \dot{M} can be set by requiring

$$(GM\dot{M}/R) \geq 4\pi D^2 F_X. \quad (3.1)$$

The inclination of the disk in 4U 1626–67 must be $i < 33^\circ$ if the companion is a $0.02 M_\odot$ star. We used $D_e = (D^2/\cos i)^{1/2}$ as one parameter, since the value of i does

not affect our fitting except that different values would result in different distance values.

In the X-ray heated disk model, the X-ray albedo of the disk η_d is a parameter to be considered. de Jong, van Paradijs, & Angusteijn (1996) concluded that LMXB accretion disks have a high effective X-ray albedo of $\eta_d \geq 0.9$. We adopted $\eta_d = 0.9$ in our fitting.

The search for best fits was therefore done in a five-dimensional parameter space ($D_e, r_i, r_o, \dot{M}, A(V)$). We used a χ^2 statistical test to find the best fits. The standard deviation of every binned point was calculated by combining the standard deviation of the mean flux at each binned point and the respective standard deviation in the extinction model (Cardelli et al. 1989).

The Inner Radius of the Accretion Disk

The results of our fitting show that the UV/optical spectrum of 4U 1626–67 can be well fitted by the X-ray heated accretion disk model. In Figure 3-6, we show both a typical fitting spectrum, with $r_i = 4.0 \times 10^8$ cm and the observed dereddened spectrum. Other parameters for this fitting spectrum are $D_e = 3.16$ kpc, $r_o = 0.92 \times 10^{10}$ cm, $\dot{M} \simeq 2 \times 10^{-10} M_\odot \text{yr}^{-1}$, and $A(V) = 0.31$. We can see from Figure 3-6 that the observed spectrum of the source is well fitted.

In the fitting, the values of four parameters D_e, r_i, r_o , and \dot{M} , were closely related with each other in order to have best fits. For example, as r_i is increased, it is obvious that r_o has to be increased too. For the best fits, the resulting $A(V)$ is always in the range consistent with the value derived from the Ly α line or the Galactic disk reddening.

However, we found the fitting was more sensitive to r_i and \dot{M} . In Figure 3-7, we show the χ^2 values at a 90% confidence level as the function of \dot{M} and r_i , with other three parameters D_e, r_o , and $A(V)$ being freely varied. The allowed values of r_i and \dot{M} can basically stretch toward both small and large values if there is no limit on other parameters. However, a lower limit can be set on \dot{M} by equation 3.1. The limit is shown as a long dashed line in Figure 3-7 at the lower-left end of the contour (here

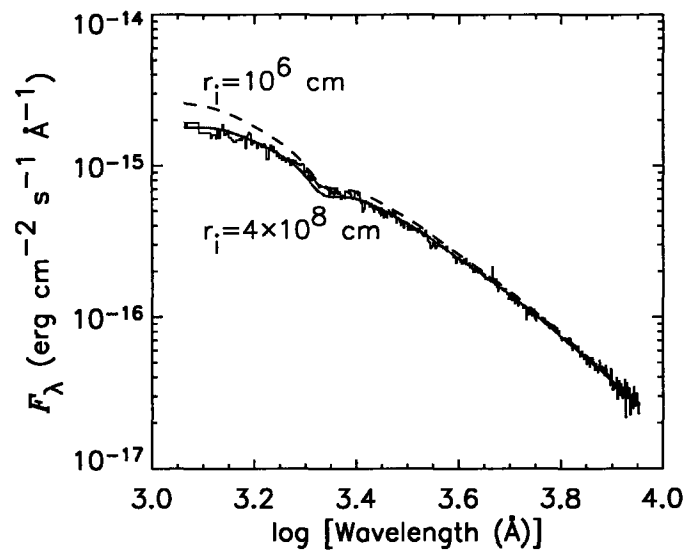


Figure 3-6 The binned spectrum of 4U 1626–67. Also plotted are a best-fit spectrum (solid curve) produced by the X-ray heated accretion disk model with $D_e = 3.16$ kpc, $r_i = 4.0 \times 10^8$ cm, $r_o = 0.92 \times 10^{10}$ cm, $A_V = 0.31$, and $\dot{M} \simeq 2 \times 10^{-10} M_\odot \text{yr}^{-1}$ and a similar spectrum (dashed curve) but with r_i changed to 10^6 cm. The difference between the two curves indicates our fitting is sensitive to r_i .

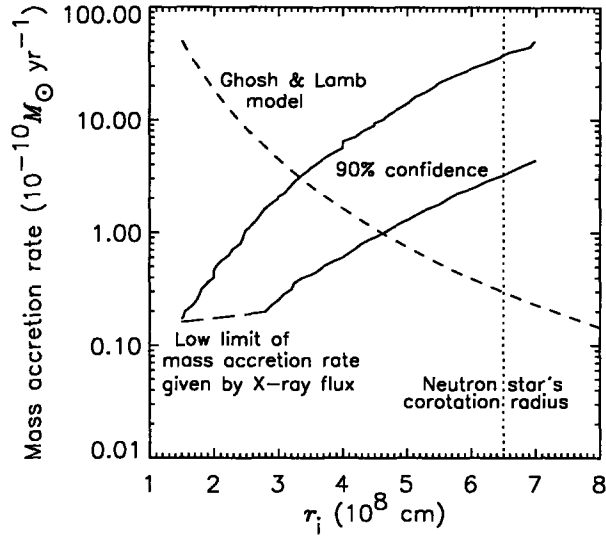


Figure 3-7 Allowed values of r_i and \dot{M} at a 90% confidence level. The long-dashed line at the low left end of the contour indicates the low limit of \dot{M} , while the dashed curve indicates the innermost radius r_0 as a function of \dot{M} (Ghosh & Lamb 1979). The neutron star's corotation radius r_{co} , presumably the upper limit on r_i , is also plotted as the dotted line. the dotted line.

we assume $i \simeq 0^\circ$; $i \simeq 33^\circ$ will lower the limit by a factor of $\cos(33^\circ) = 0.84$). Below this line, there are D_e values allowing good fits, but they can not satisfy equation 3.1. Thus, the contour and the equation 3.1 only allow r_i to have a minimum value of $\sim 1.5 \times 10^8$ cm. with $D_e \approx 1.1$ kpc.

An innermost radius r_0 , inside which the accretion disk is truncated by the strong magnetic field of a central neutron star, can be set as a function of \dot{M} (Ghosh & Lamb 1979a), $r_0 \approx 0.52r_m$, where the magnetosphere radius is $r_m = \mu^{4/7}(2GM)^{-1/7}\dot{M}^{-2/7}$ with μ the magnetic dipole moment of the neutron star. The dashed curve in Figure 3-7 indicates this r_0 . According to Ghosh & Lamb's model (Ghosh, Lamb, & Pethick 1977; Ghosh & Lamb 1979a,1979b) for an accretion disk, r_0 should be smaller than a neutron star's corotation radius r_{co} as the accreting neutron star is spinning up, or close to r_{co} as the neutron star stops spinning up; $r_{co} = (GM/\Omega_*^2)^{1/3}$ ($\sim 6.5 \times 10^8$ cm for 4U 1626-67), where Ω_* is the star's angular velocity. As can be seen from Figure 3-7, the range of r_0 with 90% confidence is between $(3.2-4.5) \times 10^8$ cm, consistent

with the theoretical model. Moreover, based on the same argument on the accretion process around neutron stars, \dot{M} is inferred as to be greater than $2 \times 10^{-10} M_{\odot} \text{ yr}^{-1}$ from spin-up rate of 4U 1626–67 (Chakrabarty et al. 1997). This implies that, if \dot{M} has not changed dramatically after the turn-over of 4U 1626–67 from spin-up to spin-down in 1990 (Chakrabarty et al. 1997), r_0 can be located approximately at 4.0×10^8 cm by this lower limit of \dot{M} and the χ^2 region.

As the accreting neutron star of 4U 1626–67 has a surface magnetic field strength of $\sim 3.2 \times 10^{12}$ G (Orlandini et al. 1998) and theoretical models have predicted the truncation of an accretion disk by a strong magnetic field of the neutron star, our result for the inner disk radius, in particular the strong lower limit on r_i , provides evidence for supporting the idea of magnetic truncation. In Figure 3-6, we indicate the difference between two spectra when r_i is changed from 4×10^8 cm to 10^6 cm while with other parameters fixed.

3.4.2 Spectral Features

Our observations indicate the absence of hydrogen lines in the optical spectra of 4U 1626–67. Although Cowley et al. (1988) mentioned a possible detection of a weak H β line, their optical spectra presented are far from convincing. More spectroscopic observations are needed to confirm our results. Using the Ly α $\lambda 1216$ absorption line profile, we derived the hydrogen column density towards the source. We show that the derived value is consistent with the assumption that the Ly α line originates from interstellar absorption. As the H β emission line is one of the prominent emission features (van Paradijs & McClintock 1995) in the optical spectra of most LMXBs, the absence of hydrogen lines probably results from zero or very low hydrogen abundance in this ultra-compact LMXB. Thus our observations provide support for the theory that ultra-compact binaries must have H-depleted donors (Nelson et al. 1986).

As the companion star in 4U 1626–67 is probably a C-O or O-Ne white dwarf (Schulz et al. 2001), a question is raised as to what the abundance of helium is in this system. Homer et al. (2002) noted that the absence of He II $\lambda 1640$ emission line is a distinct feature of 4U 1626–67 by comparing its FUV spectrum to other

observed spectra of LMXBs. Quantitatively, Table 5 of Raymond (1993), which shows the observed FUV emission line fluxes, indicates that, for other LMXBs, the strength of the He II line is comparable to those of C IV, Si IV, or O V line, while numerical simulations of the atmosphere of X-ray heated accretion disks with using typical cosmic abundance also give the similar line strengths (Raymond 1993; Ko & Kallman 1994). As a result, a more interesting question is whether the observed N III lines in our optical spectra are produced by the BF mechanism or not, since He Ly α photons are the “seeds” for producing other Bowen lines. The absence of any Bowen O III lines seems to support this speculation (note that the NUV spectrum has a total exposure time of 10.8 ks), while the observed possible helium lines in the optical are against it. Motch & Pakull (1989) compared all the observed EW ratios of N III/C III to He II and argued that the EW ratio could be used as an indicator of metallicity of LMXBs. For 4U 1626–67, a limit of 3.6 on the EW ratio is estimated, and this value is located at the far right side of Figure 2 of Motch & Pakull (1989), thus making it a source distinct from other LMXBs. In order to further study the possibility of low helium abundance in 4U 1626–67, numerical simulations of X-ray heated accretion disks with the non-standard abundance set are needed.

Our optical observations also reveal several emission features which are as broad as 50 Å or more. Since each feature probably contains several emission lines, such as a C III/N III blend which may consist of N III λ 4634, N III λ 4641, 4642, and C III λ 4647, 4651, 4652, higher resolution spectroscopic observations are required to deblend the features. However, assuming a typical FWHM value of 2000 km s⁻¹ for emission lines obtained in the X-ray (Schulz et al. 2001) and FUV observations (Holmer et al. 2002), an optical emission line can be as broad as 30 Å. Therefore it is possible that we have observed the similar line broadening in the optical as in the X-ray and FUV, and this may imply that emission features in the optical originate from an accretion disk, as suggested in the X-ray and FUV.

Chapter 4

Optical Survey of Known and Suspected Ultracompact X-Ray Binaries

4.1 Introduction

Low-mass X-ray binaries (LMXBs) containing ordinary, hydrogen-rich mass donors have a minimum orbital period around 80 min (Paczynski & Sienkiewicz 1981; Rappaport, Joss, & Webbink 1982). However, systems with hydrogen-poor or degenerate donors can evolve to extraordinarily small binary separations, with orbital periods as short as a few minutes (Nelson, Rappaport, & Joss 1986). These so-called ultracompact binaries include three X-ray bursters (two in globular clusters), a classical X-ray pulsar, and three millisecond X-ray pulsars, spanning a range of orbital periods from 11 to 50 minutes. Besides these accreting neutron stars, there is also a related class among the accreting white dwarfs, the AM CVn binaries (see Warner 1995). Together, these systems represent extreme and exotic endpoints in binary and stellar evolution (see, e.g., Podsiadlowski, Rappaport, & Pfahl 2002). In all cases, the donor stars in these systems must have extremely low mass and be either hydrogen-depleted or degenerate (Nelson, Rappaport, & Joss 1986; Yungelson, Nelemans, &

van den Heuvel 2002).

Although these systems had initially been assumed to be relatively rare, the known number has doubled in the past few years. In addition, recent X-ray spectroscopic work has identified several more candidate ultracompact binaries on the basis of comparison to the known ultracompact LMXB 4U 1626–67, with low-mass, Ne-enriched C-O white dwarfs suggested as possible donors (Juett, Psaltis, & Chakrabarty 2001; Juett & Chakrabarty 2003). Candidates may also be identified through an unusually low optical-to-X-ray flux ratio (Deutsch, Margon, & Anderson 2000). In an effort to further study the known ultracompact systems and verify the proposed candidates, we have undertaken a systematic optical survey. In the following two sections, we report our spectroscopy of the LMXB 4U 0614+091, 4U 1543–624, and 4U 1916–05 and time-resolved photometry of the LMXBs 4U 1543–624 and 4U 1822–000, respectively.

All these X-ray sources were discovered by the *Uhuru* mission over thirty years ago (Giacconi et al. 1974). Among them, 4U 0614+091 ($l = 201^\circ$, $b = -3^\circ$) and 4U 1543–624 ($l = 322^\circ$, $b = -6^\circ$) were suggested as ultracompact systems with neon-rich degenerate donors based on their X-ray spectral features by Juett et al. (2001). Both of them have been extensively observed by a series of X-ray missions (Christian & Swank, 1997; Asai et al., 2000; Juett et al., 2001; Schultz, 2003; Farinelli et al., 2003; Juett & Chakrabarty, 2003), but these observations found no evidence for orbital modulation of the X-ray flux. The optical counterparts to 4U 0614+091 and 4U 1543–624 were identified by Murdin et al. (1974) and McClintock et al. (1978) respectively. Optical spectra show no lines of H or He and support the suggestion of C-O white dwarf donor (Davidsen et al., 1974; Machin et al., 1990; Nelemans et al., 2004).

The LMXB 4U 1916–05 ($l = 31^\circ$, $b = -8^\circ$) is a known ultracompact system with an orbital period of 50 min detected in the X-rays (White & Swank 1982; Walter et al. 1982) and a 50.46 min period in the optical (Grindlay et al. 1988; Schmidtke 1988). Further extensive studies (see, e.g., Callanan et al., 1995; Homer et al., 2001b) have established it as the first known neutron star X-ray binary superhump source (Retter

et al. 2002). No optical spectroscopy has been reported, probably due to its optical faintness, $V = 21.0$ (Grindlay et al. 1988; Schmidtke 1988).

The X-ray source 4U 1822–000 ($l = 30^\circ$, $b = +6^\circ$) has been less well studied. Its $V = 22$ optical counterpart was identified by Chevalier & Ilovaisky (1985). *Chandra* observations verify that the X-ray source is coincident with the optical position and show no evidence for orbital modulation of the X-ray flux (Juett & Chakrabarty 2004). We have identified the system as a candidate ultracompact system on the basis of its optical/X-ray flux ratio.

4.2 Spectroscopy of 4U 0614+091, 4U 1543–624, and 4U 1916–05

4.2.1 Observations and Data Reduction

Our optical observations were made with the 6.5-meter Baade/Magellan I telescope at Las Campanas Observatory. A Low-Dispersion Survey Spectrograph (LDSS-2) was used for all our observations, and the CCD detector used was SITe1. On 2002 April 8, a 9 min spectrum of 4U 0614+091 was obtained using a medium/blue dispersion grism, providing a spectral scale of $5.3 \text{ \AA pixel}^{-1}$ and a wavelength coverage of 3900–8500 \AA . We used a GG375 filter to block the second order contamination. A spectrophotometric standard star LTT 3218 was observed at the same time for flux calibration. On 2002 August 10, the observations of 4U 1543–624 and 4U 1916–053 were carried with using a high dispersion grism, providing a spectral scale of $2.4 \text{ \AA pixel}^{-1}$ and a wavelength coverage of 3900–6800 \AA . The exposure times for our targets are listed in Table 4.1 respectively. The standard star observed for flux calibration was EG 274. A long slit with a width of $1''.0$ was used for all our observations, and was oriented according to the parallactic angle for minimizing light losses due to differential refraction. A log of our observations is given in Table 4.1. In the table, we also include 4U 1626–67, since we refer to its spectral features a few times in this Chapter. This source is a known ultracompact LMXB, well studied by both the X-ray

Table 4.1. Log of Magellan Observations of Ultracompact X-ray Binaries

Source	Date	Grism	Wavelength coverage (Å)	Spectral scale (Å/pixel)	Exposure time (s)
4U 0614+091	2002 Apr 08	Medium/blue	3900-8500	5.3	540
4U 1543-624	2002 Aug 10	High	3900-6800	2.4	2×1800
4U 1626-67	2002 Aug 10	High	3900-6800	2.4	2100
4U 1916-053	2002 Aug 10	High	3900-6800	2.4	2×1200

and optical observations, and its spectrum was obtained with the same instrument setup during our 2002 August observing run.

We used the IRAF packages to reduce our data. The spectral images were bias-subtracted and flat-fielded, and the IRAF package `twodspec` was used to extract the spectra. The spectra were wavelength-calibrated by using He-Ne lamp spectra. However we found that the calibration for our April run suffered from a very large uncertainty by comparing with night sky lines (Osterbrock & Martel 1992). Thus we instead used the identified sky lines to wavelength-calibrate our spectrum of 4U 0614+091. We then used the respective sensitivity spectra, derived from the standard stars, to flux-calibrate the spectra. For 4U 1543-624 and 4U 1916-053, we derived their final spectra by averaging a couple of spectra with the same exposure time (see Table 4.1).

4.2.2 Common Spectral features

The spectra of our sources are shown in Figure 4-1. For comparison, we also show a spectrum of 4U 1626-67, which was taken using the LDSS-2 and has been reported in Chapter 3. As seen in the figure, the spectra look very similar and generally are featureless. Longward of 5000 Å, there are several absorption features due to atmospheric and interstellar absorption. No hydrogen lines, such as H α and H β lines, were detected. The upper limits on equivalent widths (EWs) of the H α and H β lines are given in Table 4.2. One broad emission feature near 4650 Å is seen in all our spectra. The blue region (4000-5000 Å) of the spectrum of 4U 0614+091 was very poorly wavelength-calibrated; however, by comparing it to the spectra reported by

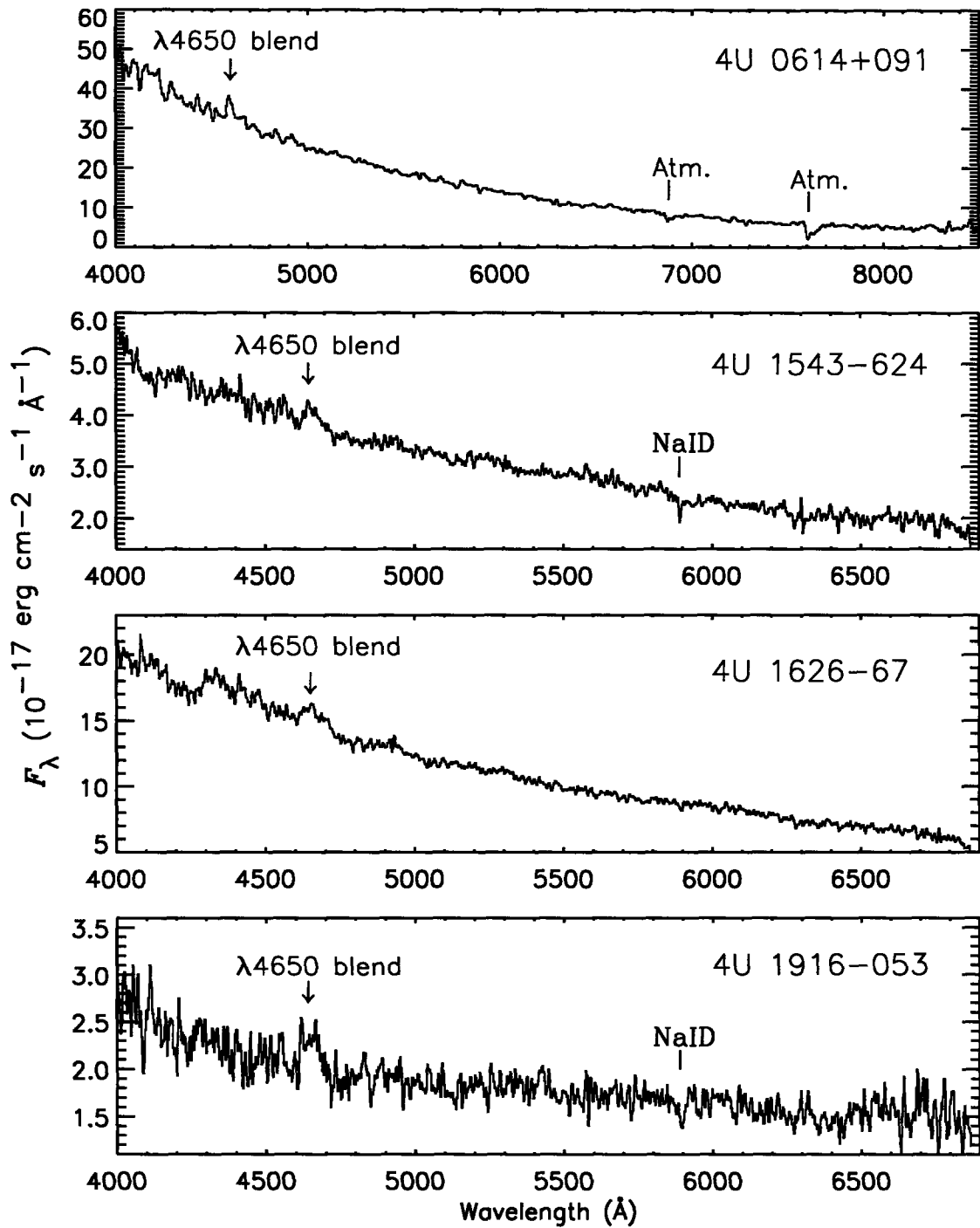


Figure 4-1 Spectra of ultracompact low-mass X-ray binaries. The indicated feature is C III/N III λ 4640-4650 \AA blend.

Table 4.2. Equivalent width measurements and 2σ upper limits (\AA) on H and He emission lines

Feature	4U 0614+091	4U 1543-624	1626-67	4U 1916-053	EXO 0748-676
He II $\lambda 4686$	$\lesssim 2.2$	$\lesssim 2.6$	$\lesssim 3.0$	$\lesssim 5.2$	5.5 ± 0.2
H β $\lambda 4861$	$\lesssim 2.0$	$\lesssim 1.8$	$\lesssim 2.0$	$\lesssim 5.2$	2.0 ± 0.2
H α $\lambda 6563$	$\lesssim 1.8$	$\lesssim 3.4$	$\lesssim 1.2$	$\lesssim 7.6$	5.9 ± 0.4

Table 4.3. Parameters of Gaussian fits to the $\lambda 4650$ feature

Source	EW (\AA)	Line flux (10^{-16} ergs $\text{cm}^{-2}\text{s}^{-1}$)	FWHM (km s^{-1})
4U 0614+091	5.26 ± 1.07	17.1 ± 3.5	1830 ± 429
4U 1543-624	8.59 ± 0.82	3.16 ± 0.30	3978 ± 459
4U 1626-67	4.15 ± 0.52	6.19 ± 0.77	3115 ± 478
4U 1916-053	23.3 ± 2.6	4.31 ± 0.48	5167 ± 728
EXO 0748-676	2.6 ± 0.2	...	1998 ± 263

Davidson et al. (1974) and Machin et al. (1990), we identified the peak (see Figure 4-1) in the spectrum as the $\lambda 4650$ blend. There may have other emission features between 4000-5000 \AA ; further high-resolution spectroscopic observations are required to identify them.

For 4U 0614+091, our spectrum is consistent with those given by Davidson et al. (1974) and Machin et al. (1990). An O I $\lambda 5577$ emission line was reported by Machin et al. (1990), but was not detected by our observation. We note that a same night sky line (Osterbrock & Martel 1992) coincides with the wavelength position. Further observations are needed to clarify.

Our spectra also show a lack of helium lines, especially the He II $\lambda 4686$ emission line. In the spectra, the He II $\lambda 4686$ regions are blended by the nearby $\lambda 4650$ features, not allowing accurate measurements of the upper limits of the He II lines (Table 4.2). However, Motch & Pakull (1989) compared the EWs of C III/N III blend and He II $\lambda 4686$ for 18 ordinary, H-rich LMXBs which have been spectroscopically studied, and

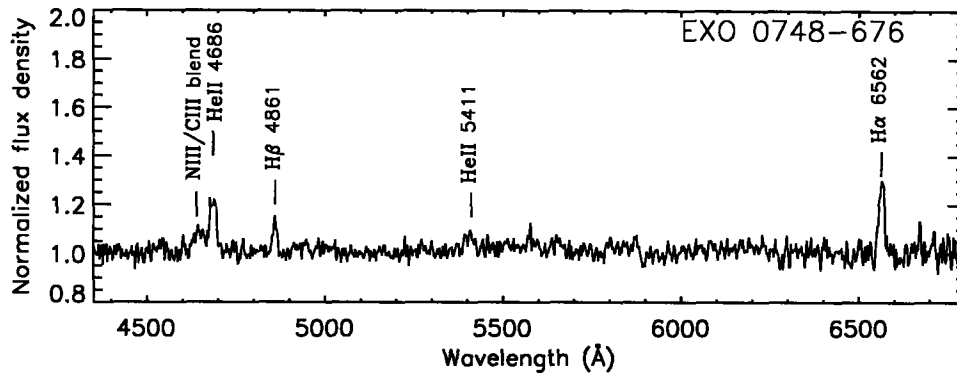


Figure 4-2 LDSS-2 spectrum of the LMXB EXO 0748–676. This spectrum shows typical strong hydrogen and helium emission lines detected from the spectra of an “ordinary” LMXB.

found that the EW ratios have a maximum value of 1.5. Thus for those LMXBs, the He II $\lambda 4686$ is comparable to or even stronger than the C III/N III blend. The absence or weakness of the He II $\lambda 4686$ line, especially compared to the $\lambda 4650$ blend, in the spectra is thus another feature to distinguish our sources from other LMXBs.

The emission feature around 4650 \AA is commonly seen in optical spectra of LMXBs (McClintock, Canizares, & Tarter 1975; van Paradijs & McClintock 1995) and probably consists of C III $\lambda\lambda 4647, 4651, 4652$, and N III $\lambda\lambda 4634, 4641, 4642$ (see, eg., Schachter, Filippenko, & Kahn 1989). The N III lines are generally considered to be produced by the Bowen fluorescence mechanism (Bowen 1934, 1935; McClintock, Canizares, & Tarter 1975). The $\lambda 4650$ blends in our spectra are not resolved while they are very broad. We fitted the features with a Gaussian profile, and the results are given in Table 4.3. We note that the EW value for 4U 0614+091 we obtained is consistent with the one reported by Machin et al. (1990).

Van Paradijs & McClintock (1995) have summarized the common prominent emission features in the optical spectra of LMXBs are $H\beta$, He II $\lambda 4686$, and C III/N III blend (van Paradijs & McClintock 1995). To illustrate these features more clearly, we show an LDSS-2 spectrum of a LMXB EXO 0748–676 in Figure 4-2 (also see Table 4.2 and 4.3 for measurements of its emission features). This binary has a 3.82 hour orbital period, and it probably contains a $0.45 M_{\odot}$ low-mass companion

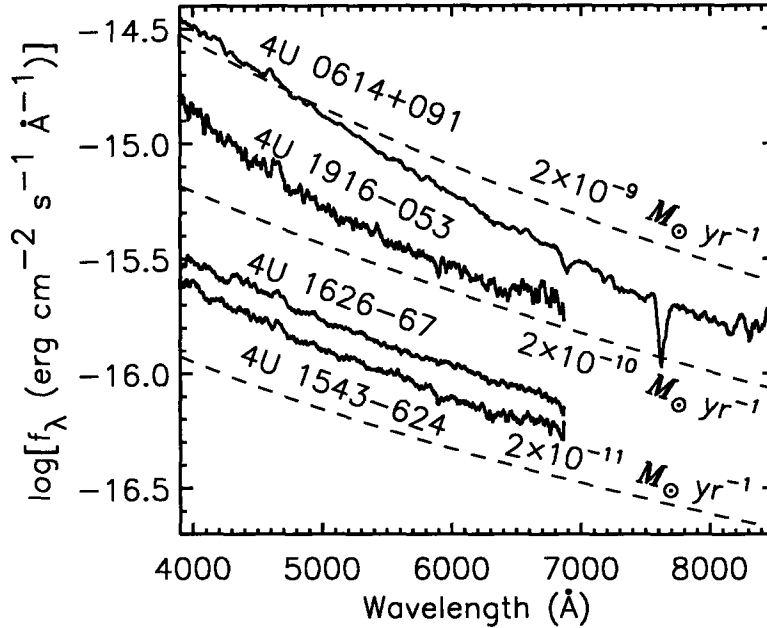


Figure 4-3 Dereddened and corrected spectra of ultracompact low-mass X-ray binaries. The dashed lines are spectra produced by an X-ray heated accretion disk with different mass accretion rate at a distance of 3 kpc.

(Parmar et al. 1986). The differences in the spectra between this LMXB and our ultracompact sources are obvious. The absence of hydrogen lines and a strong He II $\lambda 4686$ line distinguishes our sources from this typical LMXB. As 4U 1626-67 and 4U 1916-053 are known ultracompact binaries, the similarities between the spectra of our sources thus strongly suggest that 4U 0614+091 and 4U 1543-624 are also ultracompact LMXBs. In addition, the absence of hydrogen lines is consistent with the spectral features found in the AM CVn stars and the theoretical prediction that the mass donors in ultracompact binaries must be H-depleted.

4.2.3 Discussion

The optical emission from an ultracompact LMXB should be dominated by the emission from the accretion disk in this binary system. This is supported by the lack of stellar features in our spectra. We have also found that the composite spectrum

(1150-9000 Å) of 4U 1626–67 can be well fitted by an X-ray heated accretion disk (see 3.4). No attempt was made to fit the spectra due to uncertainties in the reddening, distance, and mass accretion rate of each source. However, we plot our spectra together in Figure 4-3 to show the similarity in general shape among the spectra of our sources. The spectra have been dereddened by using the approximate $E(B-V)$ values for each source as well as corrected for their inclination angles. The values we use are $E(B-V) = 0.3$ for 4U 0614+091 (Machin et al. 1990), $E(B-V) = 0.2$ for 4U 1543–624 (van Paradijs et al. 1986; Juett & Chakrabarty 2002), $E(B-V) = 0.1$ for 4U 1626–67, and $E(B-V) = 0.7$ for 4U 1916–053 (Schmidtke 1988). An inclination angle of 60° is assumed for 4U 0614+091 and 4U 1543–624, 0° for 4U 1626–67 (Schulz et al. 2001), and 70° for 4U 1916–053 (Smale et al. 1988). For comparison, we also plot the spectra emitted from an X-ray heated accretion disk with different mass accretion rates in an ultracompact LMXB (Arons & King 1993; Chakrabarty 1988) at a distance of 3 kpc. This distance is the upper limit for 4U 0614+091 (Brandt et al. 1992). As we can see, the general shapes of our spectra are consistent with the spectra emitted by the accretion disk model.

In conclusion, we have obtained very similar optical spectra from the known and candidate ultracompact LMXB systems. They all lack hydrogen lines, such as strong $H\alpha$ and $H\beta$ emission lines commonly seen in the optical spectra of ordinary LMXBs, and strong helium lines, especially the He II $\lambda 4686$ emission line, and show a broad emission feature near 4650 Å. The similarities shown in the spectra strongly suggest that 4U 0614+091 and 4U 1543–624 are also ultracompact binaries. Besides, one common feature, the absence of hydrogen lines, is consistent with the spectral features found in AM CVn stars and theoretical predictions. Therefore our spectroscopic observations suggest that optical spectroscopy may be used to identify ultracompact binaries based on the common features we have identified. Other known ultracompact LMXBs as well as candidates, such as 2S 0918–549 (Juett et al., 2001), should be targets to further test our suggestion.

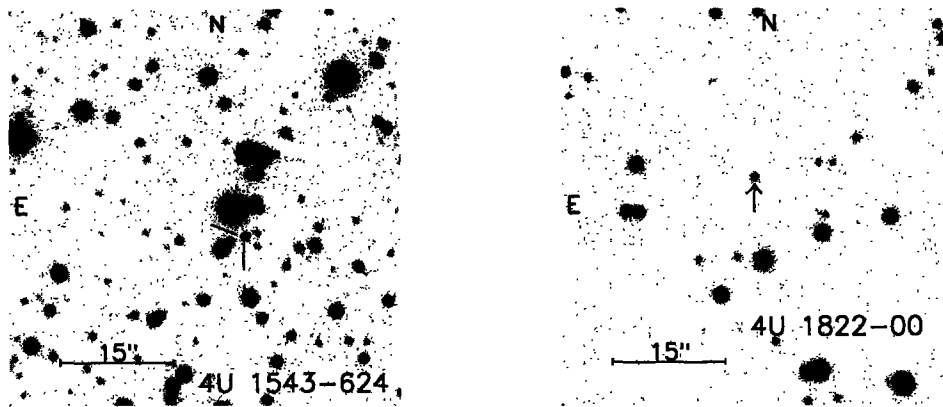


Figure 4-4 Sloan r' -band images of the fields containing 4U 1543–624 and 4U 1822–000 with their optical counterparts indicated ($r' \approx 20.4$ and 21.6 , respectively).

4.3 Time-resolved Optical Photometry of the LMXB 4U 1543–624 and 4U 1822–000

4.3.1 Observations and Data Reduction

Our optical photometric observations were made on 2003 August 2–4 using the 6.5-meter Clay/Magellan II telescope at Las Campanas Observatory in Chile. The detector was the Raymond and Beverly Sackler Magellan Instant Camera (MagIC), a 2048×2048 pixel CCD camera providing a $0''.069 \text{ pixel}^{-1}$ plate scale and a $142''$ field of view at the $f/11$ focus of the telescope. A Sloan r' filter (Fukugita et al. 1996) was used for our observations. The total observation time spanned approximately 100 min on August 2 for 4U 1822–000 with 99 CCD image frames of the targeted field taken, and 140 min on August 3 for 4U 1543–624 with 137 frames taken. The exposure time of each individual frame was 30 seconds for both targets. Since the readout time of MagIC is 20 seconds, we obtained approximately one image per minute over the course of our observations. The telescope position was dithered $5''$ once every 20 minutes during the observations. The conditions during our observations on August 2 were excellent, with $0''.6$ seeing. On August 3, the conditions were windy, with the

seeing varying over a range of $0''.6$ – $1''.0$. In addition to our science targets, the Sloan photometric standard star G 93-48 (Smith et al. 2002) was observed on August 3 for flux calibration of 4U 1543–624. A few images of both science targets were obtained on August 4, allowing us to extend our photometric calibration to 4U 1822–000 as well. In Figure 4-4, we show finder images of our two fields.

We used the IRAF analysis package for our initial data reduction, including bias subtraction and flat fielding. We then used DOHPOT (Schechter, Mateo, & Saha 1993), a point-spread function fitting photometry program, to measure brightnesses of our target and other in-field stars. In order to eliminate any systematic offsets, we used differential photometry for our timing analysis; the brightness of our targets were calculated relative to an ensemble of bright, non-variable stars in the images.

4.3.2 Results

The light curve for 4U 1543–624 is shown in the top panel of Figure 4.3.1. The average magnitude was $r' = 20.42 \pm 0.03$. However, a periodic modulation with a semiamplitude of around 0.1 magnitudes is also clearly visible. For comparison, the light curve of a check star of similar brightness in the same field is also shown. The standard deviation of the brightness of this check star is only 0.026 magnitudes, which shows that the light curve variation of our target is highly significant. We made an initial estimate of the modulation period by interpolating the data into an evenly-sampled time series and using a Fourier spectral analysis, which indicated that the modulation was periodic and essentially sinusoidal. We refined our measurement using an epoch-folding search technique on the uninterpolated data (Leahy et al. 1983) to determine a period of 18.2 ± 0.1 minutes. A plot of the data folded on this period is shown in Figure 4-6, along with the best-fit sinusoid with a semiamplitude of 0.081 ± 0.002 magnitudes. The topocentric time of phase zero (maximum brightness) was UT 2003 August 3 00:44:20, corresponding to August 3 00:48:32 (TDB) at the solar system barycenter, with an uncertainty of 66 seconds.

In the bottom panel of Figure 4.3.1, we show the light curve of 4U 1822–000. The average magnitude was $r' = 21.58 \pm 0.08$. However, the target brightness is clearly

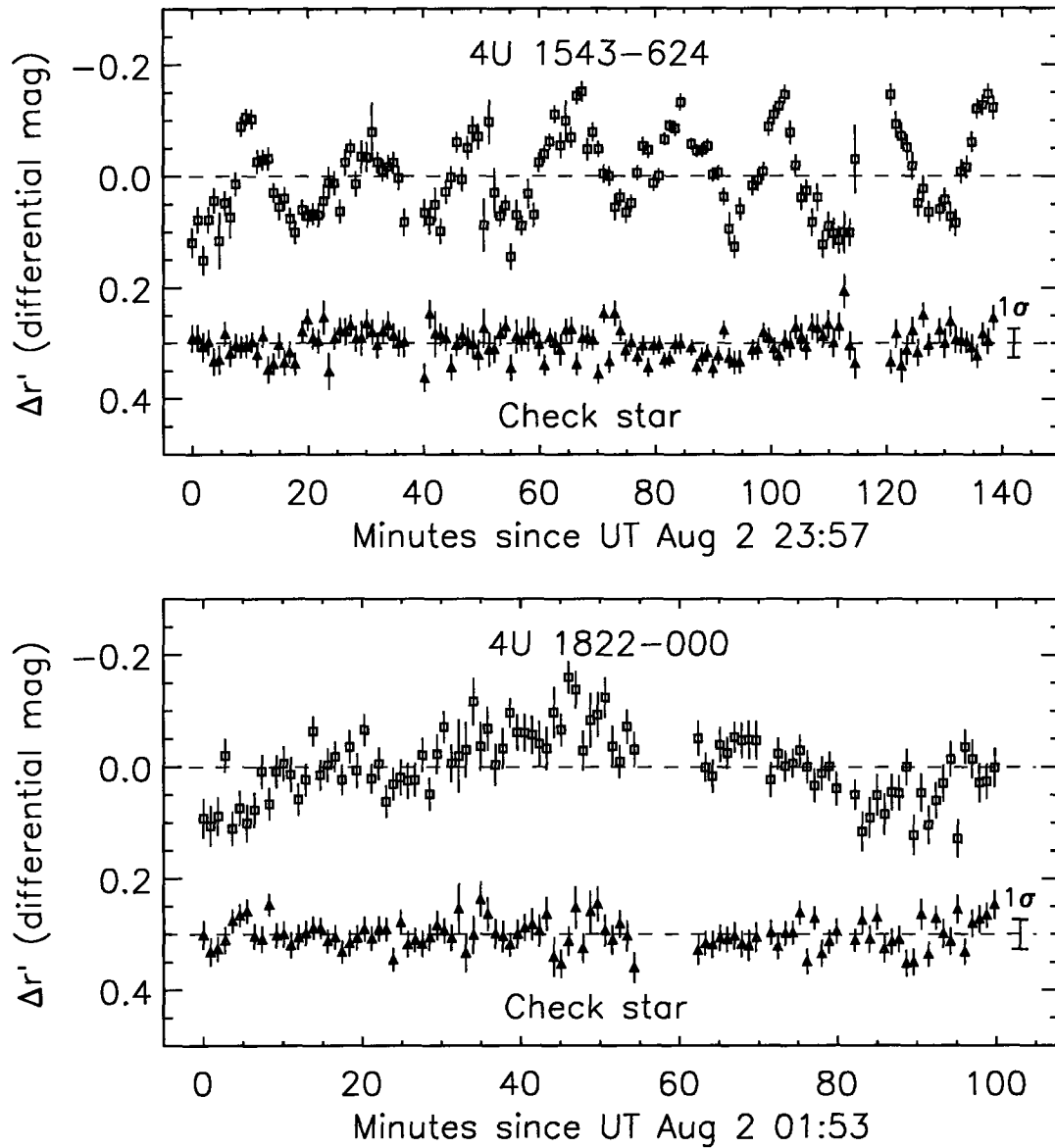


Figure 4-5 Light curves of 4U 1543-624 and 4U 1822-000 in the r' band. The light curves for nearby comparison stars with comparable brightness are also shown. A periodic modulation is clearly visible in the light curve of 4U 1543-624. The brightness of 4U 1822-000 varies significantly over the observation. The average magnitudes were $r' = 20.42 \pm 0.03$ for 4U 1543-624 and $r' = 21.58 \pm 0.08$ for 4U 1822-000.

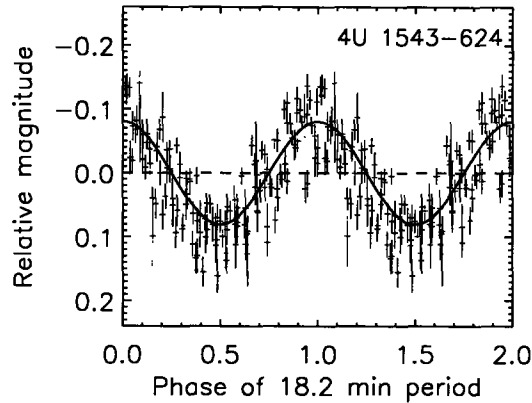


Figure 4-6 The r' band photometric data for 4U 1543–624 folded on the 18.2 min period. Phase zero is chosen to be of maximum brightness. Two cycles are displayed for clarity. The best fitting sinusoid is plotted as the solid curve.

varying systematically by a few tenths of a magnitude over the 100 min observation. These changes are quite significant compared to the 0.027 magnitude scatter observed in nearby check star. The variability could possibly be due to a ~ 90 min periodicity, but our data span is insufficient to determine this.

4.3.3 Discussion

We have found an 18.2 min periodicity in the optical light curve of 4U 1543–624. Since the modulation appears to be coherent, this is almost certainly the orbital period of the binary, verifying its ultracompact nature. This is the second shortest orbital period for an LMXB, after the 11-minute binary 4U 1820–30 (Stella, Priedhorsky, & White 1987). We note that this discovery bolsters the earlier suggestion of 4U 0614+091 and 2S 0918–549 as ultracompact binaries on the basis of X-ray and optical evidence (Juett et al. 2001; Juett & Chakrabarty 2003; Nelemans et al. 2004; Wang & Chakrabarty 2004).

Sinusoidal modulation of the optical light curve for LMXBs generally arises from X-ray heating of the companion star by the central X-ray source in a relatively low-inclination ($i < 60^\circ$) binary (see van Paradijs & McClintock 1995), with the visible

area of the heated face varying as a function of orbital phase, and the superior conjunction of the companion star corresponding to the observed brightness maximum of the light curve. For sufficiently low binary inclinations, blockage by the accretion disk does not occur, resulting in a sinusoidal profile. A possible alternative explanation is that the 18.2 min variation is a superhump oscillation (see Warner 1995 for a review). Superhumps are observed as optical photometric modulations in cataclysmic variables and LMXBs at periods a few percent longer than the binary period. These oscillations, which occur only in binaries with extreme mass ratios (like ultracompact binaries), are understood to arise because of an orbital resonance condition that leads to a precessing, eccentric accretion disk (Whitehurst 1988; Whitehurst & King 1991; Lubow 1991). Without an independent determination of the binary period from, e.g., X-ray variability or Doppler line measurements, we cannot definitively distinguish between these possibilities. In either case, however, 4U 1543–624 certainly has an orbital period around 18 min.

As an ultracompact binary, 4U 1543–624 must contain a hydrogen-depleted and degenerate donor resulting from the evolution of either an evolved main-sequence star+neutron star binary or a white dwarf+neutron star binary (see Nelson & Rappaport 2003 and references therein for a recent discussion of evolutionary scenarios for ultracompact binaries). Indeed, based on both X-ray (Juett et al. 2001; Juett & Chakrabarty 2003) and optical measurements (Nelemans et al. 2004; this chapter), it has been suggested that the donor is a low-mass C-O white dwarf. If so, we can use our orbital period measurement to estimate the mass and radius of the donor. Since the mean density of a Roche-lobe-filling companion is determined by the binary period, our 18 min period defines a mass-radius relation for the companion, shown as the solid curve in Figure 4-7. (In the absence of a measured mass function for the binary, the allowed curve extends down to $M_2 = 0$.) In comparing this to stellar models, we note that recent studies of three millisecond pulsars in ultracompact LMXBs have shown that the extremely low-mass white dwarf donors in such systems may be thermally bloated compared to cold stars, affecting their M - R relation (Bildsten 2000; Deloye & Bildsten 2003; Nelson & Rappaport 2003). For comparison,

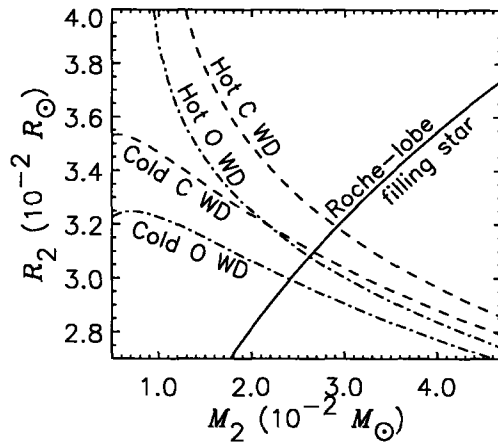


Figure 4-7 Mass-radius constraints for the companion star in 4U 1543–624. The solid curve is the M - R relation for a Roche-lobe-filling donor in an 18.2 min binary. Also shown are the model curves for low-mass carbon (dashed lines) and oxygen (dot-dashed lines) white dwarfs for both cold (10^4 K) and hot (3×10^6 K) core temperatures, taken from Deloye & Bildsten (2003). The donor must have a mass in the 0.025 – $0.03 M_{\odot}$ range with a radius around $0.03 R_{\odot}$.

Figure 4 also shows both cold and hot solutions for pure C and O white dwarfs from the models of Deloye & Bildsten (2003). For a Roche-lobe-filling donor, a mass in the 0.025 – $0.03 M_{\odot}$ range and a radius around $0.03 R_{\odot}$ is indicated. Since mass transfer in an ultracompact binary is driven by gravitational radiation, this mass estimate implies a mass transfer rate of

$$\dot{M} \approx 5.5 \times 10^{-10} M_{\odot} \text{ yr}^{-1} \left(\frac{M_1}{1.4 M_{\odot}} \right)^{2/3} \left(\frac{M_2}{0.03 M_{\odot}} \right)^2 \left(\frac{P_{\text{orb}}}{18.2 \text{ min}} \right)^{-8/3},$$

where M_1 is the mass of the compact primary, M_2 is the mass of the white dwarf donor, and P_{orb} is the binary period. Given the measured unabsorbed 0.5–10 keV X-ray flux of $\simeq 1 \times 10^{-9} \text{ erg cm}^{-2} \text{ s}^{-1}$ (Juett & Chakrabarty 2003), this suggests a source distance of $\simeq 7 \text{ kpc}$.

The ~ 90 min optical variability of 4U 1822–000 is also suggestive of a periodicity, in which case it may also provide a binary period, but a considerably longer observation will be necessary to test this. Indeed, the variability might not be periodic at

all, but could instead be only quasiperiodic or even stochastic. Strong ~ 15 min optical/UV quasiperiodic oscillations were previously detected in the 42 min ultracompact LMXB 4U 1626–67 (Chakrabarty et al. 2001), showing that photometric variability in ultracompact binaries need not only occur near the orbital period. Again, only an observation long enough to contain many modulation cycles can distinguish between a periodic and a quasiperiodic oscillation (or stochastic variability) and allow a secure measurement of its time scale.

Chapter 5

The Ultracompact X-ray Binary 4U 1820–30: Superhumper or Hierarchical Triple?

5.1 Introduction

The low-mass X-ray binary 4U 1820–30, which consists of an accreting neutron star and a Roch-lobe filling low-mass secondary, has been extensively studied since it has the shortest orbital period, $P_{\text{orb}} = 685$ s, among the known LMXBs (Stella, Friedhorsky, & White 1987; Smale, Mason, & Mukai 1987; Morgan, Remillard, & Garcia 1988; Sansom et al. 1989; Tan et al. 1991; van der Klis et al. 1993; Chou & Grindlay 2001). This period is indicated by a low amplitude X-ray flux modulation ($\sim 3\%$), and suggests that the companion star in this binary is probably a $0.06\text{--}0.08 M_{\odot}$, hydrogen-exhausted white dwarf (Rappaport et al. 1987). The ultraviolet (UV) observations (in the wavelength range $1265\text{--}2510 \text{ \AA}$), made with the *HST*, also revealed a periodic modulation with a 16% amplitude (Anderson et al. 1997). The reported UV period is 687.6 ± 2.4 s, and may reflect the orbital period if the modulation is assumed to arise from the X-ray heating of the secondary star (Arons & King 1993). This X-ray source is near the center of the globular cluster (GC) NGC 6624 (Grindlay

et al. 1984). The X-ray observations over the past three decades have found that it has a negative orbital period derivative of $\dot{P}/P \approx -3.5 \times 10^{-8} \text{ yr}^{-1}$ (van der Klis et al. 1993; Tan et al. 1991; Chou & Grindlay 2001).

In addition, a long-term modulation with a period of about 171 days has been detected (Priedhorsky & Terrell 1984; Chou & Grindlay 2001). It has been suggested that this long-term modulation indicates that this source is a hierarchical triple system (Grindlay 1988; Chou & Grindlay 2001). The inner binary would have an orbital period of $P_{\text{inner}} = 685 \text{ s}$ while a third companion, orbiting the inner system with a period of $P_{\text{outer}} \sim 1 \text{ day}$, induces the inner binary eccentricity variation with the 171 day period. The variation makes the mass accretion rate as well as the X-ray luminosity of this source modulated with the same period.

In this chapter, we report the detection of a period, about 1% longer than the X-ray period, from the far-ultraviolet (FUV) observations of 4U 1820–30. This FUV period is approximately consistent with the triple system model (Grindlay 1988). One of the two periods, either the X-ray or FUV, is P_{inner} while the other one is the beat period between P_{inner} and P_{outer} . However, a similar source, the LMXB 4U 1916–05 which has an optical period of 50.46 min and an X-ray period of 50.00 min (see, e.g., Retter et al. 2002 for a review), reminds us that the period difference between the X-ray and FUV probably indicates superhumps in 4U 1820–30. Recently it was verified that 4U 1916–05 is a superhump source by the detection of negative superhumps by the X-ray observations (Retter et al. 2002). We further note that a long term modulation (199 day; Priedhorsky & Terrell 1984; Smale & Lochner 1992) in the X-ray light curve of 4U 1916–05 has also been reported, although recently Homer et al. (2001) only found a likely 83 day modulation. Due to the similarities between these two sources, we thus propose a superhump model for 4U 1820–30.

Superhumps are periodic modulations observed in binary systems with periods a few percent longer than the orbital periods. This phenomenon was first discovered in super-outbursts of the SU UMa Dwarf Novae (Vogt 1974; Warner 1975), and since then, it has been commonly detected in short-period cataclysmic variables (Patterson 1998). It is now believed that superhumps arise from an elliptical accretion disk,

which is developed when the disk extends beyond a resonance radius and precesses in the inertial frame due to the tidal force of the secondary star (e.g. Whitehurst & King 1991). The resonance requires the condition that the mass ratio of a secondary to a primary $q \lesssim 0.33$ (Whitehurst & King 1991), and this condition has been proven to also work for X-ray binaries as superhumps have been detected in both black hole soft X-ray transients (SXTs; O'Donoghue & Charles 1996) and neutron star LMXB 4U 1916–053 and GX 9+9 (Haswell et al. 2001). Indeed, Haswell et al. (2001) have further suggested that neutron star LMXBs with orbital period below ~ 4.2 hr are potential superhump sources with the superhump modulation reflecting the area changes of an X-ray irradiated accretion disk over the course of superhump cycles.

5.2 Observations and Data Reduction

The *HST* observations were made on 1998 March 14 using the Space Telescope Imaging Spectrograph (STIS; Woodgate et al. 1998). A low-resolution grating G140L was used, providing a FUV wavelength coverage of 1150–1730 Å. The aperture was a $52'' \times 0'.5$ long slit. The data were taken in TIME-TAG mode with using the solar-blind CsI multi-anode microchannel array (STIS/FUV-MAMA) detector. The TIME-TAG mode allows us to record the position and detection time of every photon, and the timing precision is 125 microsecond. We extracted the data from the *HST* archive service. The datasets consist of five exposures with a total exposure time of about 12.1 ks. Except the first dataset which has a short exposure time of 1830 s, the other four each has an exposure time of 2580 s. The total time span was $T_s \approx 24.7$ ks.

The data were first corrected for the barycenter arrival times. The IRAF task `odelaytime` in the *HST* calibration package STIS was used. The *HST* ephemeris (ORX) file at the observation time was obtained using the Starview program.¹ Photons within the spectra position range in the STIS images were selected except those of Ly α $\lambda 1216$ Å line, which are due to strong geocoronal emission. The light curve of the data is shown in Figure 5-1. For clarity, the data points were binned in 16 s time

¹see <http://starview.stsci.edu/html/>

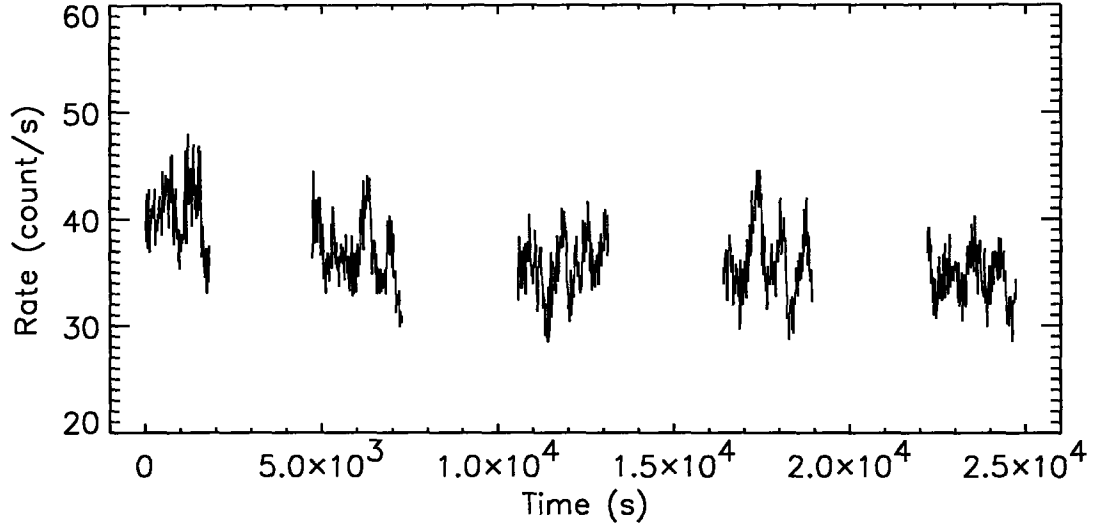


Figure 5-1 FUV light curve of 4U 1820–30. The data points were selected photons binned in 16 s time intervals.

intervals.

5.3 Period Determination

We first used an epoch-folding technique (Leahy et al. 1983) to search for periodicity with the data folded to 10 phase bins per period. The result of χ^2 period searching is shown in Figure 5-2, and clearly indicates the detection of the periodicity with a period $P = 690.3$ s. This period is 5.3 s longer than the 685 s X-ray period. However, based on the epoch-folding technique, the frequency spacing used in the search was $1/2T_s = 2.02 \times 10^{-5}$ Hz. This corresponds to a temporal spacing of 9.6 s near 690 s, which is too coarse to determine if the period difference between the FUV and X-ray is significant. Therefore the period resolution is not high enough to resolve the period difference because of the limited time span.

In order to obtain the period more accurately, we 10 times over-sampled our data and used a discrete Fourier transform technique to construct an overresolved power spectrum (Chakarbarty 1998). The original data were binned evenly in 1 s time inter-

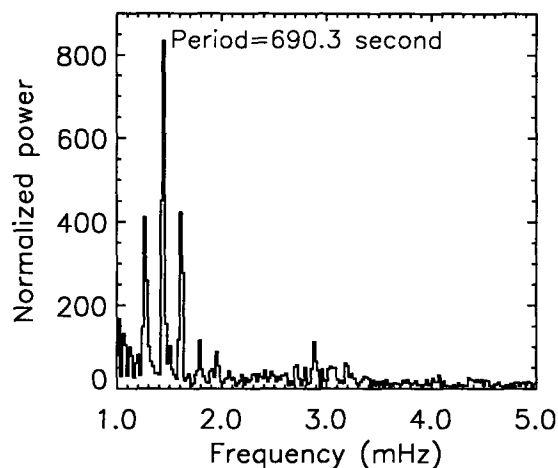


Figure 5-2 Result of χ^2 folded period searching. A period of 690.3 s is detected. Two major sidebands are artifacts due to the observation gaps.

vals for the Fourier transform. Figure 5.3 shows the overresolved power spectrum in the vicinity of the main power peak. We fitted the peak with a Gaussian to obtain the peak frequency, $f = 1.44407$ mHz, corresponding to a period of 692.5 s. The uncertainty of the peak frequency is 0.0021 mHz (Ransom, Eikenberry, Middleditch 2002), corresponding to $\sigma_P = 1.1$ s. Although this uncertainty value probably represents the theoretical best we are able to obtain from our data, it helps indicate that the period difference between the FUV and X-ray is at about $7\sigma_P$ confidence.

In Figure 5-4, we show the folded light curves, made in the same way as the UV light curve reported by Anderson et al. (1997) for direct comparison, with the 692.5 s period and with the X-ray period. As can be seen, neither of them has a sinusoidal shape. However, it is clear that the FUV data cannot be folded nicely with the X-ray period. There are four phase bins forming a flat bottom with a 4% amplitude (from average to bottom). The 692.5 s light curve is different from the reported UV light curve (Anderson et al. 1997), which has a smooth sinusoidal shape. The semi-amplitude is about 6%, similar to yet 2% smaller than the amplitude value Anderson et al. (1997) reported. We note that the time spans of both our data were approximately equal, while their wavelength coverage was between 1265-2510 Å, 2

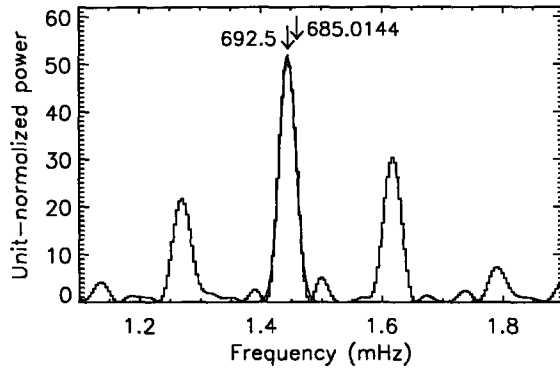


Figure 5-3 A 10 times overresolved power spectrum in the vicinity of the main power peak resulted from the Fourier transform. Two major sidebands are artifacts due to the observation gaps. The fitting of the peak with a Gaussian profile gives a period of 692.50 s.

times wider than ours and their observations were made in 1996, two years earlier than our data. Thus the light curve differences may be due to the intrinsic variations of the source in the UV as well as different wavelength coverages.

5.4 Discussion

The X-ray observations have consistently obtained the 685 s period over the past decades, and thus it is convincingly believed that the X-ray period is the orbital period of 4U 1820–30. We note that the negative X-ray period derivative not only implies a decrease of the period as a function of time, but also is too small ($\Delta P \sim 0.03 \text{ ms yr}^{-1}$) to account for any period changes comparable to the 7.5 s difference between the X-ray and FUV periods. On the other hand, as the X-ray periodic modulation is probably caused by the occultation by a bulge near the impact point where the mass transfer stream hits the accretion disk (Stella et al. 1987), the low modulation amplitude ($\sim 3\%$) probably indicates a lower inclination. Assuming that the UV/optical modulation is due to X-ray heating of the companion star, the resulting light curve of a LMXB with low inclination is typically a sinusoid (see, e.g., van Paradijs & McClintock 1995 for a review). Using this model (see Arons & King 1993), Anderson et

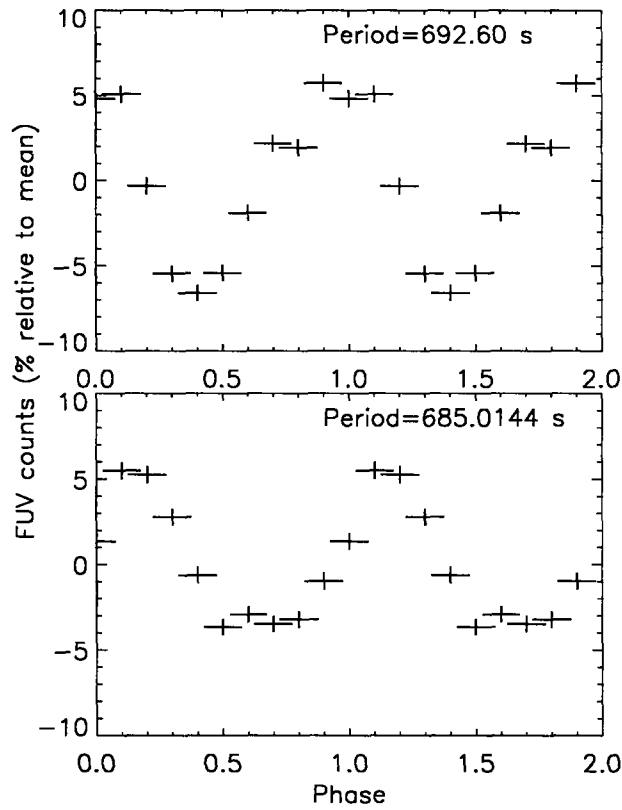


Figure 5-4 Folded light curves with the FUV period 692.50 s (*top*) and the X-ray period 685.0144 s (*bottom*). The error bars indicate the standard deviations in phase bins (horizontal) and counts (vertical). For clarity, two cycles are displayed.

al. (1997) actually found the inclination of 4U 1820–30, $i \approx 43^\circ \pm 9^\circ$. However, as we have shown in Figure 5-4, the folded light curve with the X-ray period (or the orbital period) is significantly different from a sinusoid. This provides additional evidence supporting the idea that we have detected a different periodicity in the FUV light curve than the orbital periodicity.

The existence of the FUV period, about 1% longer than the orbital period, is consistent with the scenario of 4U 1820–30 being a triple system (Grindlay 1988). The FUV period is the beat period between P_{inner} and P_{outer} . This model naturally explains the observed 171 day modulation as that caused by the inner binary eccentricity variation with a period of $P_{\text{long}} \sim P_{\text{outer}}^2/P_{\text{inner}}$ (Mazeh & Shaham 1979; Chou & Grindlay 2001). Numerical simulations also suggest that a few percent of binaries in a GC could be triple systems due to binary-binary encounters (see, e.g., McMillan et al. 1991) with observational evidence that one triple system, PSR B1620–26 in the GC M4, has been identified as one neutron star and white dwarf inner binary with a substellar mass third companion (Sigurdsson et al., 2003).

However, given the similarities between 4U 1820–30 and 4U 1916–053, 4U 1820–30 could also be a superhump source with the X-ray and FUV periods being the orbital period P_{orb} and the superhump period P_{sh} respectively. Its superhump excess is $\epsilon = (P_{\text{sh}} - P_{\text{orb}})/P_{\text{orb}} \approx 0.011$, similar to those found for 4U 1916–053 (e.g. Haswell et al. 2001) and SXTs (O’Donoghue & Charles 1996). We may estimate the mass ratio q using a relation between the superhump excess and mass ratio (Patterson 2001), $q = 0.051$ for $\epsilon \approx 0.011$. Assuming the standard neutron star mass $M_1 = 1.4 M_\odot$, the mass ratio corresponds to a companion mass $M_2 \approx 0.071 M_\odot$. This value is consistent with the mass range in a standard scenario derived for 4U 1820–20 (Rappaport et al. (1987).

According to the superhump model, the period difference between the X-ray and FUV indicates an accretion disk precessing with a period $P_{\text{prec}} = (1/P_{\text{orb}} - 1/P_{\text{sh}})^{-1} \approx 0.7$ day. This period should be searched by further X-ray observations, as a 3.9 day beat period between the X-ray and optical periods has been found in the X-ray light curve of 4U 1916–05 (Chou et al. 2001; Homer et al. 2001). However, we note that

the triple system model also predicts that the third companion has an orbital period $P_{\text{outer}} \sim 1$ day (Chou & Grindlay 2001). Thus, an accurate measurement of the FUV period would help identify if 4U 1820–30 is a superhump source or not. The triple system model predicts $P_{\text{long}} = KP_{\text{outer}}^2/P_{\text{inner}}$, where K is a constant of order unity (Mazeh & Shaham 1979). It would be possible to test if P_{outer} , derived from the FUV period, is consistent with the $P_{\text{long}} = 171$ day modulation or not.

The long term 171-d modulation may be due to the nodal precession of a warped accretion disk. If 4U 1820–30 is a superhump source, both the 171-d and 692-s periodicities are related to the accretion disk. Correlations between them may exist and be detectable. Thus, further timing observations at different phases of the 171-d modulation should be made, in searching for correlations and identifying whether the FUV periodicity originates from the accretion disk or not.

Finally, in a standard scenario with mass transfer driven by gravitational radiation, a positive orbital period derivative for 4U 1820–30 is expected (Rappaport et al. 1987). The observed negative period derivative has been a puzzling feature for this source (Chou & Grindlay 2001). We note that the precession of an elliptical accretion disk, existing in the superhump model, may be responsible for this. Indeed it was suggested by van der Klis et al. (1993) that, if the azimuth of the impact point in the disk varies due to the precession, the phase of the observed X-ray light curve is shifted and thus there may not be any changes for the true orbital period.

Chapter 6

The Optical Counterpart of the Accreting Millisecond Pulsar SAX J1808.4–3658 in Outburst

6.1 Introduction

It is generally believed that millisecond radio pulsars are formed during sustained mass transfer onto neutron stars in X-ray binaries (e.g., Alpar et al. 1982; Joss & Rappaport 1983). The X-ray transient SAX J1808.4–3658 ($l = 355.4^\circ$, $b = -8.1^\circ$) was discovered in 1996 September by the *BeppoSAX* Wide Field Cameras during a ~ 20 day transient outburst (in 't Zand et al. 1998). Based on the detection of Eddington-limited thermonuclear X-ray bursts during these observations, the source distance is estimated to be 2.5 kpc (in 't Zand et al. 2001). A second source outburst was detected with the *Rossi X-ray Timing Explorer (RXTE)* in 1998 April (Marshall 1998). Timing analysis of the 2–30 keV *RXTE* data revealed the presence of a 401 Hz pulsar in a 2-hr binary with a low-mass companion (Wijnands & van der Klis 1998; Chakrabarty & Morgan 1998).

Shortly after the initial *RXTE* detection of the 1998 X-ray outburst, we observed a $V \approx 16$ star located 19 arcsec from the center of the *BeppoSAX* error circle; this

star was not present on the Digitized Sky Survey image of the field to a limiting magnitude of $V \gtrsim 19$, leading to its identification as the optical counterpart of SAX J1808.4–3658 (Roche et al. 1998). The optical intensity of this source faded as the X-ray source declined, and a 2-hr orbital modulation was marginally detected in the optical flux (Giles, Hill, & Greenhill 1999). This 2-hr optical modulation was subsequently confirmed in observations during quiescence (Homer et al. 2001). The optical counterpart has been designated V4580 Sagittarii (Kazarovets, Samus, & Durlevich 2000). In this chapter, we report on optical/IR photometry obtained during the 1998 outburst.

6.2 Observations

Tariq Shahbaz (at Instituto de Astrofísica de Canarias, Spain) helped us obtain multi-band optical photometry of the SAX J1808.4–3658 field at several epochs during the 1998 X-ray outburst using the $f/15$ Cassegrain CCD imager on the 1-m Jacobus Kapteyn Telescope (JKT) at the Observatorio del Roque de los Muchachos, La Palma, Canary Islands, Spain. Additional optical observations were obtained at various epochs during the outburst using the Keck 10-m telescope in Mauna Kea, Hawaii; the 3.5-m New Technology Telescope (NTT) at the European Southern Observatory (ESO) in La Silla, Chile; and the 1.9-m telescope at the South African Astronomical Observatory. Infrared photometry was also obtained at several epochs using the 3.8-m United Kingdom Infrared Telescope (UKIRT). A summary of these observations is given in Table 1. For completeness, we have also included the photometry obtained by other groups as well (Giles et al. 1999; Percival et al. 1998; Homer et al. 2001).

6.3 Results

The V -band flux history is shown in Figure 1, along with the X-ray flux history measured by the *RXTE* Proportional Counter Array (PCA; Gilfanov et al. 1998).

Table 6.1. Optical/IR Photometry of SAX J1808.4–3658^a

UT Date	MJD	Telescope	Magnitudes							Ref.
			B	V	R	I	J	H	K	
1998 Apr 16.6	50919.6	Keck 10-m	16.19(3)	1	
1998 Apr 18.2	50921.2	JKT 1-m	...	16.51(9)	16.19(15)	15.89(13)	1	
1998 Apr 18.6	50921.6	UKIRT 3.8-m	15.06(2)	14.34(1)	1	
1998 Apr 18.7	50921.7	Mt. Canopus 1-m	...	16.72	...	16.11(5)	2	
1998 Apr 22.7	50925.7	Mt. Canopus 1-m	...	16.77	2	
1998 Apr 24.2	50927.2	JKT 1-m	17.43(10)	17.12(7)	16.82(6)	16.50(8)	1	
1998 Apr 27.7	50930.7	Mt. Canopus 1-m	...	17.81	...	17.36(13)	2	
1998 Apr 28.0	50931.0	SAAO 1.9-m	...	17.74(8)	...	17.13(11)	1	
1998 Apr 29.7	50932.7	Mt. Canopus 1-m	...	18.17(6)	...	17.67(6)	2	
1998 May 02.6	50935.6	UKIRT 3.8-m	17.17(4)	3	
1998 May 02.7	50935.7	Mt. Canopus 1-m	...	18.58(11)	...	17.83(10)	2	
1998 May 04.6	50937.6	UKIRT 3.8-m	17.33(4)	3	
1998 May 04.7	50937.7	Mt. Canopus 1-m	...	18.36(7)	...	17.83(13)	2	
1998 May 05.1	50938.1	JKT 1-m	18.67(18)	18.51(15)	18.06(14)	17.92(25)	1	
1998 May 05.7	50938.7	Mt. Canopus 1-m	...	18.50(9)	...	18.12(15)	2	
1998 May 16.7	50949.7	Mt. Canopus 1-m	...	18.36(14)	...	17.80(15)	2	
1998 May 17.5	50950.5	Mt. Canopus 1-m	...	18.44(5)	...	17.84(6)	2	
1998 Jun 02.4	50966.4	NTT 3.5-m	...	18.59(5)	1	
1998 Jun 27.7	50991.7	Mt. Canopus 1-m	...	> 20.5	1	
1998 Sep 07.6	51063.6	UKIRT 3.8-m	>19.3	>18.3	1	
2000 Jul 03	51728	SAAO 1.9-m	22.0(1)	21.5(1)	20.9(1)	4	

^aWhere multiple measurements were obtained on the same day from a given observatory, we present the average value. Measurement uncertainties are quoted at the 1σ level.

References. — (1) This work; (2) Giles et al. 1999; (3) Percival et al. 1998; (4) Homer et al. 2001.

On both plots, we have also indicated the quiescent flux levels measured well after outburst (Wijnands et al. 2001; Homer et al. 2001). It is interesting to compare the behavior of the X-ray and optical light curves. In the X-ray band, the intensity shows a steady exponential decay ($\tau = 10.9$ d) until about MJD 50929, when there is a sharp break to a steeper decay ($\tau = 2.2$ d), as shown previously by Gilfanov et al. (1998). The optical *V*-band light curve also shows an initially exponential decay in intensity ($\tau = 8.4$ d) until MJD 50936, when it abruptly reaches a plateau lasting at least 30 d. Despite the fact that the optical light curve appears to roughly follow the X-ray light curve early in the outburst, the breaks from the initial decay are spaced by a week, and the behavior after the break is quite different in the two bands.

The broadband optical/IR spectrum is shown in Figure 2 for several epochs during the outburst, as well as a quiescent measurement. The shape of the *BVRI* spectrum during the outburst remains roughly constant. There is an obvious infrared excess on MJD 50921, with the *JHK* points lying well above an extrapolation of the *BVRI* spectrum. By contrast, the *K* point for MJD 50938 is consistent with the extrapolated optical spectrum. Since the origin of the IR excess early in the outburst is unclear, we restrict our accretion disk fitting in the next section to the optical *BVRI* bands, which (along with the ultraviolet and soft X-ray) is where most of the disk emission from an LMXB accretion disk is expected.

One point of concern is the discrepancy between optical intensities measured at different observatories a short time apart. This is particularly evident in the JKT and Mt. Canopus observations on MJD 50921, which were spaced by half a day but differ by 0.2 magnitudes in *V* and *I*. One possible contribution to this discrepancy is the 2-hr orbital flux modulation reported by Giles et al. (1999), with amplitude of $\simeq 0.07$ magnitudes. To account for this in our fits, we added a systematic uncertainty of this size in quadrature to the statistical uncertainties quoted in Table 1. However, even this systematic uncertainty is insufficient to explain the discrepancy, which we conclude largely arises from further systematic errors due to calibration uncertainties in the JKT data. In particular, several of the JKT service observations suffered from limited or insufficient calibration measurements. We therefore adopt a systematic

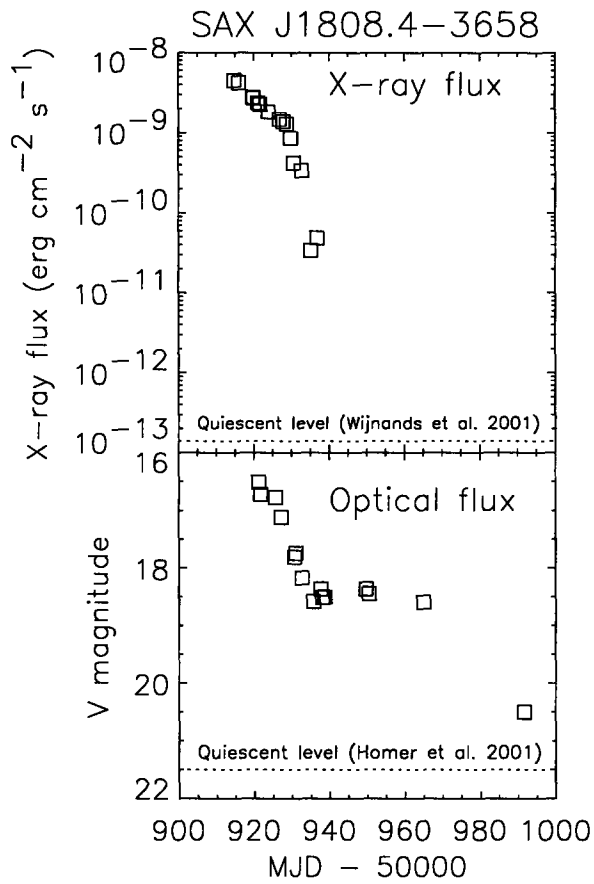


Figure 6-1 X-ray (3–150 keV) and optical flux histories during the 1998 outburst of SAX J1808.4–3658. The quiescent levels well after the outburst are also indicated. The X-ray history (taken from Gilfanov et al. 1998) contains a sharp break at MJD 50929, while the optical history shows a break at MJD 50936.

uncertainty of 0.2 magnitudes for all the JKT measurements in our model fitting.

6.4 Discussion

The optical data during outburst may be fitted by an X-ray-heated accretion disk model (see Vrtilik et al. 1990, Chapter 1.1, and references therein). Especially for SAX J1808.4–3658, many of the model parameters are well-constrained. We may adopt the distance $D = 2.5$ kpc inferred from radius-expansion X-ray bursts (in 't Zand et al. 2001). Since this is a disk-accreting pulsar, we may assume that the inner disk is truncated by the pulsar's magnetosphere at a radius r_{in} of order the corotation radius $r_{\text{co}} = (GM_{\text{x}}P_{\text{spin}}^2/4\pi^2)^{1/3} \approx 30$ km (Psaltis & Chakrabarty 1999); in fact, the optical spectrum is not very sensitive to the exact value of this parameter, since the optical emission primarily arises from radii in excess of 10^8 cm. The outer disk will be cut off sharply near the neutron star's tidal radius, $\approx R_{\text{Roche}}$ (Frank et al. 1992), which will in turn depend upon the mass ratio and thus the binary inclination (Eggleton 1983). We may infer the X-ray luminosity from the X-ray flux through $L_{\text{x}} = 4\pi D^2 F_{\text{x}}$, and hence deduce the mass transfer rate \dot{M} . Finally, for the X-ray albedo of the disk, we can use the results of previous studies of X-ray reprocessing in LMXBs which found that $\eta_{\text{d}} \gtrsim 0.90$, indicating that only a small fraction of the incident X-ray flux is absorbed by the accretion disk and reprocessed into the optical band (Kallman, Raymond, & Vrtilik 1991; de Jong, van Paradijs, & Augusteijn 1996).

With the model parameters set as described above, we fit the heated disk model to the observed photometry with two free parameters, $\cos i$ and the optical V -band extinction A_V . However, we found that the optical spectrum at outburst was much too bright to be fitted by this X-ray heated disk model, even though we tested to change the distance to values in a reasonable range ($D = 3.4$ kpc), suggested by the studies of its burst recurrence times (Galloway, private communication). Careful tests by varying parameters in our model indicated that the mass accretion rate, estimated from the X-ray flux, was about 6 times lower than our model needs. Therefore we conclude that the X-ray heated model may not work when the disk is under an

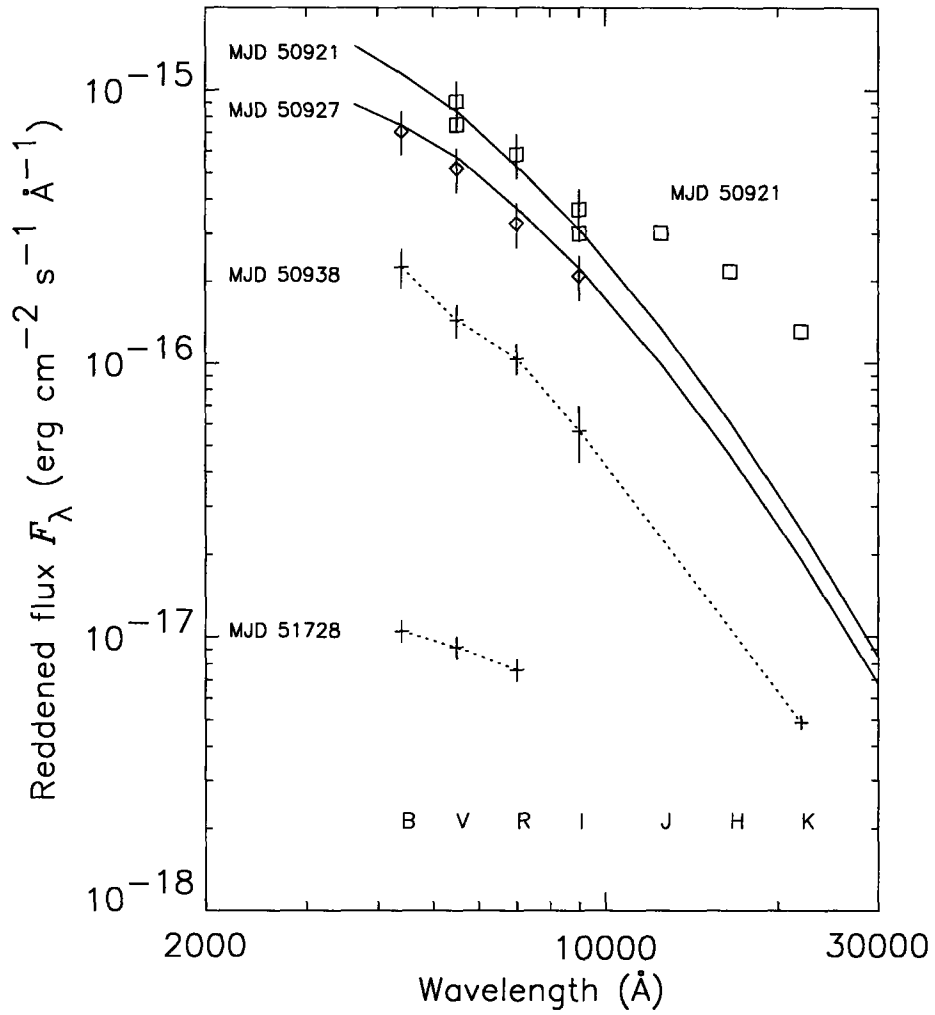


Figure 6-2 Broadband optical/IR spectra of SAX J1808.4–3658 at various epochs during the 1998 outburst. The solid curves are model fits with assumption of larger mass accretion rates than estimated from the X-ray flux, while the dotted curves simply indicate a rough interpolation of the data. There is a clear IR excess with respect to an accretion disk model on MJD 50921, but not on MJD 50938.

outburst event with quantities, such as mass accretion rate, varying dramatically in a short time scale. On the other hand, it is also possible that the underlying mass accretion rate during the outburst is far larger than estimated from the X-ray flux. This may be due to mass loss or outflow from the binary system, or even blockage of a major fraction of X-ray flux.

The strong infrared excess measured on MJD 50921 is clearly inconsistent with optical emission (see Figure 6-2). It is also orders of magnitude too bright to be due to the companion; even X-ray heating does not mitigate this, due to the small solid angle subtended by the star. On the other hand, the infrared emission on MJD 50938 is consistent with optical emission, indicating that the cause of the earlier IR excess is transient in nature. It is interesting to note that the flux density of the IR excess is comparable to the radio flux density measured from the source a week later (Gaensler, Stappers, & Getts 1999). Radio/IR emission due to synchrotron processes have been previously detected from some X-ray binaries during outburst (see, e.g., Fender 2001). The possibility of a synchrotron origin for the IR excess on MJD 50921 (as well as the radio emission) is explored in detail elsewhere (Chakrabarty, Gaensler, & Stappers 2004, in preparation).

Chapter 7

Search for Optical/IR

Counterparts to X-ray Millisecond Pulsars

7.1 Introduction

The X-ray millisecond X-ray pulsars (MSPs) are highly evolved X-ray binaries with their neutron star primaries spun up to millisecond spin period by the mass flow accreted from the companion stars. Their existence as progenitors of radio MSPs was predicted by theory (see, e.g., Alpar et al. 1982; Joss & Rappaport 1983) long before the discovery of the first X-ray MSP SAX J1808.4–3658 in 1998 (Wijnards & van der Klis 1998; Chakrabarty & Morgan 1998). Since then, a monitoring program (Swank & Markwardt 2001) searching for the X-ray transients in the Galactic bulge region, has become successful in discovering new X-ray MSPs (see 1.2.2).

In this chapter, we report our search for the optical/IR counterparts to the newly discovered MSPs. The observations were made when the MSPs were in either outburst, in order to identify the counterparts and obtain their optical/IR outburst light curves, or quiescence, in order to identify the companion stars in the binary systems and seek for the chances for further studies.

7.2 Observations

We obtained our imaging or spectral data with the Magellan telescopes at Las Campanas observatory (LCO). The observations were arranged through an intervention program, proposed to obtain prompt optical/IR data of interesting X-ray transients, within the few days after the discoveries of the new X-ray millisecond pulsars (MSPs) were reported. Depending on the available instruments on the Magellan telescopes at the time, either optical or near-IR observations were made. In Table 7.1, we summarized our observations of SAX J1808.4–3658, XTE J1751–305, XTE J0929–314, XTE J1807–294, and XTE J1814–338.

Table 7.1 Log of the Magellan imaging observations of the X-ray MSPs.

Sources	Instruments	Observation time (UT)	Filter	Exposure time (s)	Seeing (arcsec)
SAX J1808–366	MagIC	2001 Nov 02 20:44	r'	120	0.5
XTE J1751–309	Classic_CAM	2002 Apr 09 06:48	J	540	0.6
	Classic_CAM	2002 Apr 09 07:20	K_s	540	0.6
	Classic_CAM	2002 Apr 09 08:28	J	4×360	0.6
XTE J0929–314	MagIC	2002 Dec 09 06:53	r'	360	1.0
XTE J1807–294	MagIC	2003 Feb 27 00:34	i'	300	0.7
	MagIC	2003 Mar 17 09:49	i'	2×180	0.5
	MagIC	2003 Apr 24 08:10	i'	300	1.2
XTE J1814–338	LDSS-2	2003 Jun 06 10:25	BR	150	1.2
	LDSS-2	2003 Jun 07 10:01	BVR	150	1.2

In addition, we obtained one 1800 s spectrum of XTE J0929–314 during its outburst on 2002 June 7, using the Baade/Magellan I telescope. The B&C spectrograph was used with a 1200 l/mm grating, providing a wavelength coverage of 3800–5400 Å and a spectral dispersion of 0.80 Å/pixel. A 0".8 slit was used for the observation.

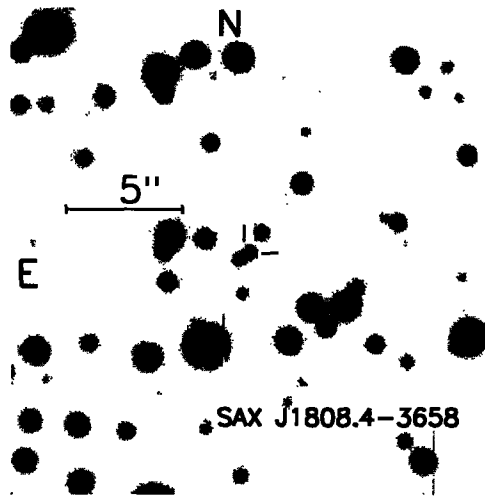


Figure 7-1 Sloan r' image of the SAX J1808.4–3658 field with its quiescent optical counterpart indicated.

7.3 Results

7.3.1 The Optical Counterpart to SAX J1808.4–3658 in Quiescence

The image we obtained on 2001 November 02 was under excellent conditions, with 0.5" seeing. We compared this MagIC image to the Keck LRIS image during the outburst, and constructed an astrometric solution by using 51 in-field stars. The quiescent optical counterpart of SAX J1808.4–3658 was identified (see Figure 7-1). Note that our image clearly indicates the counterpart while previous reported images were not be able to resolve the counterpart due to either low imaging quality or poor seeing conditions. The magnitude was $r' = 21.2 \pm 0.1$.

7.3.2 XTE J1751–305

The second X-ray MSP, XTE 1751–305, was discovered on 2002 April 3 during its X-ray outburst. The K_s image of the XTE 1751–305 field, taken during the outburst,

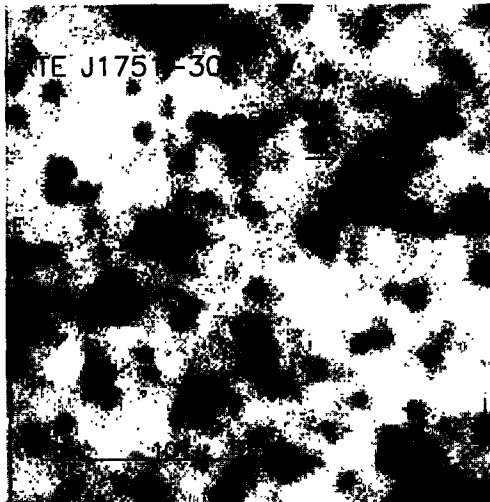


Figure 7-2 K_s image of the XTE J1751–305 field with its $0.7''$ *Chandra* error circle indicated. No stars were detected in the error circle.

is shown in Figure 7-2 with the *Chandra* error circle indicated. Two faint stars outside the error circle once were proposed as the possible candidates (Jonker et al., 2003). It is very likely that the counterpart was not detected. The upper limits for the counterpart in the optical/IR bands were $R > 23.1$, $I > 21.6$, $Z > 20.6$, $J > 19.6$, and $K > 19.2$ (Jonker et al., 2003).

7.3.3 XTE 0929–314

XTE J0929–314 was discovered in 2002 April by the All Sky Monitor on board the *RXTE* (Remillard 2002). Radio and optical counterparts were identified immediately after the discovery (Rupen et al. 2002; Greenhill et al. 2002; Cacella 2002). The detection of C III/N III $\lambda\lambda 4640\text{--}4650$ and $H\alpha$ $\lambda 6563$ in its optical spectrum was reported (Castro-Tirado et al. 2002). However, our Magellan spectrum is featureless (Figure 7-3) with no hydrogen emission lines detected (note that $H\alpha$ is not covered by our spectrum.) There is marginal evidence for the detection of C III/N III $\lambda\lambda 4640\text{--}4650$. We note our observation was made one month later than the one reported by Castro-Tirado et al. (2002). Even though this source has a high Galactic latitude ($l = 260^\circ$, $b = 14^\circ$) and thus probably low extinction ($E(B - V) \approx 0.14$; Schlegel et

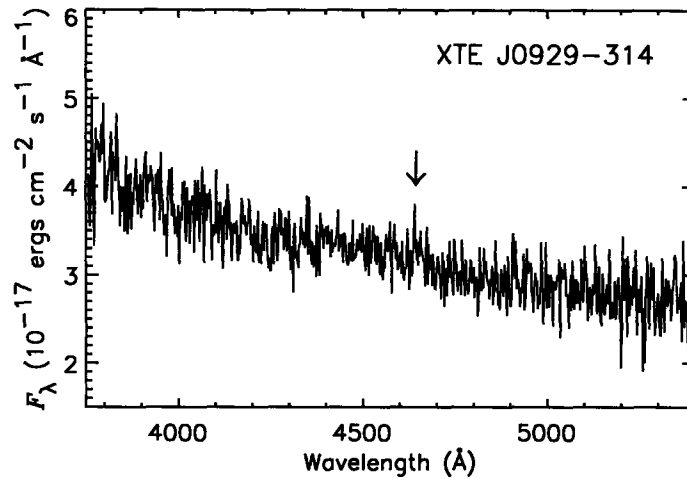


Figure 7-3 Optical spectrum of XTE J0929–314, with the C III/N III $\lambda\lambda 4640\text{--}4650$ line position indicated.

al. 1998), further imaging observations did not detect the quiescent optical counterpart (Figure 7-4). The limiting magnitude was $r' > 24$.

7.3.4 XTE J1807–294

The third X-ray MSP, XTE J1807–294, was discovered on 2003 February 21. Over the following couple of months we obtained images of its field at three epochs, in detecting variability from candidates and thereby identifying the counterpart. An astrometric solution was derived by matching 19 in-field stars with the USNO-A2.0 catalog of astrometric standards (Monet et al.1998). Two objects (labeled as object A and B in Figure 7.3.4) were found within the $1''$ *Chandra* error circle. However, no variability was detected from either of the two candidates in our images, indicating that these two objects are likely front stars due to high density of stars in the field.

7.3.5 XTE J1814–338

The X-ray MSP XTE J1814–338 was discovered as a binary with the 4.3 hour orbital period (Markwardt et al., 2003). The optical counterpart was identified soon after the discovery of this source (Krauss et al., 2003). Our optical photometry of the

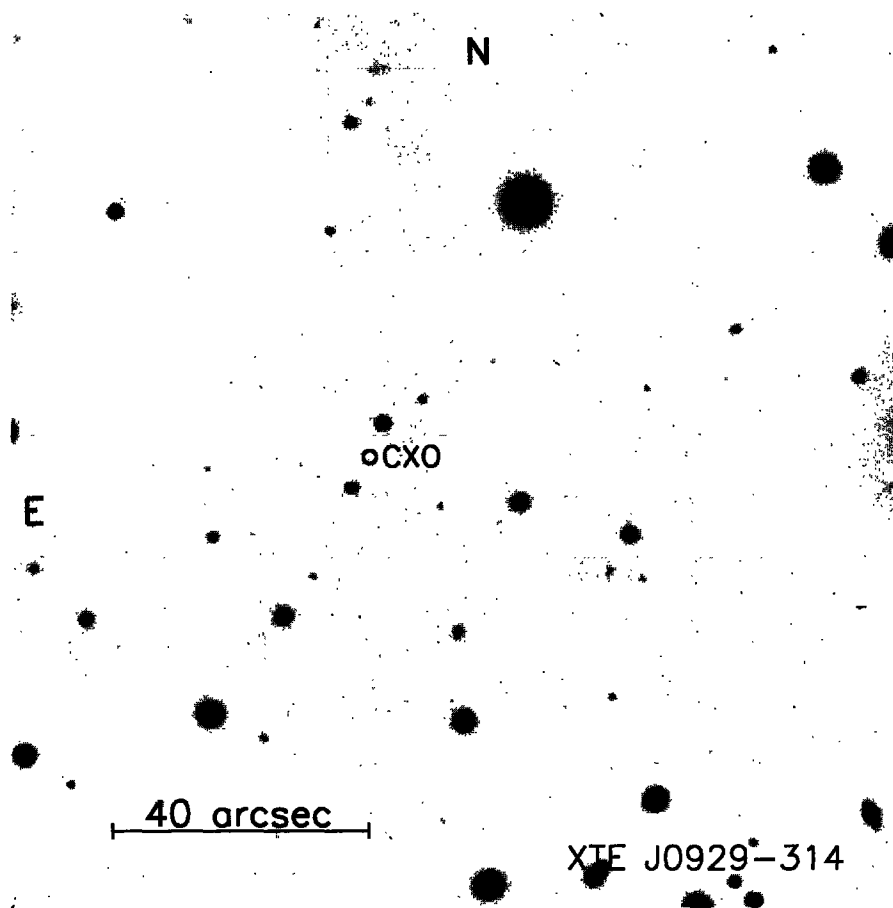


Figure 7-4 Sloan r' image of the XTE J0929-31 field. The quiescent counterpart was not detected with its position indicated by the *Chandra* error circle.

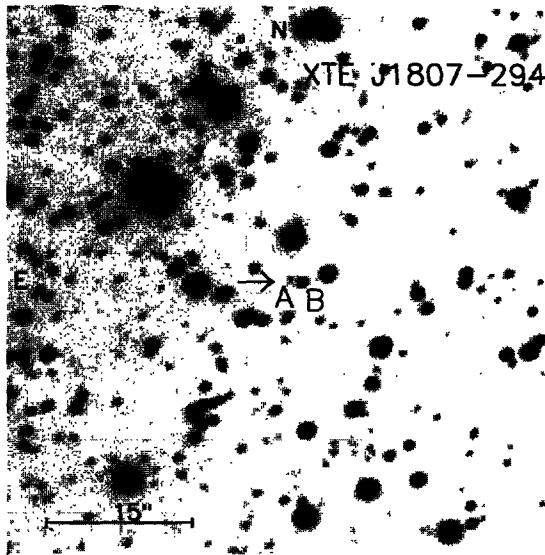


Figure 7-5 Sloan i' image of the XTE J1807-294 field with two candidate objects within the $1''$ *Chandra* error circle indicated as A and B. No variability was detected from these two objects over the course of two months after the discovery of XTE J1807-294.

counterpart found its magnitudes $B = 18.96$, $V = 18.59$, and $R = 18.26$ with the calibration error being 0.06 magnitudes (see also Krauss et al., 2004). To fit a main-sequence star to the Roche-lobe in a 4.3 hours binary, the companion star would have a mass of $0.54 M_{\odot}$ and the binary has an inclination of 21° . Assuming that the optical emission comes from the accretion disk during the outburst and fitting the broad band flux with the X-ray heated disk model, we derived a range of inclination values consistent with the 21° . Thus this source is likely a LMXB with low inclination and a $0.5 M_{\odot}$ low-mass companion.

7.4 Summary

Even though our studies have been limited by high extinction to each MSP source since the X-ray monitoring program is focused on the Galactic buldge region, we have (1) identified the optical counterpart to the X-ray MSP SAX J1808.4-3658, which was not resolved by previous optical observations; (2) set flux density limits on the

IR counterpart to XTE J1751–305, optical counterpart to XTE J1807–294, both in outburst, and the optical counterpart to XTE J0929–314 in quiescence; (3) obtained the optical spectrum of XTE J0929–314, which is featureless and shows a lack of hydrogen emission lines such as $H\beta$ and $H\gamma$, consistent with the scenario that this MSP has a H-depleted mass donor as an ultracompact binary (its orbital period is 43.6 min); (4) identified the optical counterpart to XTE J1814–338.

Chapter 8

The possible Near-Infrared Counterpart to the Bursting X-Ray Pulsar GRO J1744–28

8.1 Introduction

The bursting pulsar GRO J1744–28 is a unique LMXB which presents both type II X-ray bursts and 2.1-Hz periodic pulsations (Finger et al. 1996). This source was discovered by the Burst and Transient Source Experiment (BATSE) on board the *Compton Gamma-Ray Observatory* (CGRO) in 1995 December (Fishman et al. 1995). From then to 1997 April, when it became quiescent, it was extensively studied. The source lies in the direction of the Galactic center ($l=0^{\circ}04$, $b=0^{\circ}3$), and the high column density of $5\text{--}6\times 10^{22}\text{ cm}^{-2}$ derived from *ASCA* observations may indicate that it is located near the Galactic center (Nishiuchi et al. 1999). However, given that its persistent X-ray luminosity (Giles et al. 1996) should not exceed the Eddington limit, a distance of ~ 4 kpc can be estimated. It has an orbital period of 11.83 days and a mass function of $1.3\times 10^{-4}M_{\odot}$ (Finger et al. 1996), implying that the companion star in this system is likely a low mass giant (Daumerie et al. 1996; Sturmer & Dermer 1996; Rappaport & Joss 1997).

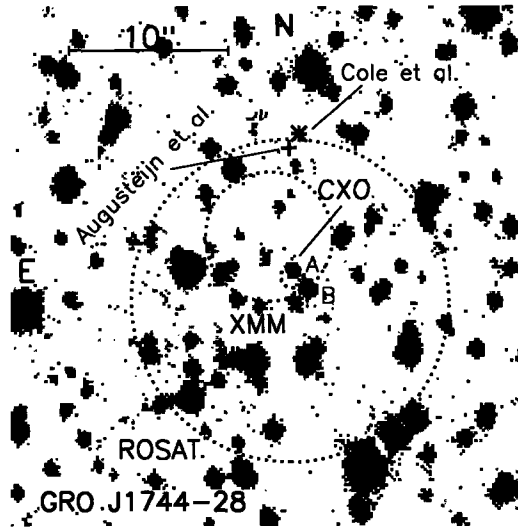


Figure 8-1 Near-infrared image of the region around GRO J1744–28. The indicated *ROSAT*, *XMM*, and *Chandra* positions are consistent. One object (A) is found within the *Chandra* error circle, while the nearest object (B) is about $1''.4$ away. The positions of the possible counterparts reported by Cole et al. (1997) and Augusteijn et al. (1997) are indicated as asterisk and plus sign respectively.

In this chapter, we report on the near-infrared observations of GRO J1744–28. Recent *Chandra* and *XMM-Newton* X-ray observations (Wijnands & Wang 2002; Daigne et al. 2002) indicated that the previous IR identifications of the counterparts to this source (Cole et al. 1997; Augusteijn et al. 1997) were wrong.

8.2 Observation

We obtained *JHK_s* near-infrared images of the GRO J1744–28 field on 2002 February 25 using the Ohio State Infrared Imager/Spectrometer (OSIRIS; Depoy et al. 1993) at the $f/14$ tip-tilt focus of the 4 m Blanco telescope at the Cerro Tololo Inter-American Observatory (CTIO) in Chile. The detector in OSIRIS was a Rockwell HAWAII HgCdTe 1024×1024 array. We used the OSIRIS $f/7$ camera, which had a $0''.161 \text{ pixel}^{-1}$ plate scale and a $93''$ field of view. For each wavelength band, we obtained four images in a 2×2 grid with offsets of about $10''$ to allow for correction

of the rapidly varying infrared sky background and to minimize the effect of bad pixels. These individual images were shifted and combined in the course of the data reduction. We obtained 20 s exposures in each J and H bands, and 80 s in the K_s band. During the night the seeing was good, varying from $0\prime.8$ to $1\prime.2$.

On 2004 February 12, we obtained JHK_s images of the source field under good conditions with the seeing being $0\prime.5$, using the Baade telescope. The IR imager we used was Persson's Auxilliary Nasmyth Infrared Camera (PANIC), which contains a Rockwell 1024×1024 detector with $0.125''$ pixels. The exposures were 5 min in J band and 2.5 min in HK_s .

The general IRAF packages were used to reduce the data. The new faint standard stars (Persson et al. 1998) were used for flux calibrations of both observations.

8.3 X-ray position and Astrometry

We derived the position of GRO J1744–28 using data from the *Chandra X-Ray Observatory* public data archive. The source was observed with the Advanced CCD imaging Spectrometer (ACIS-I) on 2001 July 18 for 10.8 ks (Wang, Gotthelf, & Lang 2002). We analyzed these data using the CIAO v2.2 data analysis package.¹ To maximize the absolute positional accuracy of the data, we used the CIAO thread (processing recipe) `fix_offset` to check for systematic aspect offsets and apply the latest alignment file (2002 May 2) as necessary. Using the CIAO tool `celldetect`, we obtained the following source position: R.A. = $17^{\text{h}}44^{\text{m}}33^{\text{s}}.09$ and Decl. = $-28^{\circ}44'27''.5$ (equinox J2000.0), with an error radius of $0\prime.6$ (90% confidence) dominated by the spacecraft attitude uncertainty. We note that the position we derived is almost the same as the one given by Wijnands & Wang (2002). There are a few other sources detected in the image. We identified one of them as the Arches cluster (Yusef-Zadeh et al. 2002). The position of this cluster in the *Chandra* image is consistent with the reported position (Nagata et al. 1995; Yusef-Zadeh et al. 2002). This partly assures the general accuracy of the *Chandra* position of GRO J 1744–28 although the Arches

¹See <http://asc.harvard.edu/ciao/>

cluster is not a point source. In addition, the *Chandra* position is consistent with the the position reported by Daigne et al. (2002) from *XMM-Newton* observations: R.A. = $17^{\text{h}}44^{\text{m}}33^{\text{s}}.2$, Decl. = $-28^{\circ}44'25''$ (equinox J2000.0), with an error radius of $4''$.

An astrometric solution for the infrared images was derived by matching 25 field stars with the 2MASS catalog (Cutri et al. 2001)². The total nominal uncertainty for locating the *Chandra* source position on our images is $0''.7$ (90% confidence), which includes the systematic uncertainty of the 2MASS catalog ($0''.2$; Curti et al. 2001), the transformation uncertainty between the infrared images and the 2MASS catalog ($0''.1$), and the uncertainty of *Chandra* observation. For the *XMM-Newton* position, the quoted $4''$ uncertainty dominates. In Figure 8-1, we show our *H* image of the field of GRO J1744–28 with the error circles of both *Chandra* and *XMM-Newton* plotted.

8.4 Results and Discussion

As seen in Figure 8-1, the positions of the proposed counterparts to the source reported by Cole et al. (1997) and Augusteijn et al. (1997) are definitely not consistent with both the *Chandra* and *XMM-Newton* positions, and we did not detect any object at their positions. One object (labeled as *A*) is located within the *Chandra* $0''.7$ error circle, and the closest object (labeled as *B*) is about $1''.4$ away from the *Chandra* error circle and at the edge of the *XMM* error circle. Thus we identified object *A* as the candidate counterpart to GRO J1744–28. We measured the magnitudes of object *A*, yielding $J > 18.7$, $H = 16.0 \pm 0.1$, and $K_s = 14.5 \pm 0.1$ for the CTIO observations. For the Magellan observation, we obtained $J = 19.21$, $H = 16.16$, and $K_s = 14.69$. The uncertainty of the Magellan measurements was 0.05 mag. The two sets of HK_s measurements have a small offset consistent with the derived uncertainties.

Using our Magellan results and the interstellar reddening law given by Rieke & Lebofsky (1985), we established the relations for the intrinsic colors of object *A* as $(J-H)_0 = 3.05 - 0.107A_V$ and $(H-K_s)_0 = 1.47 - 0.063A_V$, where A_V is the reddening in *V* band. We compared the relations to intrinsic colors of different types of stars

²See <http://www.ipac.caltech.edu/2mass/releases/second/doc/explsup.html>

(Bessell & Brett 1988). Either dwarfs or supergiants have marginally consistent colors with $A_V \sim 20 - 22$, but require unreasonable distances (360 pc for dwarfs or 100 kpc for supergiants) by their brightnesses. A wide range of giants have consistent colors if $A_V = 19 \sim 22$ (see the bottom panel of Figure 8-2). Further comparing the magnitudes of giants and the object *A* (see the top panel of Figure 8-2), we found object *A* is likely a K giant.

However, a normal K giant has a mass of $\sim 2 M_\odot$, much higher than the most probable mass range 0.2-0.7 M_\odot for the mass donor suggested by theoretical calculations (see, e.g., Rappaport & Joss 1997). We thus used *JHK* magnitude results, $(H - K)_0 = 0.0-0.2$, $(J - H)_0 = 0.2-0.6$, and $K_0 = -(0.9-0.1)$, provided by Rappaport & Joss (1997) to check if our candidate counterpart could have the consistent colors and magnitudes. The shaded region in the bottom panel of Figure 8-2 indicates the expected colors given by their evolutionary simulations. As we can see, the colors could be consistent and require $A_V \approx 22$ or larger. Assuming $A_V = 22$ and let *K* magnitude equal 14.7, we found a distance of 3.5 kpc, indicated by the top panel of Figure 8-2. This distance actually is consistent with the value derived from the Eddington luminosity limit (Giles et al. 1996), but it is probably too small to have an $A_V = 22$, even though we note that the major extinction perhaps results from the clouds of dust and gas within 4 kpc of the Sun (Sanders, Scoville, & Solomon 1985; Cotera et al. 2000).

As the Galactic center (GC) has been found an extremely dense region containing evolved KM giants, supergiants, and OB dwarfs (Blum, Sellgren, & DePoy 1996; Cotera et al. 2000), the stars brighter than object *A* in our images have a density of 0.13 stars/arcsec², giving an 18% high chance coincidence probability. Therefore, in order to verify whether object *A* is the counterpart or not, further spectroscopic or time-resolved photometric observations are needed.

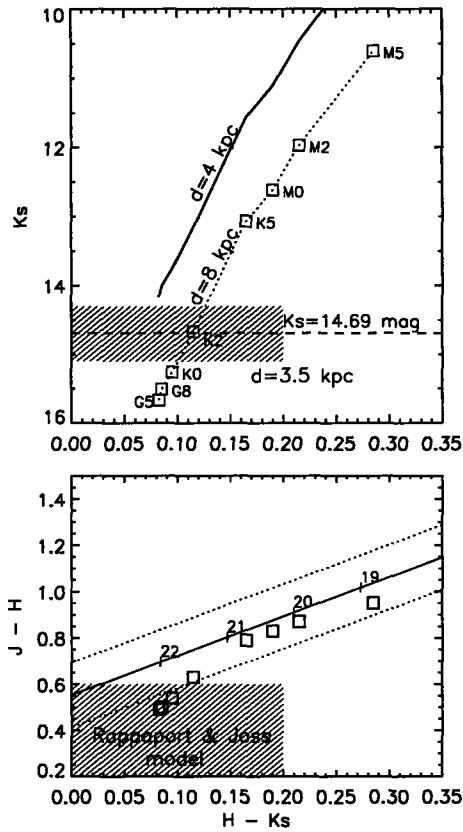


Figure 8-2 Color-magnitudes and color-color diagrams of red giants. *Top:* $H - K_s$ and K_s diagram of red giants at distances of 4 kpc (solid curve) and 8 kpc (dotted curve) with a reddening of $A_V = 21$. Different types of giants are indicated. The dashed line indicates the K_s magnitude of the candidate counterpart object A. The shaded region indicates that, in order to have the theoretical color-magnitude area consistent with $K_s = 14.69$, $d = 3.5$ kpc with $A_V = 22$. *Bottom:* $H - K_s$ and $J - H$ colors of red giants. The dotted lines indicate the color region derived from the colors of the object A. A wide range of giants from K2 to M5 can have consistent colors with $A_V = 19 \sim 22$. The shaded region indicates the expected colors given by evolutionary simulations (Rappaport & Joss 1997).

Chapter 9

The likely Near-Infrared Counterpart to the Anomalous X-Ray Pulsar 1E 1048.1–5937

9.1 Introduction

The anomalous X-ray pulsars (AXPs) are a small group of neutron stars with spin periods falling in a narrow range (6–12 s), very soft X-ray spectra, and with no evidence of binary companions (see Mereghetti et al. 2002 for a recent review). Their X-ray luminosities greatly exceed the power available from spin-down of the pulsars. These objects are thus believed to be isolated neutron stars either having extremely strong ($\sim 10^{14}$ G) surface magnetic fields (“magnetars”) or accreting from a residual accretion disk. X-ray bursts detected from the AXPs 1E 1048.1–5937 (Gavriil, Kaspi, & Woods 2002) and 1E 2259+586 (Kaspi & Gavriil 2002) have strengthened an already suspected connection to the soft gamma-ray repeaters (SGRs). The recent identification of optical/infrared counterparts to the AXPs 4U 0142+61 (Hulleman, van Kerkwijk, & Kulkarni 2000) and 1E 2259+586 (Hulleman et al. 2001) and the discovery of optical pulsations from 4U 0142+61 (Kern & Martin 2002) favor the magnetar scenario for these objects. In this chapter, we report on the detection of a

third AXP counterpart, and the first measurement of infrared colors for one of these objects.

The AXP 1E 1048.1–5937 ($l=288^{\circ}3$, $b=-0^{\circ}5$) was discovered serendipitously in 1979 during an *Einstein* observation of the Carina Nebula (Seward, Charles, & Smale 1986). It has since been extensively observed by a series of X-ray missions including *EXOSAT* (Seward et al. 1986), *Ginga* (Corbet & Day 1990), *ROSAT* (Mereghetti 1995), *ASCA* (Corbet & Mihara 1997; Paul et al. 2000), *RXTE* (Mereghetti, Israel, & Stella 1998; Baykal et al. 2000; Kaspi et al. 2001; Gavriil et al. 2002), and *XMM-Newton* (Tiengo et al. 2002). These observations establish the source as a 6.4 s pulsar that is spinning down, with an absorbed power-law + blackbody X-ray spectrum and occasional SGR-like bursts. The high column density to the source indicates that it lies behind the Carina Nebula, setting a lower limit on its distance of $d \gtrsim 2.8$ kpc (Seward et al. 1986; Özel, Psaltis, & Kaspi 2001). Previous searches for an optical counterpart have been unsuccessful (Seward et al. 1986; Mereghetti, Caraveo, & Bignami 1992) with the resultant limiting magnitudes $BVR \gtrsim 24.3$ (Israel, Mereghetti, & Stella 2001).

9.2 Optical/Infrared Observations

We obtained optical images of the field around 1E 1048.1–5937 on 2001 March 24 using the Raymond and Beverly Sackler Magellan Instant Camera (MagIC) at the west f/11 Nasmyth focus of the 6.5 m Baade (Magellan I) telescope at Las Campanas Observatory in Chile. MagIC is a 2048×2048 SITe CCD with a $0''.069$ pixel $^{-1}$ plate scale and a $142''$ field of view. Our observations were made using the Sloan filter set (Fukugita et al. 1996). We obtained 10 min exposures in the r' and i' bands. The seeing during the night was around $1''$. The limiting magnitudes (3σ) reached were $r' = 24.8$ and $i' = 24.4$. Photometric standards GD 108 and RU 152F were observed at various airmasses for calibration (Landolt 1992)

We also obtained JHK_s near-infrared images of the 1E 1048.1–5937 field on 2002 February 25 using the Ohio State Infrared Imager/Spectrometer (OSIRIS; Depoy

et al. 1993) at the f/14 tip-tilt focus of the 4 m Blanco telescope at the Cerro Tololo Inter-American Observatory (CTIO) in Chile. The detector in OSIRIS was a Rockwell HAWAII HgCdTe 1024×1024 array. We used the OSIRIS f/7 camera, which had a 0′161 pixel⁻¹ plate scale and a 93″ field of view. For each wavelength band, we obtained nine images in a 3×3 grid with offsets of about 10″ to allow for correction of the rapidly varying infrared sky background and to minimize the effect of bad pixels. These individual images were shifted and combined in the course of the data reduction. Our total exposure in each band was 4.5 min in J , 9 min in H , and 4.5 min in K_s . During the night the seeing was good, varying from 0′8 to 1′2. The limiting magnitudes (3σ) reached were $J = 21.3$, $H = 20.2$, and $K_s = 19.3$. The near-IR photometric standards 9136 and LHS 2397a of Persson et al. (1998) were observed for calibration.

We obtained deeper JHK_s images of the target field on 2002 April 8 with the “Classic Cam” near-infrared imager (Persson et al. 1992, 2001) at the west f/11 Nasmyth focus on the 6.5 m Baade telescope. The detector was a Rockwell NIC-MOS3 HgCdTe 256×256 array. We selected the camera in its low-resolution mode, with a 0′112 pixel⁻¹ plate scale and a 29″ field of view. The total exposure for 1E 1048.1–5937 in each band was 10.5 min in J , 18 min in H , and 15 min in K_s . The same dithering and data reduction scheme was employed as with the CTIO observations. The conditions were good, with the seeing around 0′8. The limiting magnitudes (3σ) reached were $J = 21.7$, $H = 20.8$, and $K_s = 19.7$. The same IR standards were used as in the CTIO observations.

We used the IRAF data analysis package to reduce our data, including the DAOPHOT routines for crowded field photometry.

9.3 X-Ray Position and Astrometry

We derived the position of 1E 1048.1–5937 using data from the *Chandra X-Ray Observatory* public data archive. The source was observed with the imaging detector of the *Chandra* High-Resolution Camera (HRC-I; Zombeck et al. 1995) on 2001 July 4

for 9.87 ks. We analyzed these data using the CIAO v2.2 data analysis package.¹ To maximize the absolute positional accuracy of the data, we used the CIAO thread (processing recipe) `fix_offset` to check for systematic aspect offsets and apply the latest alignment file (2002 May 2) as necessary. Using the CIAO tool `celldetect`, we obtained the following source position: R.A. = $10^{\text{h}}50^{\text{m}}07^{\text{s}}.14$ and Decl. = $-59^{\circ}53'21''.4$ (equinox J2000.0), with an error radius of $0''.6$ (90% confidence) dominated by the spacecraft attitude uncertainty. No other sources were detected in the *Chandra* image.

We note that our *Chandra* position differs significantly ($7''.6$) from the position reported by Tiengo et al. (2002) from *XMM-Newton* observations: R.A. = $10^{\text{h}}50^{\text{m}}06^{\text{s}}.3$, Decl. = $-59^{\circ}53'17''$ (equinox J2000.0), with an error radius of $4''$. We reanalyzed these data and obtained a position consistent with that of Tiengo et al. (2002). However, an examination of the *XMM-Newton* spacecraft attitude history during this observation indicates an unusually large and oscillating offset between the commanded and attitude-reconstructed viewing directions, with a mean value of $10''.5$ and an amplitude of $2''$. In consulting with the *XMM-Newton* User Support Group, we learned that such offsets usually (but not always) reflect problems with the attitude measurement accuracy rather than a pointing error, resulting in an erroneous reconstruction of the spacecraft attitude and the source coordinates (M. Santos-Lleo 2002, private communication). We were later informed by the *XMM-Newton* project that they have revised their attitude determination algorithm, placing less emphasis on the satellite pitch angle as determined from the fine sun sensor in the unusual case of tracking on a single guide star, as in this observation (F. Jansen 2002, private communication). This has led to a revised *XMM-Newton* position: R.A. = $10^{\text{h}}50^{\text{m}}07^{\text{s}}.31$, Decl. = $-59^{\circ}53'23''.1$, equinox J2000.0, error radius $4''$. This is consistent with the *Chandra* position. We show both the original and the revised positions in Figure 9-1. We thus disregard the *XMM-Newton* position reported by Tiengo et al. (2002).

An astrometric solution for the optical images was derived by matching about 20 unsaturated field stars with the USNO-A2.0 catalog of astrometric standards (Monet

¹See <http://asc.harvard.edu/ciao/>

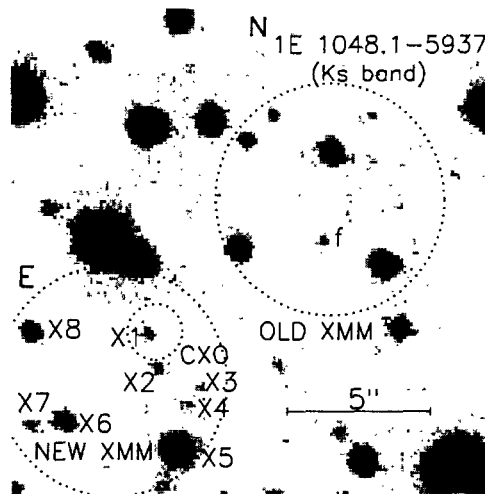
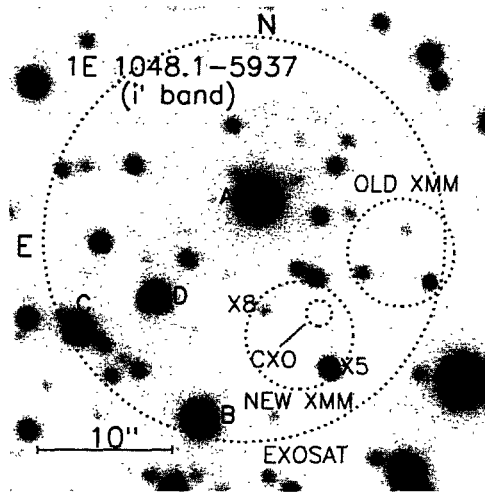


Figure 9-1 Optical and near-infrared images of the 1E 1048.1–5937 field. *Top panel:* i' -band image. *Bottom panel:* K_s -band Magellan image. On both images the *Chandra* (CXO) and *XMM-Newton* (old and new) error circles are shown. Also shown is the 15" *EXOSAT* error circle on the optical image. The candidates X1–X2 are discussed in §4. Objects A, B, C, and D in the optical image were studied by Mereghetti et al. (1992). Our proposed counterpart is object X1.

et al. 1998). Since the field of view of our infrared images is too small to allow a direct tie to the USNO-A2.0 system, we derived an astrometric solution for these images indirectly by matching stars with our optical images. The total nominal uncertainty for locating the *Chandra* source position on our optical/infrared images is 1" (90% confidence), which includes the systematic uncertainty of the USNO-A2.0 catalog (0".25; Monet et al. 1998), the transformation uncertainty between the optical image and the USNO-A2.0 catalog (0".4), and the uncertainty of *Chandra* observation. For the *XMM-Newton* position, the quoted 4" uncertainty dominates. In Figure 1, we show our *i'* and K_s images of the field of 1E 1048.1–5937 with the error circles of both *Chandra* and *XMM-Newton* plotted.

9.4 Results

As seen in the top panel of Figure 9-1, no objects were detected within the *Chandra* error circle in our optical images, although two objects (labeled *X5* and *X8*) were detected within the revised *XMM-Newton* error circle. Also indicated in that panel are the candidates (*A*, *B*, *C*, and *D*) previously studied by Mereghetti et al. (1992). In the bottom panel of Figure 1, we detected one object (*X1*) within the *Chandra* error circle in our deep infrared images and another (*X2*) just outside. In addition, we detected six other objects (labeled as *X3*–*X8*) within the revised *XMM-Newton* error circle. Object *X3* was detected only in the K_s band; since we cannot derive colors for this object, it is excluded from further consideration below. The faint objects *X3*, *X4*, and *X1* were not detected in our CTIO *JHK_s* observations, which were not as deep as the Magellan observations. The positions and optical/infrared magnitudes of our candidates are summarized in Table 1.

Figure 9-2 shows color-color diagrams for our seven candidates as well as all other field stars in our Classic Cam images. We note that the inferred hydrogen column density to 1E 1048.1–5937, $N_{\text{H}} = 1.04(8) \times 10^{22} \text{ cm}^{-2}$ (Tiengo et al. 2001), implies a visual extinction of $A_V \simeq 5.8$ for a typical dust-to-gas ratio (Predehl & Schmitt 1995). For comparison in Figure 9-2, we also show the expected colors for main sequence

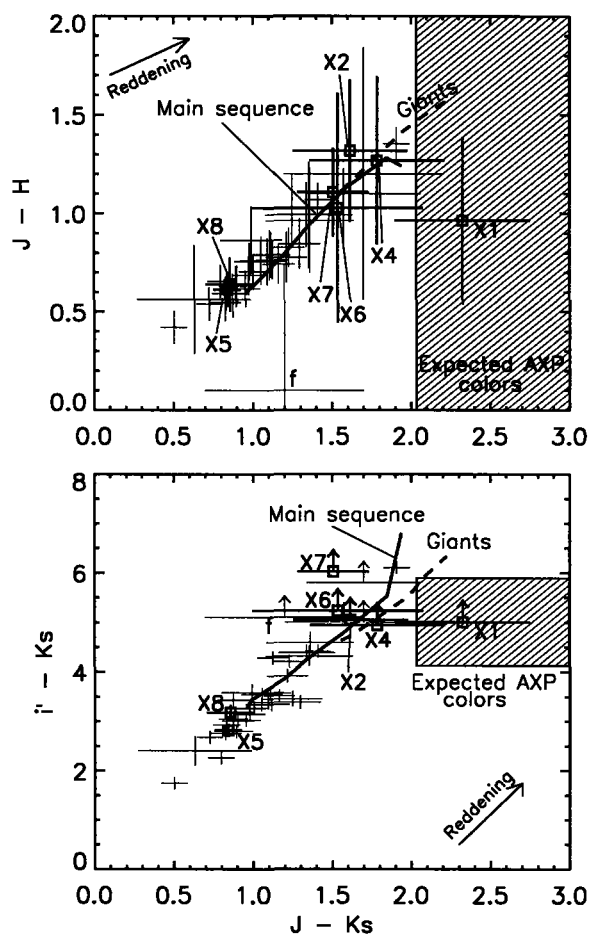


Figure 9-2 Color-color diagrams for the objects in the field of 1E 1048.1–5937. The dark squares indicate the candidates discussed in Chapter 9.4 and the light crosses indicate other field stars. The direction of increasing reddening is indicated by the arrow. The dark solid and dashed lines indicate the expected colors for main sequence and giant stars, respectively, with a reddening of $A_V = 5.8$. The shaded region indicates the expected counterpart colors based on the properties of the two other known AXP counterparts. Only our proposed counterpart (X1) lies in this region; it is also the only detected source in the *Chandra* error circle.

and giant stars (Bessell & Brett 1988; Cox 2000) reddened by $A_V = 5.8$ (Rieke & Lebofsky 1985; Fan 1999). The reddening vector lies roughly parallel to this locus of points. Most of our candidates (as well as the other field stars) have colors consistent with those of normal stars. However, two objects, *f* and *X1*, stand out with unusual colors. Assuming that the counterpart of 1E 1048.1–5937 is similar to those of the AXPs 4U 0142+61 ($V = 25.62 \pm 0.08$, $R = 24.99 \pm 0.07$, $I = 23.84 \pm 0.06$, $K = 19.6$, $A_V = 5.4$; Hulleman et al. 2000; Hulleman 2002) and 1E 2259+586 ($R > 26.4$, $I > 25.6$, $J > 23.8$, $K_s = 21.7 \pm 0.2$, $A_V = 5.2$; Hulleman et al. 2001), we have also indicated in Figure 9-2 the region of color-color space in which we would expect to find the counterpart. Only candidate *X1* has colors consistent with these predictions. We further note that *X1* is the only object detected within the *Chandra* error circle. We therefore conclude that this object is the near-infrared counterpart to 1E 1048.1–5937.

9.5 Summary

We have identified the likely near-infrared counterpart to 1E 1048.1–5937, on the basis of coincidence with the *Chandra* X-ray source position, unusual colors, and similarity to the two other known AXP counterparts. We note, however, that this conclusion relies strongly on our *i'* non-detection. A sufficiently faint *i'* magnitude could push this candidate out of the expected AXP region in the bottom panel of Figure 9-2. This is the first AXP counterpart with infrared detections in more than one band, allowing the intrinsic infrared colors to be inferred. Assuming $A_V = 5.8$ as determined in §4, the dereddened infrared magnitudes of the counterpart are $J_0 = 20.1$, $H_0 = 20.0$, and $K_{s0} = 18.8$. We plot these magnitudes and limits in Figure 9-3. For comparison, we plot the inferred spectral shape of the 4U 0142+61 counterpart (Hulleman et al. 2000; Hulleman 2002). While there is marginal evidence for a spectral flattening or even a turnover at the K_s band, the data are also consistent with a flat νF_ν infrared spectrum at the 1σ level. We note that there is clear evidence for spectral flattening in the infrared in the spectrum of 4U 0142+61 (Hulleman 2002). It would

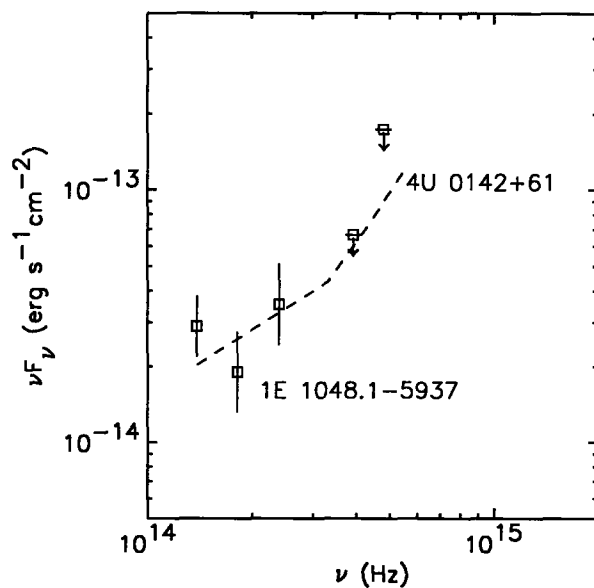


Figure 9-3 Dereddened flux from object *X1*, the counterpart to 1E 1048.1–5937. For comparison, the dashed line indicates the interpolated dereddened flux from AXP 4U 0142+61 (Hulleman et al. 2000; Hulleman 2002).

thus be of great interest to search for emission at longer wavelengths to constrain the spectral shape of AXPs further. While there has been relatively little theoretical work presented on the expected AXP optical/infrared emission in the magnetar scenario, we note that models involving X-ray illumination of a “fallback” accretion disk predict a spectral turnover leading to strong emission in the infrared and submillimeter bands (e.g., Chatterjee, Hernquist, & Narayan 2000; Perna, Hernquist, & Narayan 2000).

Table 9.1. Astrometry and Photometry of Candidate Counterparts

ID	R.A. (J2000)	Decl. (J2000)	r'	i'	J	H	K_s
$X1^a$	10 ^h 50 ^m 07 ^s .13	−59°53′21″.3	>24.8	> 24.4	21.7(3)	20.8(3)	19.4(3)
$X2$	10 ^h 50 ^m 07 ^s .09	−59°53′22″.5	>24.8	> 24.4	21.0(2)	19.7(3)	19.3(3)
$X3$	10 ^h 50 ^m 06 ^s .89	−59°53′23″.2	>24.8	> 24.4	>21.7	>20.8	20.3(4)
$X4$	10 ^h 50 ^m 06 ^s .94	−59°53′23″.8	>24.8	> 24.4	21.2(3)	20.0(3)	19.5(3)
$X5$	10 ^h 50 ^m 07 ^s .00	−59°53′25″.5	19.8(1)	19.0(1)	17.04(2)	16.42(8)	16.20(8)
$X6$	10 ^h 50 ^m 07 ^s .09	−59°53′24″.4	>24.8	> 24.4	19.9(2)	18.8(1)	18.4(1)
$X7$	10 ^h 50 ^m 07 ^s .67	−59°53′24″.4	>24.8	> 24.4	20.7(5)	19.7(3)	19.2(2)
$X8$	10 ^h 50 ^m 07 ^s .66	−59°53′21″.2	22.3(1)	21.3(1)	19.0(1)	18.3(1)	18.1(1)
f	10 ^h 50 ^m 06 ^s .29	−59°53′18″.2	>24.8	> 24.4	20.5(4)	20.4(5)	19.3(3)
A	10 ^h 50 ^m 07 ^s .71	−59°53′12″.9	16.5(1)	16.2(1)	14.875(6)	14.45(8)	14.37(8)
B	10 ^h 50 ^m 08 ^s .31	−59°53′29″.3	17.6(1)	17.0(1)	15.170(7)	14.69(8)	14.49(8)
C	10 ^h 50 ^m 09 ^s .52	−59°53′22″.6	18.5(1)	17.8(1)	14.783(7)	13.71(8)	13.37(8)
D	10 ^h 50 ^m 08 ^s .74	−59°53′20″.1	19.1(1)	17.8(1)	16.46(3)	15.90(9)	15.65(9)

^aProposed counterpart to 1E 1048.1−5937.

Chapter 10

Search for IR Counterparts of the Central X-ray Point Sources in Young Supernova Remnants

10.1 Introduction

There are now five young supernova remnants (SNRs) known to contain radio-quiet, nonplerionic X-ray point sources (XPSs) near their geometric center (see Pavlov et al. 2002a for a review). These objects have X-ray spectra roughly consistent with the expected surface emission from young cooling neutron stars (NSs). However, they differ from “typical” young NSs (e.g., the Crab pulsar) in SNRs in that they lack strong non-thermal emission components and (except in one case) they have no detectable pulsations. Along with the anomalous X-ray pulsars and the soft gamma-ray repeaters, these objects challenge our standard framework for understanding young neutron stars. Deep multiwavelength observations to establish the overall spectrum of these objects can provide important constraints. In this chapter, we report on our search for optical/infrared counterparts to such objects in the Southern Hemisphere.

Our targets are 1E 1614–5055 in SNR RCW 103 (Tuohy & Garmire 1980), 1E 1207–5209 in SNR PKS 1209–52 (Helfand & Becker 1984), RX J0822–4300

in SNR Puppis A, and RX J0852–4617 in SNR RX J0852.0–4622. The first three sources were discovered using the *Einstein Observatory*. The XPS in RCW 103 is unique among the five XPSs in showing considerable X-ray variability (Gotthelf, Petre, & Vasisht 1999; Pavlov et al. 2002b), and was suggested as a low-mass X-ray binary in a supernova remnant (Becker & Aschenbach 2002). The XPS in SNR PKS 1209–52 is the only confirmed pulsar among the five ($P_{\text{spin}}=424$ ms; Zavlin et al. 2000), and it is the only known neutron star with detectable absorption lines in its X-ray spectrum (Sanwal et al. 2002). A possible detection of a 75.3 ms period was reported (Pavlov et al., 1999) for RX J0822–4300. Previous searches for optical counterparts of the targets have been unsuccessful (Tuohy et al. 1983; Garmire et al. 2000; Matsui, Long, & Tuohy 1988; Bignami, Caraveo, & Mereghetti 1992; Mereghetti, Bignami, & Caraveo 1996; Petre et al., 1996). The last one, XPS RX J0852–4617, was detected by a series of X-ray missions, including *ROSAT* (Aschenbach et al., 1999), *ASCA* (Slane et al., 2001), *BeppoSAX* (Mereghetti, 2001), and *Chandar* (Pavlov et al., 2001). Previous observations indicated the limiting magnitudes on its optical counterpart were $B > 22.5$, $R > 21.0$ (Pavlov et al., 2001).

We report here on the possible identification of a near-infrared counterpart to RCW 103 and the observations of a near-infrared object near the PKS 1209–52 *Chandra* error circle. In the case of RCW 103, our counterpart may correspond to one proposed independently by Pavlov et al. (2002a).

10.2 Optical and Infrared Observations

We obtained optical images of the fields around the XPSs 1E 1614–5055, 1E 1207–5209, RX J0822–4300 on 2001 March 24–25 and June 12 using the Magellan Instant Camera (MagIC) at an $f/11$ Nasmyth focus of the 6.5 m Baade (Magellan 1) Telescope at Las Campanas Observatory in Chile. MagIC is a 2048×2048 SITe CCD with a $0''.069$ pixel $^{-1}$ plate scale and a $142''$ field of view. Our observations were made using the Sloan filter set. We obtained 9–10 min exposures of both fields in the r' and i' bands on March 24–25. For the high-latitude field of 1E 1207–5209, we also obtained

a 10 min exposure in the g' band on March 24 and a 5 min exposure in the u' band on June 12. The seeing for these observations was around $1''$.

We also obtained JHK_s near-infrared images of the 1E 1207–5209 and RX J0822–4300 fields on 2002 February 25 and RX J0852–4617 field on 2002 February 26, using the Ohio State Infrared Imager/Spectrometer (OSIRIS; Depoy et al. 1993) at the $f/14$ tip-tilt focus of the 4 m Blanco Telescope at the Cerro Tololo Inter-American Observatory (CTIO) in Chile. The detector in OSIRIS was a Rockwell HAWAII HgCdTe 1024×1024 array. We used the OSIRIS $f/7$ camera, which had a $0''.161$ pixel $^{-1}$ plate scale and a $93''$ field of view. For each wavelength band, we obtained nine images in a 3×3 grid with offsets of about $10''$ to allow for correction of the rapidly variable infrared sky background and to minimize the effect of bad pixels. These individual images were shifted and combined in the course of the data reduction. Our total exposure in each band was 9 min in J , 18 min in H , and 30 min in K_s for each target. During the nights the seeing was good, varying from $0''.8$ to $1''.2$.

In addition, we obtained JHK_s images of our target fields on 2002 April 8 and on 2003 January 21 with the “ClassicCam” near-infrared imager (Persson et al. 1992, 2001) at an $f/11$ Nasmyth focus on the 6.5 m Baade Telescope. The detector was a Rockwell NICMOS3 HgCdTe 256×256 array. We operated the camera in its low-resolution mode, with a $0''.112$ pixel $^{-1}$ plate scale and a $29''$ field of view. The total exposure for 1E 1614–5055 in each band was 10 min in J , 18 min in H , and 15 min in K_s . For 1E 1207–5209, we obtained a single 15 min exposure in J band. We also obtained a single 30 min K_s exposure for each RX J0822–4300 and RX J0852–4617. The same dithering and data reduction was employed as with the CTIO observations. The conditions were good, with the seeing being around $0''.8$.

On 2004 February 12, we obtained deep images of the 1E 1207–5209 field under excellent conditions with the seeing being $0''.5$, using the Baade telescope. The IR imager we used was Persson’s Auxilliary Nasmyth Infrared Camera (PANIC), which contains a Rockwell 1024×1024 detector with $0.125''$ pixels. The exposures were 30 min in J band and 40 min in K_s . The telescope position was dithered five times (using

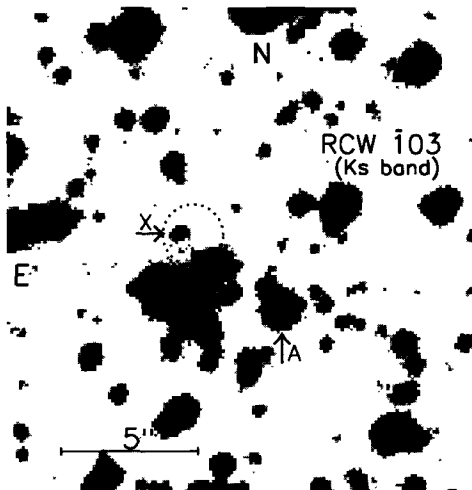
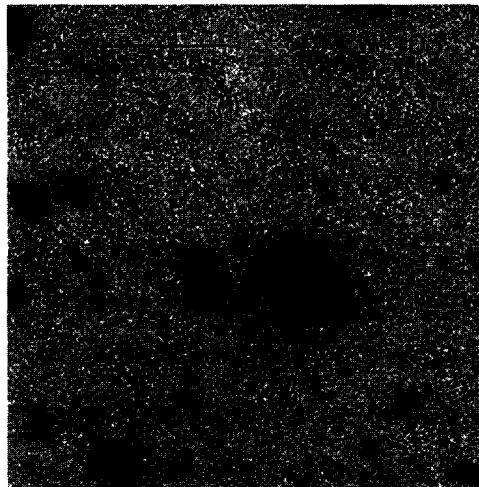


Figure 10-1 Optical and near-infrared images of the region around RCW103 (1E 1614–5055). Object X, the possible counterpart, is within the $0''.8$ dotted circle, which is the X-ray position derived from *Chandra*/ACIS observation. Object A was identified as a subdwarf M star by Tuohy et al. (1983).

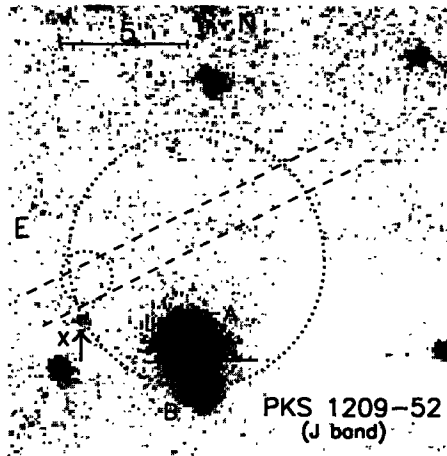


Figure 10-2 *J*-band image of the PKS 1209–52 (1E 1207–5209) region. A 5'' dotted circle indicates the *Einstein*/HRI position (Seward 1990) and 1''1 dotted error circle indicates the *Chandra* position. Two parallel dashed lines with the width of 1''4 between them, which cross the HRI error circle, are drawn to indicate the position derived from *Chandra*/ACIS observation. A faint object (labeled as *X*) right near the *Chandra* position and on the error circle is detected in this image.

a dither pattern “dice-5”), with a 15'' dither step, over the course of each exposure.

10.3 Astrometry

We derived positions for the X-ray sources using data from the *Chandra X-Ray Observatory* public data archive. The SNR RCW 103 was observed with *Chandra* Advanced CCD Imaging Spectrometer (ACIS) on 1999 September 26 for 13.6 ks. We analyzed these data using the CIAO v2.2 data analysis package.¹ We obtained the following position of 1E 1614–5055: R.A. = 16^h17^m36^s.25 and Decl. = –51°02'24''5 (equinox J2000.0), with a 90% confidence error radius of 0''6 dominated by the spacecraft attitude uncertainty. We note that this position is consistent with the one reported by Garmire et al. (2000). The source 1E 1207–5209 was observed by *Chandra*/ACIS on 2000 January 6 for 32.47 ks. These observations were made in continuous clocking

¹See <http://asc.harvard.edu/ciao/>

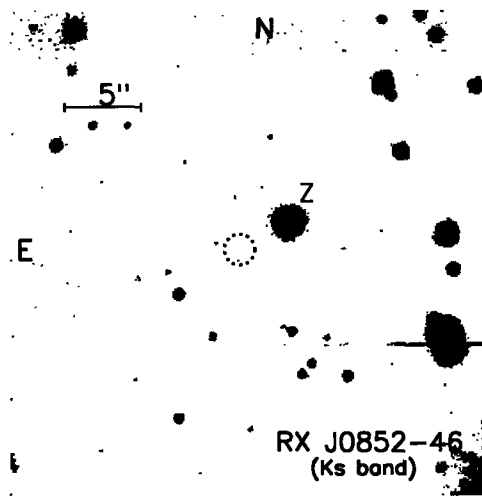


Figure 10-3 Classicam K_s image of the RX J0852-4617 field with the *Chandra* error circle (dotted circle) indicated. No near-IR counterparts were found near the error circle.

mode, so that only a 1-D position constraint is given; the derived direction is along northwest with an angle of $63^{\circ}3$ to the north and an uncertainty (90% confidence) of $0''.7$. The source was also observed by *Chandra*/ACIS on 2003 June 17, allowing us obtaining its position, R.A. = $12^{\text{h}}10^{\text{m}}00^{\text{s}}.92$, Decl. = $-52^{\circ}26'28''.3$ (equinox J2000.0). The uncertainty was dominated by the $0''.6$ (90% confidence) spacecraft attitude uncertainty. We note that the X-ray position derived from *Einstein* High Resolution Imager observations (Seward 1990) was R.A. = $12^{\text{h}}07^{\text{m}}23^{\text{s}}.4$, Decl. = $-52^{\circ}09'46''$ (equinox 1950.0).

We derived an astrometric solution for each of the optical images by matching about 50 unsaturated field stars to the USNO-A2.0 catalog of astrometric standards (Monet et al. 1998). Since the size of our infrared images is too small to allow a direct tie to the USNO-A2.0 system, we derived an indirect astrometric solution for these images by matching stars with our optical images. In Figures 10-1 and 10-2, we show our i' and K_s images of the field of 1E 1614-5055 and the J image of 1E 1207-5209 with their X-ray positions respectively plotted.

For 1E 1614-5055, the total nominal uncertainty (90% confidence) is $1''.1$, which

has included the systematic uncertainty of the USNO-A2.0 catalog ($0''.25$; Monet et al. 1998), the uncertainty of transforming between the optical image and the USNO-A2.0 catalog ($0''.5$), and the uncertainty of *Chandra* observation. The uncertainty of transforming between the optical image and the IR image is negligible. The dotted circle plotted in Figure 10-1 indicates this $1''.1$ uncertainty. For 1E 1207–5209, the uncertainty of transforming between the optical image and the USNO-A2.0 catalog is $0''.3$, and the uncertainty of transforming between the optical image and the IR image is negligible. The resulting nominal uncertainty is $0''.9$ (90% confidence). In Figure 10-2, the 1-D position derived from the *Chandra* observations is plotted as two parallel dashed lines, and it well matches the 2-D *Chandra* and *Einstein* error circles.

The sky position of XPS RX J0852–4617 given by the *Chandra* observations is R.A. = $08^{\circ}52'01''.38$, Decl. = $-46^{\circ}17'53''.3$ (equinox J2000.0; Pavlov et al., 2001). This position is indicated in Figure 10-3 as the dotted error circle.

The *Chandra* ACIS data for Puppis A were retrieved from the *Chandra* data Archive. We derived the position of XPS RX J0822–4300: R.A. = $08^{\circ}21'57''.46$ and Decl. = $-43^{\circ}00'15''.8$ (equinox J2000.0), with an error radius of $0''.7$ (90% confidence). This position is indicated as an solid circle in the top panel of Figure 10-4.

10.4 Results

10.4.1 RCW 103 (1E 1614–5055)

As seen in the bottom panel of Figure 10-1, one object (*X*) was detected at the *Chandra* position in both the *H* and *K_s* band images (bottom panel of the figure), while it was not detected in our *J* band images and optical images (top panel of the figure). Star *A*, indicated in both panels, is a subdwarf M star previously identified by Tuohy et al. (1983). We used IRAF package DAOPHOT to measure the magnitudes of object *X*, yielding $H = 19.4 \pm 0.2$ and $K_s = 18.1 \pm 0.1$. We also estimated the limiting magnitudes for the optical and *J* band images. The results are summarized in Table 10.1.

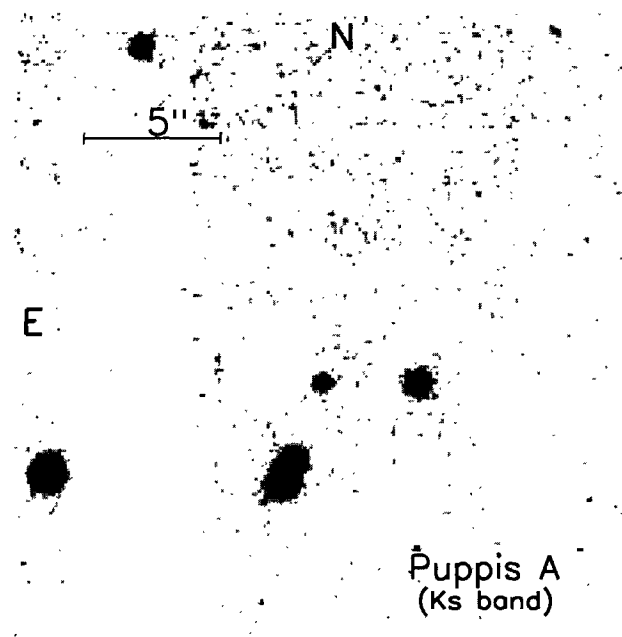
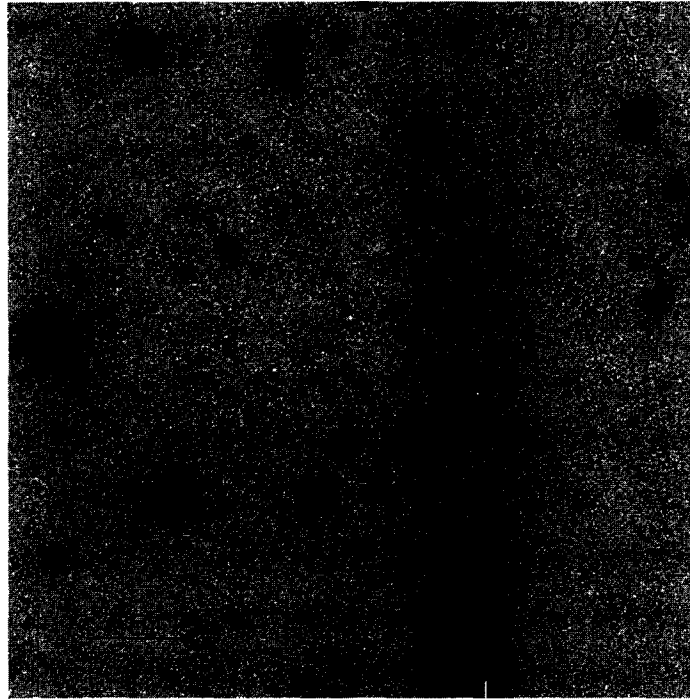


Figure 10-4 Sloan i' and IR K_s images of the Puppis A field with the *Chandra* error circle (solid circle) of XPS RX J0822-4300 indicated. No optical/IR counterparts were found near the error circle.

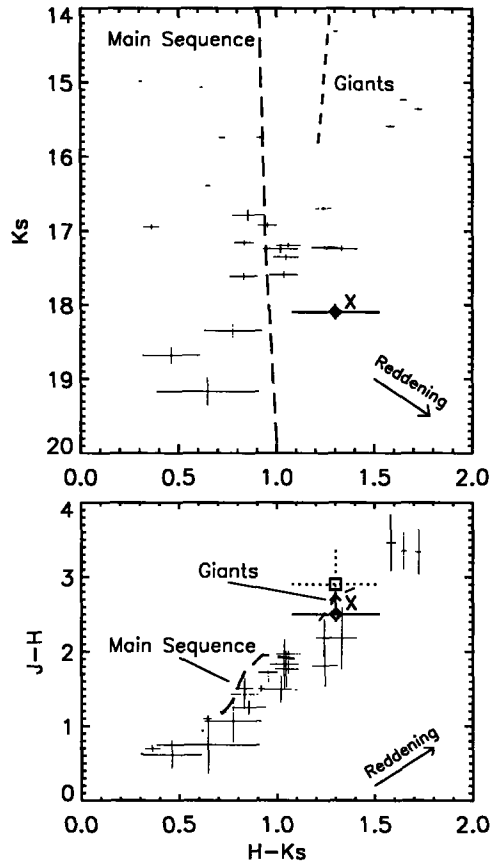


Figure 10-5 Color-magnitude and color-color diagrams for objects near the X-ray source position of 1E 1614-5055. The long-dashes line and dashed line are the main sequence with $A_V = 15$ and the giants with $A_V = 18$ respectively, both at a distance of 10 kpc. The diamond indicates the colors and K_s magnitude of the possible counterpart with using its J limit, while the square indicates its color $J - H$ with $J = 22.3 \pm 0.5$ (Pavlov et al. 2002a). The arrow at the low right corner of each diagram shows the reddening direction.

Table 10.1 Optical/IR photometry of XPSs

Filter	Wavelength (Å)	1E 1207–5209	1E 1614–5055	RX J0822–4300	RX J0852–4617
<i>u'</i>	3540	>22.5
<i>g'</i>	4770	>23.9
<i>r'</i>	6230	>24.3	>24.8	>25.0	...
<i>i'</i>	7620	>24.0	>24.4	>24.4	...
<i>J</i>	12500	>23.4	>21.9	>21.7	>21.7
<i>H</i>	16500	>21.3	19.4±0.2	>20.6	>20.6
<i>K_s</i>	21400	>22.0	18.1±0.1	>20.1	>20.1

Since the direction of 1E 1614–5055 is along the Galactic plane ($l = 332.4, b = -0.4$), its field is crowded. The estimated density of the stars which are at least as bright as object *X* in the field is 0.14 arcsec^{-2} , corresponding to a 30% chance coincidence probability. Accordingly it is possible that this object is an unrelated background star. In order to identify object *X*, we compare its colors with those of nearby stars. We measured the *JHK_s* magnitudes of 24 nearby stars. Their colors and *K_s* magnitudes are shown in the color-color and color-magnitude diagrams of Figure 10-5. Object *X* is also shown in the diagrams, where we use its *J* limiting magnitude. As seen in the bottom panel of Figure 10-5, the colors of nearby stars indicate that they are consistent with being main sequence stars (Bessell & Brett 1988), while the colors of object *X* have the tendency of staying away from the main sequence, which is indicated by its low limit of *J* – *H*. We note that Pavlov et al. (2002a) reported a possible IR counterpart which has very similar *H* and *K_s* values to ours. Assuming that we find the same object and thus using their measurement, $J = 22.3 \pm 0.5$, the *J* – *H* color of object *X* is redder than those of main sequence stars.

The colors of object *X* actually can be of an M giant reddened by $A_V = 18$. To show this, dashed lines are plotted in Figure 10-5 to represent colors and *K_s* magnitudes of giant stars (Bessell & Brett 1988) reddened by the extinction (Rieke & Lebofsky 1985). However, given that in the direction of 1E 1614–5055 the edge of the Galactic disk is about 20 kpc from us and the total extinction caused by the Galactic disk is roughly $A_V \simeq 40$ (Schlegel et al. 1998), object *X* should be at a distance of about 10 kpc to have $A_V = 18$. With this distance, a giant star is much

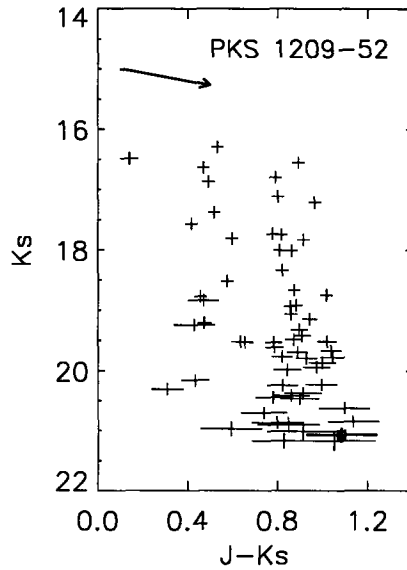


Figure 10-6 Color-magnitude diagram of the objects near the XPS 1E 1207–5209 position. The square indicates the object *X*, and the arrow indicates the reddening direction.

brighter in K_s band than the object, which can be clearly seen in the upper panel of Figure 10-5. In fact, to have $K_s \simeq 18$ with extinction $A_V = 18$, a faint giant star must approximately be at a distance of 29 kpc, beyond the edge of the Galactic disk. Therefore it is unlikely that object *X* is a red giant.

Based on coincidence with the *Chandra* X-ray position and the colors and K_s magnitude of object *X*, it is likely that we have identified the near-infrared counterpart to 1E 1614–5055. However, we note that our magnitude measurements suffer large uncertainties, thus excluding a definite conclusion. As a result, if object *X* is the counterpart, which has a distance of 3.3 kpc (Caswell et al. 1975) and extinction $A_V = 4.5$ (Leibowitz & Danziger 1983), its absolute IR magnitudes were $M_J \gtrsim 8.1$, $M_H \simeq 6.0$, and $M_{K_s} \simeq 5.0$.

10.4.2 PKS 1209–52 (1E 1207–5209)

In Figure 10-2, the *J* band image of the field of 1E 1207–5209, there is no object within the error region confined by the *Chandra* and *Einstein* observations. Two

blended stars (star *A* and *B*) within the *Einstein* error circle were studied by Matsui et al. (1988) and Bignami et al. (1992) and identified as two main sequence stars. However one faint object (object *X* in Figure 10-2) appears right outside the *Chandra* error area. It is about $1''.5$ (3σ) away from the *Chandra* position and at the edge of the *Einstein* error circle. This is the only object ever detected near the error region (Mereghetti et al. 1996) other than star *A* and *B*. We measured its *J* magnitude: $J = 22.2 \pm 0.2$ and $K_s = 21.1 \pm 0.1$. Comparing its $J - K_s$ color and K_s magnitude to those of nearby objects, it is among other objects (see Figure 10-6) and it could be a high red-shift galaxy (Chen 2004, private communication). Therefore based on its position and magnitudes, object *X* probably is not the counterpart. The upper limits, without detection in the optical and other IR images, were derived and are given in Table 10.1.

10.4.3 RX J0822–4300 and RX J0852–4617

No near-IR object near the error circles was detected by our images for either target. In the images of RX J0852–4617, the closest object, object *Z* (see Figure 10-3; Pavlov et al., 2001), is about $4''$ away from the *Chandra* position. Its optical colors indicate that it is likely a G type main sequence star (Pavlov et al., 2001). The respective limiting magnitudes were given in Table 10.1

10.5 Discussion

If the object we find in the *Chandra* error circle is the counterpart of 1E 1614–5055 our observations may provide strong constraints on understanding its nature. Figure 10-7 shows the unabsorbed νL_ν from 1E 1614–5055, whose general shape is inconsistent with the spectrum from a black body $kT \sim 0.6$ keV (Gotthelf et al. 1997). In addition, the unabsorbed K_s band flux $\nu_{K_s} F_{\nu, K_s}^u \simeq 8.2 \times 10^{-14}$ erg cm⁻² s⁻¹ is much larger than the inferred infrared flux from the black-body model for 1E 1614–5055. This consequently excludes the thermal emission origin of the observed infrared flux. One possibility is XPSs are low mass X-ray binaries (LMXBs),

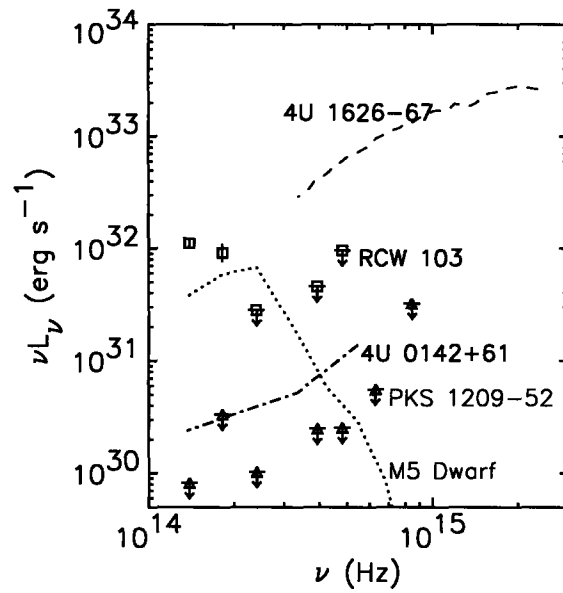


Figure 10-7 Unabsorbed energy spectra of 1E 1614-5055 and 1E 1207-5209. The squares are the values of 1E 1614-5055 derived with using distance = 3.3 kpc and $A_V = 4.5$, while the triangles are those of 1E 1207-5209 with using distance = 2.1 kpc and $A_V = 0.47$. Also plotted are those of M5 dwarf (dotted line), ultra-compact LMXB 4U 1626-67 (dashed line), and AXP 4U 0142+61 (dash-dotted line).

as suggested for 1E 1614–5055 (Becker & Aschenbach, 2002). In Figure 10-7, we show both the unabsorbed νL_ν from an M5 dwarf (Cox 2000; Bassell & Brett 1988) and the LMXB 4U 1626–67, where we use a distance of 3.2 kpc and $A_V = 0.3$ for 4U 1626–67 (Chapter 3.4.1). As seen in the figure, the J upper limits of 1E 1614–5055 is below the energy spectrum of an M5 star, and thus sets a strong constraint on the possible companion star. The LMXB 4U 1626–67 is an ultracompact binary with a white dwarf as the companion, and the optical emission from its accretion disk dominates (Chapter 3.4). By comparing the spectral shapes shown in Figure 10-7, it is unlikely that 1E 1614–5055 has an accretion disk similar to 4U 1626–67, because an accretion disk limited by the orbital size of an ultracompact LMXB should brighten the binary system in optical bands more than in infrared bands. For interesting comparison, we plot the energy spectrum from one anomalous X-ray pulsar (AXP) 4U 0142+61 (Hulleman, van Kerkwijk, & Kulkarni 2000) since they are another small group of pulsars showing different properties from “typical” pulsars (see Mereghetti 2002 for a review). As shown in Figure 10-7, the shapes of the energy spectra for the XPS and AXP are quite different. This may be evidence indicating that they are two different classes of neutron stars.

The XPS 1E 1207–5209 is a high Galactic latitude source ($l = 296^\circ 5, b = 9^\circ 9$). The low limit of the extinction to this source can be estimated by using the extinction caused by the Galactic disk (Schlegel et al. 1998). This gives $A_V \simeq 0.47$, which is consistent to the N_H value derived from X-ray observations (Mereghetti et al. 1996). We use this A_V value and the distance of 2.1 kpc (Giacani et al. 2000) to derive its unabsorbed νL_ν upper limits. Our observations are deep enough to exclude that 1E 1207–5209 has the similar optical emission to AXPs for the assumed distances. In addition, its upper limits are about one order of magnitude lower than those of 1E 1614–5055. Thus, if the XPSs are a uniform class of objects with very similar emission, we may have to suspect that our proposed counterpart to 1E 1614–5055 is not the real one. However, given that RCW 103 is different in its X-ray behavior than other XPSs, our observations could actually imply that the XPSs differ with each other substantially.

Chapter 11

Summary and Future Work

This thesis presents the studies of phenomena related to accretion disks in ultracompact low-mass X-ray binaries (LMXBs), in X-ray millisecond pulsars (MSPs), and around young neutron stars with strong X-ray emission.

11.1 Ultracompact LMXBs

Our studies of ultracompact LMXBs through both spectroscopy and time-resolved photometry have successfully verified the ultracompact nature of one candidate source, 4U 1543–624, and identified common spectral features of ultracompact sources. The absence of hydrogen lines in their optical spectra strongly supports the theoretical prediction that the mass donors are H-depleted. The lack of strong He lines, especially He II $\lambda 4686$ which is one of the prominent emission features for most “ordinary” LMXBs, probably indicates that the mass donors in our sources are helium-deficient white dwarfs, as suggested by the X-ray observations. Our work thus shows that optical spectroscopy may provide a means for discriminating ultracompact binary systems.

An interesting question about the origin of the N III lines in the $\lambda 4650$ blends, which were detected in every spectrum of our sources, is raised. These N III lines (see Figure 11-1) are believed to be produced by the Bowen Fluorescence (BF) process (McClintock et al. 1975; Kallman & McCray 1980) with He II Ly α photons

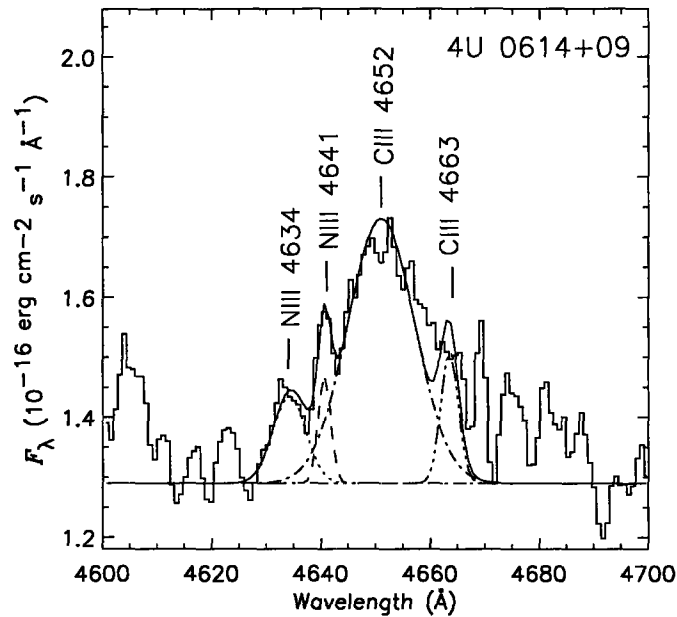


Figure 11-1 Resolved $\lambda\lambda 4640\text{--}4650$ C III/N III feature.

as the “seeds”, contrary to our suggestion that the mass donors in our sources are also helium-deficient. The follow-up high resolution spectroscopic observations were thus made recently, and our preliminary spectral analysis indicate a strong C III line and two relatively weak N III lines (Figure 11-1) in the $\lambda 4650$ blend of 4U 0614+09, distinguishing this source from other ordinary LMXBs which generally have the opposite in their optical spectra (Schachter et al. 1989). Further clarifications should be conducted by searching for the other Bowen lines such as the secondary O III lines between 3200-4000 Å in optical spectra of ultracompact sources. A non-detection of the O III lines would strongly support the exotic WD scenario for the binaries and challenge the conventional view that the N III lines are due to BF for every LMXB. This would also help establish our understanding of the possible evolutionary paths of these ultracompact sources.

11.2 X-ray MSPs

We have obtained interesting results from our intervention program carrying out follow-up optical/IR observations of X-ray millisecond (MSPs). However, since the X-ray monitoring program, which is successfully detecting X-ray MSPs, was designed to search for X-ray transients in the Galactic bulge region, high extinction along the source direction has made it difficult for our optical/IR identifications of the counterparts to the X-ray MSPs and limited any studies of the sources in quiescence. So far, the only X-ray MSP with identified quiescent counterpart is SAX J1808.4–3658. Our high quality Magellan image has shown the real optical counterpart which previous optical observations were not be able to resolve. Orbital-phase photometry of the binary system has been proposed by us, in an effort to derive its optical light curve and hence estimate its orbital inclination. As its mass function is known, any limit on its inclination would help identify its companion star by combining with multiband photometric measurements in quiescence. Several scenarios have been proposed for this system, which predicts different companion stars (see, e.g., Bildsten & Chakrabarty 2001; Nelson & Rappaport 2003). The identification would clarify these uncertainties, and thus help our understanding of the evolutionary scenarios for the X-ray MSPs.

11.3 Searching For Fallback Disks

Our program, searching for optical/IR counterparts to anomalous X-ray pulsars (AXPs) and the X-ray point sources (XPSs) with using Magellan telescopes, has successfully identified the IR counterpart to a third AXP of a group of 6 AXP sources. We made the first measurement of IR colors for these objects. Further observations made by other research groups demonstrated the IR variability of this source ($\Delta K_s > 1.3$ mag). The optical/IR measurements we made cannot rule out the accretion disk scenario; however, other evidence favors a “magnetar” scenario (neutron stars with extremely strong surface magnetic fields). For X-ray point sources (XPSs) in young supernova

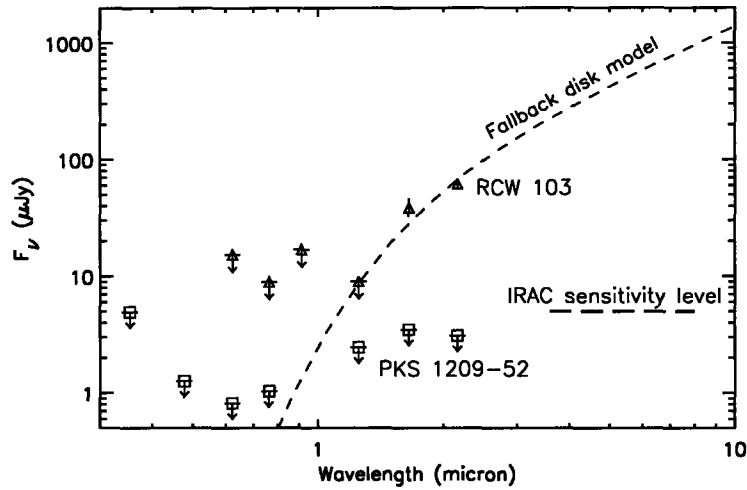


Figure 11-2 Dereddened fluxes and flux limits of RCW103 and PKS1209–52. Spectral fluxes from a fallback disk at a distance of 3.3 kpc (the distance of RCW103) is also shown, indicating strong emission in the mid-IR.

remnants (SNRs), we have likely identified the IR counterpart to 1E 1614–5055 in SNR RCW 103 and set strong constraints on the optical/near-IR flux densities of other XPSs. The near IR flux densities are consistent with a fallback disk with a mass of $10^{-4} M_{\odot}$ (Figure 11-2).

As theory predicts that fallback disks around young neutron stars should be strong mid/far-IR emitters, we are further obtaining mid-IR imaging of AXP and XPSs with using the Infrared Array Camera (IRAC) on board the *Spitzer Space Telescope*. The on-going imaging observations would verify if abnormal IR emission from the counterpart of 1E 1614–5055 is due to a fallback disk or not, thus potentially providing the first confirmed detection of fallback disks around young neutron stars in SNRs. In addition, combined with our optical and near-IR data, the observations would give strong constraints or detections of fallback disks.

Appendix A

FUV spectrum of the Ultracompact LMXB 4U 1820-30

The source 4U 1820–30 has the shortest orbital period, $P = 685$ s (Stella et al., 1987), among the known LMXBs. Its companion star is probably a $0.06\text{--}0.08 M_{\odot}$, hydrogen-exhausted white dwarf (Rappaport et al. 1987).

The far-ultraviolet (FUV) spectral data were extracted from the *HST* archive service. The *HST* observations were made on 1998 March 14 using the STIS (Woodgate et al. 1998). A low-resolution grating G140L was used, providing a FUV wavelength coverage of 1150–1730 Å. The aperture was a 52×0.5 arcsec² long slit. The data were taken in TIME-TAG mode with using the solar-blind CsI multi-anode microchannel array (STIS/FUV-MAMA) detector. The TIME-TAG mode allows to record the position and detection time of every photon. The timing analysis of the data is reported in Chapter 8.

The spectrum is presented in Figure A-1 with the identified lines indicated. It is interesting to note that all these lines are interstellar medium absorption lines (see, e.g., Cox 2000). Comparing it to the FUV spectrum of 4U 1626–67, which shows strong C/O emission lines, it is puzzling that no emission lines were detected in the 4U 1820–30 spectrum. Using the Ly α λ 1216 absorption line (Diplas & Savage 1994; Chapter 3.3.1), we obtained the H column density to the source $N(\text{H I}) = (1.1 \pm 0.4) \times 10^{21} \text{ cm}^{-2}$ (Figure A-2).

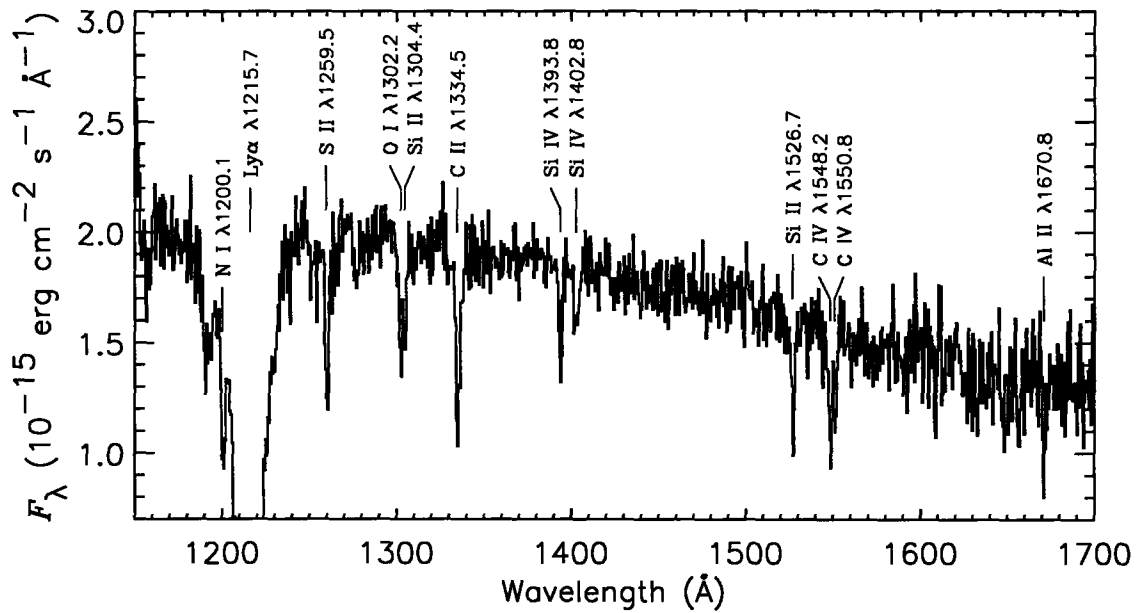


Figure A-1 *HST/STIS* FUV spectrum of the ultracompact LMXB 4U 1820–30. The identified lines are due to interstellar medium absorption.

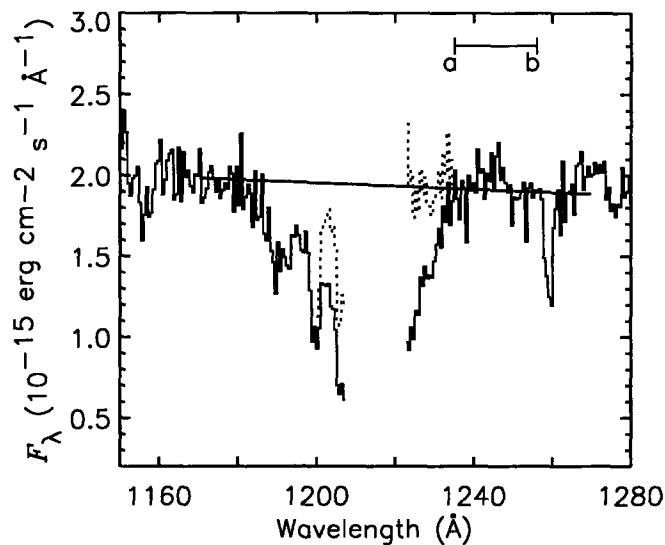


Figure A-2 Reconstruction of Ly α λ 1216 absorption line. The solid line is the estimated continuum over the Ly α while the dotted curve is the reconstructed spectrum. Following the method of Diplás & Savage (1994a), the spectral region marked between a and b was used for deriving the noise level in the continuum.

Bibliography

- Anderson, S.F., et al. (1997). Time-Resolved Ultraviolet Observations of the Globular Cluster X-Ray Source in NGC 6624: The Shortest Known Period Binary System. *The Astrophysical Journal*, **482**, L69.
- Alpar, M. A., Cheng, A. F., Ruderman, M. A., & Shaham, J. (1982). A new class of radio pulsars. *Nature*, **300**, 728.
- Angelini, L., White, N. E., Nagase, F., Kallman, T. R., Yoshida, A., Takeshima, T., Becker, C. M., & Paerels, F. (1995). Neon Line Emission in the X-Ray Spectrum of the Pulsar 4U 1626-67. *The Astrophysical Journal*, **449**, L41.
- Arons, J. & King, I. R. (1993). A reprocessing model for the ultraviolet and optical light from 4U 1820-30. *The Astrophysical Journal*, **413**, L121.
- Asai, K., Dotani, T., Nagase, F., & Mitsuda, K. (2000). Iron K Emission Lines in the Energy Spectra of Low-mass X-ray Binaries Observed with ASCA. In *The Astrophysical Journal Supplement Series*. **131**, 571
- Aschenbach, B., Iyudin, A. F., & Schönfelder, V. (1999). Constraints of age, distance and progenitor of the supernova remnant RX J0852.0-4622/GRO J0852-4642. *Astronomy and Astrophysics*, **350**, 997.
- Augusteijn, T., et al. (1997). ROSAT Position of GRO J1744-28 and Search for Its Near-Infrared Counterpart. *The Astrophysical Journal*, **486**, 1013.
- Baldwin, J. A., Verner, E. M., Verner, D. A., Ferland, G. J., Martin, P. G., Korista, K. T., & Rubin, R. H. (2000). High-Resolution Spectroscopy of Faint Emission Lines in the Orion Nebula. *The Astrophysical Journal Supplement Series*, **129**, 229.
- Baykal, A., Strohmayer, T., Swank, J., Alpar, M. A., & Stark, M. J. (2000). Differences between the two anomalous X-ray pulsars: variations in the spin-down rate of 1E 1048.1-5937 and an extended interval of quiet spin-down in 1E 2259+586. *Monthly Notices of the Royal Astronomical Society*, **319**, 205.
- Becker, W. & Aschenbach, B. (2002). X-ray Observations of Neutron Stars and Pulsars: First Results from XMM-Newton. In *Neutron Stars, Pulsars and Supernova Remnants*. Becker, W., Lesch, H., & Trümper, J., Editors. Bad Honnef, 64.

- Bessell, M. S. & Brett, J. M. (1988). JHKLM photometry - Standard systems, passbands, and intrinsic colors. *The Publications of the Astronomical Society of the Pacific*, **100**, 1134.
- Bhattacharya, D. & van den Heuvel, E.P.J. (1991). Formation and evolution of binary and millisecond radio pulsars. *Physics Reports*, **203**, 1.
- Bignami, G. F., Caraveo, G. A., & Mereghetti, S. (1992). On the optical counterpart of 1E 1207.4-5209, the central X-ray source of a ring-shaped supernova remnant. *The Astrophysical Journal*, **389**, L67
- Bildsten, L. (2002). Hot white dwarf donors in ultracompact X-ray Binaries. *The Astrophysical Journal*, **577**, L27
- Bildsten L. & Chakrabarty, D. (2001). A Brown Dwarf Companion for the Accreting Millisecond Pulsar SAX J1808.4-3658. *The Astrophysical Journal*, **557**, 292
- Blum, R. D., Sellgren, K., & DePoy, D. L. (1996). JHKL Photometry and the K-Band Luminosity Function at the Galactic Center. *The Astrophysical Journal*, **470**, 864.
- Bohlin R. C. (1975). Copernicus observations of interstellar absorption at Lyman alpha. *The Astrophysical Journal*, **200**, 402.
- Bowen, I. S. (1934). The Excitation of the Permitted O III Nebular Lines. *The Publications of the Astronomical Society of the Pacific*, **46**, 146.
- Bowen, I. S. (1935). The Spectrum and Composition of the Gaseous Nebulae. *The Astrophysical Journal*, **81**, 1.
- Brandt, S., Castro-Tirado, A. J., Lund, N., Dremin, V., Lapshov, I., & Syunyaev, R. (1992). *Astronomy and Astrophysics*, **262**, 15.
- Brazier, K. T. S. & Johnston, S. (1999). The implications of radio-quiet neutron stars. *Monthly Notices of the Royal Astronomical Society*, **305**, 671
- Brown, T., et al. (2002). In HST STIS Data Handbook, version 4.0, Mobasher, B. editor.
- Callanan, P. J., Grindlay, J. E., Cool, A. M. (1995). Optical Observations of 4U 1915-05, and the Stability of the Long Term Ephemeris. *Publication of the Astronomical Society of Japan*, **47**, 153.
- Canizares, C. R., McClintock, J. E., & Grindlay, J. E. (1979). A spectroscopic study of the optical counterparts of three X-ray bursters. *The Astrophysical Journal*, **234**, 556.
- Cardelli, J. A., Clayton, G. C., & Mathis, J. S. (1989) The relationship between infrared, optical, and ultraviolet extinction. *The Astrophysical Journal*, **345**, 245.

- Casswell, J. L., Murray, J. D., Roger, R. S., Cole, D. J., & Cooke, D. J. (1975). Neutral hydrogen absorption measurements yielding kinematic distance for 42 continuum sources in the galactic plane. *Astronomy and Astrophysics*, **45**, 239
- Chakrabarty, D. (1998). High-Speed Optical Photometry of the Ultracompact X-ray Binary 4U 1626-67. *The Astrophysical Journal*, **492**, 342
- Chakrabarty, D. & Morgan, E. H. (1998). The two-hour orbit of a binary millisecond X-ray pulsar. *Nature*, **394**, 346
- Chakrabarty, D., Homer, L., Charles, P. A., & O'Donoghue, D. (2001). Millihertz Optical/Ultraviolet Oscillations in 4U 1626-67: Evidence for a Warped Accretion Disk. *The Astrophysical Journal*, **562**, 985
- Chakrabarty, D., Pivovarov, M., Hernquist, L. E., Heyle, J., & Narayan, R. (2001). The Central X-ray Point Source in Cassiopeia A. *The Astrophysical Journal*, **548**, 800.
- Chakrabarty, D., et al. (1997). Torque Reversal and Spin-down of the Accretion-powered Pulsar 4U 1626-67. *The Astrophysical Journal*, **474**, 414.
- Chatterjee, P., Hernquist, L., & Narayan, R. (2000). An Accretion Model for Anomalous X-ray Pulsars. *The Astrophysical Journal*, **534**, 373.
- Chevalier, C. & Ilovaisky, S. A. (1985). Optical Identifications of Faint X-ray Sources - New CCD Candidates for 0918-549 1822-00 and 1905-000. *Space Science Review*, **40**, 443
- Chou, Y., & Grindlay, J. E. (2001). Binary and Long-Term (Triple?) Modulations of 4U 1820-30 in NGC 6624. *The Astrophysical Journal*, **563**, 934.
- Chou, Y., Grindlay, J. E., & Bloser, P. F. (2001). Timing Analysis of the Light Curve of the Dipping-Bursting X-Ray Binary X1916-053. *The Astrophysical Journal*, **549**, 1135.
- Christian, D.J., & Swank, J.H. (1997). The Survey of Low-mass X-ray Binaries with the Einstein Observatory Solid-state Spectrometer and Monitor Proportional Counter. *The Astrophysical Journal Supplement Series*. **109**, 177
- Cole, D. M., et al. (1997). Optical/Near-Infrared Observations of GRO J1744-28. *The Astrophysical Journal*, **480**, 377.
- Corbet, R. H. D. & Day, C. S. R. (1990). GINGA observations of the 6-s X-ray pulsar 1E 1048.1-5937. *Monthly Notices of the Royal Astronomical Society*, **243**, 553.
- Corbet, R. H. D. & Mihara, T. (1997). The Spin-down Rate and X-ray Flux of 1E 1048.1-5937. *The Astrophysical Journal*, **475**, L127.
- Cotera, A. S., Simpson, J. P., Erickson, P. S., Colgan, S. W. J., Burton, M., & Allen, D. A. (2000). Interstellar Extinction in the Vicinity of the Galactic Center. *The Astrophysical Journal Supplement Series*, **129**, 123.

- Cowley, A. P., Crampton, D., & Hutchings, J. B. (1982). A model for 0921-63 - A second halo X-ray source. *The Astrophysical Journal*, **256**, 605.
- Cowley, A.P., Hutchings, J.B., & Crampton D. (1988). Spectroscopy and kinematics of the low-mass X-ray binaries. *The Astrophysical Journal*, **333**, 906.
- Cox, A. N. (2000). *Allen's Astrophysical Quantities*, 4th ed. New York: Springer.
- Cunningham, C. (1976). Returning radiation in accretion disks around black holes. *The Astrophysical Journal*, **208**, 534
- Daigne, F., Goldoni, P., Ferrando, P., Goldwurm, A., Decourchelle, A., & Warwick, R. S. (2002). XMM-Newton observation of the bursting pulsar GRO J1744-28 in quiescence. *Astronomy and Astrophysics*, **386**, 531.
- Daumerie, P., Kalogera, V., Lamb, F. K., & Psaltis, D. (1996). A strongly magnetic neutron star in a nearly face-on binary system. *Nature*, **382**, 141.
- Davidson, A., Malina, R., Smith, H., Spinrad, H., Margon, B., Mason, K., Hawkins, F., & Sanford, P. (1974). Optical and X-ray observations of 3U 0614+09. *The Astrophysical Journal*, **193**, L25.
- de Jong, J. A., van Paradijs, J., & Augusteijn, T. (1996). Reprocessing of X-rays in low-mass X-ray binaries. *Astronomy and Astrophysics*, **314**, 484
- Deguchi, S. (1985). Bowen fluorescence mechanism in X-ray binaries. *The Astrophysical Journal*, **291**, 492.
- Deloye, C.J., & Bildsten L. (2003). White Dwarf Donors in Ultracompact Binaries: The Stellar Structure of Finite-Entropy Objects. *The Astrophysical Journal*, **598**, 1217
- Depoy, D., Atwood, B., Byard, P. L., Frogel, J., & O'Brien, T. P. (1993). Ohio State Infrared Imager/Spectrometer (OSIRIS). *Proc. SPIE*, **1946**, 667
- Deutsch, E. W., Margon, B., & Anderson, S. F. (2000). Ultracompact X-ray Binaries in Globular Clusters: Variability of the Optical Counterpart of X1832-330 in NGC 6652. *The Astrophysical Journal*, **530**, L21
- Diplas, A. & Savage, B. D. (1994). An IUE survey of interstellar H I LY alpha absorption. 1: Column densities. *The Astrophysical Journal Supplement Series*, **93**, 211.
- Diplas, A. & Savage, B. D. (1994). An IUE survey of interstellar H I LY alpha absorption. 2: Interpretations. *The Astrophysical Journal*, **427**, 274.
- Eggleton, P. P. (1983). Approximations of the radii of Roche lobes. *The Astrophysical Journal*, **268**, 368.
- Fahlman, G. G., & Gregory, P. C. (1981). An X-ray pulsar in SNR G109.1-1.0. *Nature*, **293**, 695.

- Fan, X. (1999). Simulation of Stellar Objects in SDSS Color Space. *The Astronomical Journal*, **117**, 2528.
- Farinelli, R., et al. (2003). BeppoSAX observations of two unclassified LMXBs: X1543-624 and X1556-605. *Astronomy and Astrophysics*, **402**, 1021.
- Fender, R. (2001). Energetics of jets from X-ray binaries. In *Microquasars*, Castro-Tirado, A. J., Greiner, J., & Paredes, J. M., Editors. Dordrecht: Kluwer, astro-ph/0010613.
- Finger, M. H., Koh, D. T., Nelson, R. W., Prince, T. A., Vaughan, B. A., & Wilson, R. B. (1996). Discovery of hard X-ray pulsations from the transient source GRO J1744-28. *Nature*, **381**, 291.
- Fishman, G. J., et al. (1995). *International Astronomical Union Circular*, **6338**.
- Fitzpatrick, E. L. (1999). Correcting for the Effects of Interstellar Extinction. *The Publications of the Astronomical Society of the Pacific*, **111**, 63.
- Frank, J., King, A., & Raine, D. (1992). *Accretion Power in Astrophysics*. 2nd ed., Cambridge: Cambridge Univ. Press.
- Fukugita, M. et al. (1996). The Sloan Digital Sky Survey Photometric System. *The Astronomical Journal*, **111**, 1748.
- Gaensler, B. M., Stappers, B. W., & Getts, T. J. (1999). Transient Radio Emission from SAX J1808.4-3658. *The Astrophysical Journal*, **522**, L117.
- Garmire, G. P., Pavlov, G. G., Garmire, A. B., & Zavlin, V. E. (2000). *International Astronomical Union Circular*, **7350**.
- Gavriil, F. P., Kaspi, V. M., Woods, P. M. (2002). Magnetar-like X-ray bursts from an anomalous X-ray pulsar. *Nature*, **419**, 142.
- Giacani, E. B., Dubner, G. M., Green, A. J., Goss, W. M., & Gaensler, B. M. (2000). The Interstellar Matter in the Direction of the Supernova Remnant G296.5+10.0 and the Central X-ray Source 1E 1207.4-5209. *The Astrophysical Journal*, **119**, 281.
- Giacconi, R., Murray, S., Gursky, H., Kellogg, E., Schreier, E., Matilsky, T. Koch, D., & Tananbaum, H. (1974). The Third UHURU catalog of X-ray sources. *The Astrophysical Journal Supplement Series*, **27**, 37.
- Giles, A. B., Hill, K. M., & Greenhill, J. G. (1999). The optical counterpart of SAX J1808.4-3658, the transient bursting millisecond X-ray pulsar. *Monthly Notices of the Royal Astronomical Society*, **304**, 47.
- Giles, A. B., Swank, J. H., Jahoda, K., Zhang, W., Strohmayer, T., Stark, M. J., & Morgan, E. H. (1996). The Main Characteristics of GRO J1744-28 Observed by the Proportional Counter Array Experiment on the Rossi X-Ray Timing Explorer. *The Astrophysical Journal*, **469**, L25.

- Gilfanov, M., Revnivtsev, M., Sunyaev, R., & Churazov, E. (1998). The millisecond X-ray pulsar/burster SAX J1808.4-3658: the outburst light curve and the power law spectrum. *Astronomy and Astrophysics*, **338**, L83.
- Ghosh, P. & Lamb, F. K. (1979a). Accretion by rotating magnetic neutron stars. II - Radial and vertical structure of the transition zone in disk accretion. *The Astrophysical Journal*, **232**, 259.
- Ghosh, P. & Lamb, F. K. (1979b). Accretion by rotating magnetic neutron stars. III - Accretion torques and period changes in pulsating X-ray sources. *The Astrophysical Journal*, **234**, 296.
- Ghosh, P., Lamb, F. K., & Pethick, C. J. (1977). Accretion by rotating magnetic neutron stars. I - Flow of matter inside the magnetosphere and its implications for spin-up and spin-down of the star. *The Astrophysical Journal*, **217**, 578.
- Gotthelf, E. V., Petre, R., & Hwang, U. (1997). The Nature of the Radio-quiet Compact X-ray Source in SNR RCW 103. *The Astrophysical Journal*, **487**, L175.
- Gotthelf, E. V., Petre, R., & Vasishth, G. (1999). X-ray Variability from the Compact Source in the Supernova Remnant RCW 103. *The Astrophysical Journal*, **514**, L107
- Grindlay, J. E. (1988). X-ray binaries in globular clusters. In *IAU Symp. 126, Globular Cluster System in Galaxies*, Grindlay, J. E. & Philip, A. G. D., editors. Dordrecht: Reidel, 347.
- Grindlay, J. E., Hertz, P., Steiner, J. E., Murray, S. S., Lightman, A. P. (1984). Determination of the mass of globular cluster X-ray sources. *The Astrophysical Journal*, **282**, L13.
- Grindlay, J. E., Bailyn, C. D., Cohn, H., Lugger, P. M., Thorstensen, J. R., Wegner, G. (1988). Discovery of a possible X-ray triple - 4U 1915-05. *The Astrophysical Journal*, **334**, L25.
- Haswell, C. A., King, A. R., Murray, J. R., & Charles, P. A. (2001). Superhumps in low-mass X-ray binaries. *Monthly Notices of the Royal Astronomical Society*, **321**, 475.
- Helfand, D. J. & Becker, R. H. (1984). Observation of stellar remnants from recent supernovae. *Nature*, **307**, 215.
- Homer, L., Anderson, S.F., Wachter, S., & Margon, B. (2002). The Ultraviolet Spectrum of the Ultracompact X-Ray Binary 4U 1626-67. *The Astronomical Journal*, **124**, 3348.
- Homer, L., Charles, P. A., Chakrabarty, D., & van Zyl, L. (2001). The optical counterpart to SAX J1808.4-3658: observations in quiescence. *Monthly Notices of the Royal Astronomical Society*, **325**, 1471.

- Homer, L., Charles, P. A., Hakala, P., Muhli, P., Shih, I.-C., Smale, A. P., Ramsay, G. (2001). On the multi-periodicities in the X-ray dipper XB1916-053. *Monthly Notices of the Royal Astronomical Society*, **bfv322**, 827.
- Hulleman, F., van Kerkwijk, M. H., & Kulkarni, S. R. (2000). An optical counterpart to the anomalous X-ray pulsar 4U0142+61. *Nature*, **408**, 689.
- Hulleman, F., Tennant, A. F., van Kerkwijk, M. H., Kulkarni, S. R., Kouveliotou, C., & Patel, S. K. (2001). A Possible Faint Near-Infrared Counterpart to the Anomalous X-ray Pulsar 1E 2259+586. *The Astrophysical Journal*, **563**, L49.
- in 't Zand, J. J. M., Heise, J., Muller, J. M., Bazzano, A., Cocchi, M., Natalucci, L., & Ubertini, P. (1998). Discovery of the X-ray transient SAX J1808.4-3658, a likely low-mass X-ray binary. *Astronomy and Astrophysics*, **331**, L25
- in 't Zand, J. J. M. et al. (2001). The first outburst of SAX J1808.4-3658 revisited. *Astronomy and Astrophysics*, **372**, 916
- Israel, G. L., Mereghetti, S., Stella, L. (1994). The Discovery of 8.7 second pulsations from the ultrasoft X-ray source 4U 0142+61. *The Astrophysical Journal*, **433**, L25.
- Israel G., Mereghetti, S., & Stella, L. (2001). Observations of Anomalous X-ray Pulsars. In *Soft Gamma Repeaters: The Rome 2000 Mini-workshop*. Editors, Feroci M. and Mereghetti S. in press (astro-ph/0111093).
- Jerkins, E.B. (1971). A Closer Look at Interstellar Lyman-Alpha Absorption. *The Astrophysical Journal*, **169**, 25.
- Jonker, P. G., et al. (2003). A search for the optical and near-infrared counterpart of the accreting millisecond X-ray pulsar XTE J1751–305. *Monthly Notices of the Royal Astronomical Society*, **344**, 201
- Joss, P. C. & Rappaport, S. A. (1983). On the origin of the 6.1-ms pulsar. *Nature*, **304**, 419.
- Joss, P. C., Avni, Y., & Rappaport, S. (1978). Accreting neutron stars in highly compact binary systems and the nature of 3U 1626-67. *The Astrophysical Journal*, **221**, 645.
- Juett, A.M., & Chakrabarty, D. (2003). The X-ray Spectroscopy of the Low-Mass X-ray Binaries 2S 0918-549 and 4U 1543-624: Evidence for Neon-rich Degenerate Donors. *The Astrophysical Journal*, **599**, 498.
- Juett, A.M., Psaltis, D., & Chakrabarty, D. (2001). Ultracompact X-ray Binaries with Neon-rich Degenerate Donors. *The Astrophysical Journal*, **560**, L59.
- Juett, A. M., Marshall, H. L., Chakrabarty, D., & Schulz, N. S. (2002). Chandra High-Resolution Spectrum of the Anomalous X-ray Pulsar 4U 0142+61. *The Astrophysical Journal*, **568**, L31.

- Kallman, T. R., & McCray R. (1980). Efficiency of the Bowen fluorescence mechanism in static nebulae. *The Astrophysical Journal*, **242**, 615.
- Kallman, T. R., Raymond, J. C., & Vrtilik, S. D. (1991). The ultraviolet spectrum of Scorpius X-1 as observed by IUE - 1978-1988. *The Astrophysical Journal*, **370**, 717.
- Kaspi, V. M. & Gavriil, F. P. (2002). *International Astronomical Union Circular*, **7924**.
- Kaspi, V. M., Gavriil, F. P., Chakrabarty, D., Lackey, J. R., & Muno, M. (2001). Long-Term Rossi X-ray Timing Explorer Monitoring of the Anomalous X-ray Pulsar 1E 1048.1-5937. *The Astrophysical Journal*, **558**, 253.
- Kazarovets, E. V., Samus, N. N., & Durlevich, O. V. (2000). *Information Bulletin on Variable Stars*, **4870**, 1.
- Kern, B. & Martin, C. (2002). Optical pulsations from the anomalous X-ray pulsar 4U0142+61. *Nature*, **417**, 527.
- Kim Quijano, J., et al. (2003). STIS Instrument Handbook, Version 7.0, (Baltimore: STScI).
- Ko, Y. K., & Kallman T. R. (1994). Emission lines from X-ray-heated accretion disks in low-mass X-ray binaries. *The Astrophysical Journal*, **431**, 273.
- Krauss, M. I., Dullighan, A., Chakrabarty, D., van Kerkwijk, M. H., & Markwardt, C. B. (2003). *International Astronomical Union Circular*, **8154**.
- Krauss, M. I., et al. (2004). in preparation.
- Lampton, M., Margon, B., & Bowyer, S. (1976). Parameter estimation in X-ray astronomy. *The Astrophysical Journal*, **208**, 177.
- Landolt, A. U. (1992). UBVRI photometric standard stars in the magnitude range 11.5-16.0 around the celestial equator. *The Astronomical Journal*, **104**, 340.
- Leahy, D.A., Darbro, W., Elsner, R.F., Weisskopf, M.C., Sutherland, P.G., Kahn, S., & Grindlay, J.E. (1983). On searches for pulsed emission with application to four globular cluster X-ray sources - NGC 1851, 6441, 6624, and 6712. *The Astrophysical Journal*, **266**, 160.
- Leibowitz, E. M. & Danziger, I. J. (1983). Spectrophotometry in the galactic supernova remnants RCW 86, 103 and Kepler. *Monthly Notices of the Royal Astronomical Society*, **204**, 273.
- Levine, A., Ma, C. P., McClintock, J., Rappaport, S., van der Klis, M., & Verbunt, F. (1988). 4U 1626-67 - The binary with the smallest known mass function. *The Astrophysical Journal*, **327**, 732.

- Liu, Q. Z., van Paradijs, J., & van den Heuvel, E. P. J. (2001). A catalogue of low-mass X-ray binaries. *Astronomy and Astrophysics*, **368**, 1021.
- Lubow, S. H. (1991). A model for tidally driven eccentric instabilities in fluid disks. *The Astrophysical Journal* **381**, 259.
- Machin, G., et al. (1990). Optical and X-ray Observations of 4U: 0614+09. *Monthly Notices of the Royal Astronomical Society*, **247**, 205.
- Markwardt, C. B. & Swank, J. H. (2003). *International Astronomical Union Circular*, **8144**.
- Markwardt, C. B., Smith, E., & Swank, J.H. (2003). *International Astronomical Union Circular*, **8080**.
- Markwardt, C. B., Swank, J. H., Strohmayer, T. E., Zand, J. J. M. I., & Marshall, F. E. (2002). Discovery of a Second Millisecond Accreting Pulsar: XTE J1751-305. *The Astrophysical Journal*, **575**, L21.
- Marshall, F. E. (1998). *International Astronomical Union Circular*, **6876**.
- Martini, P., et al. (2004). PANIC: A Near-infrared Camera for the Magellan Telescopes. Astro-ph/0406666.
- Matsui, Y., Long, K. S., Tuohy, I. R. (1988). X-ray imaging observation of the supernova remnant PKS 1209-52 and its central compact X-ray source. *The Astrophysical Journal*, **329**, 838.
- Mazeh, T., & Shaham, J. (1979). The orbital evolution of close triple systems - The binary eccentricity. *Astronomy and Astrophysics*, **77**, 145.
- McClintock, J. E., Canizares, C. R., Tarter, C. B. (1975). On the origin of 4640-4650 A emission in X-ray stars. *The Astrophysical Journal*, **198**, 641.
- McClintock, J. E., Canizares, C. R., Hiltner, W. A., & Petro. L. (1978). Optical Candidates for Two X-ray Sources. *International Astronomical Union Circular*, **3251**.
- McClintock, J. E., Canizares, C. R., Bradt, H. V., Doxsey, R. E., Jernigan, J. G., & Hiltner, W. A. (1977). Optical candidates for two X-ray bursters and an X-ray pulsar. *Nature*, **270**, 320.
- McMillan, S., Hut, P., & Makino, J. (1991). Star cluster evolution with primordial binaries. II - Detailed analysis. *The Astrophysical Journal*, **371**, 111.
- Mereghetti, S. (1995). A Spin-down Variation in the 6 Second X-Ray Pulsar 1E 1048.1-5937. *The Astrophysical Journal*, **455**, 598.
- Mereghetti, S. (2001). The X-ray Sources at the Center of the Supernova Remnant RX J0852.0-4622. *The Astrophysical Journal*, **548**, L213.

- Mereghetti, S., Bignami, G. F., & Caraveo, P. A. (1996). The X-ray Source at the Center of G296.5+10.0 as a Young Isolated Neutron Star. *The Astrophysical Journal*, **464**, 842.
- Mereghetti, S., Caraveo, P., & Bignami, G.F. (1992). CCD imaging and spectroscopy in the field of the X-ray pulsar 1E 1048.1-5937. *Astronomy and Astrophysics*, **263**, 172.
- Mereghetti, S., Chiarlone, L., Israel, G. L., & Stella, L. (2002). The Anomalous X-ray Pulsars. In *Neutron Stars, Pulsars, and Supernova Remnants*, Becker, W., Lesch, H., & Trümper, J., Editors. Bad Honnef, in press. astro-ph/0205122.
- Mereghetti, S., Israel, G. L., & Stella, L. (1998). New limits on the orbital parameters of 1E 1048.1-5937 and 1E 2259+586 from RXTE observations. *Monthly Notices of the Royal Astronomical Society*, **296**, 689.
- Middleditch, J., Mason, K. O., Nelson, J. E., & White, N. E. (1981). 4U 1626-67 - A prograde spinning X-ray pulsar in a 2500 S binary system. *The Astrophysical Journal*, **244**, 1001.
- Monet, D. E. A., et al. (1998). A catalogue of astrometric standards. In *The PMM USNO-A2.0 Catalog*. U.S. Naval Observatory, Washington DC.
- Morgan, E. H., Remillard, R. A., & Garcia, M. R. (1988). SAS 3 and Einstein observations of the 11 minute orbital period of the globular cluster X-ray source 4U 1820-30. *The Astrophysical Journal*, **324**, 851.
- Motch, C. & Pakull, M. W. (1989). The strength of N III-C III complex emission in low-mass X-ray binaries as a possible indicator of metallicity. *Astronomy and Astrophysics*, **214**, 1.
- Murdin, P., et al. (1974). Optical observations of stars near Copernicus X-ray positions. *Monthly Notices of the Royal Astronomical Society*, **169**, 25.
- Nagata, t., Woodward, C. E., Shure, M., Kobayashi, N. (1995). Object 17: Another cluster of emission-line stars near the galactic center. *The Astronomical Journal*, **109**, 1676.
- Nelemans, G., Jonker, P.G., Marsh, T.R., & van der Klis, M. (2004). Optical spectra of the carbon-oxygen accretion discs in the ultra-compact X-ray binaries 4U 0614+09, 4U 1543-624 and 2S 0918-549. *Monthly Notices of the Royal Astronomical Society*, **348**, L7.
- Nelson, L. A., & Rappaport, S. A. (2003). Theoretical Considerations on the Properties of Accreting Millisecond Pulsars. *The Astrophysical Journal*, **598**, 431.
- Nelson, L.A., Rappaport, S.A. & Joss P.C. (1986). The evolution of very low mass stars. *The Astrophysical Journal*, **304**, 231.

- Nishiuchi, M., et al. (1999). ASCA Observations of GRO J1744-28. *The Astrophysical Journal*, **517**, 436.
- O'Donoghue, D., & Charles, P. (1996). Have superhumps been seen in black hole soft X-ray transients? *Monthly Notices of the Royal Astronomical Society*, **282**, 191.
- Oosterbroek, T., Parmar, A. N., Mereghetti, S., & Israel, G. L. (1998). The two-component X-ray spectrum of the 6.4 pulsar 1E 1048.1-5937. *Astronomy and Astrophysics*, **334**, 925.
- Orlandini, M. et al. (1998). BEPPOSAX Observation of 4U 1626-67: Discovery of an Absorption Cyclotron Resonance Feature. *The Astrophysical Journal*, **500**, L163.
- Osterbrock, D. E. & Martel, A. (1992). Sky spectra at a light-polluted site and the use of atomic and OH sky emission lines for wavelength calibration. *The Publications of the Astronomical Society of the Pacific*, **104**, 760.
- Özel, F., Psaltis, D., & Kaspi, V. M. (2001). Constraints on Thermal Emission Models of Anomalous X-ray Pulsars. *The Astrophysical Journal*, **563**, 255.
- Parmar, A. N., White, N. E., Giommi, P., & Gottwald, M. (1986). The discovery of 3.8 hour periodic intensity dips and eclipses from the transient low-mass X-ray binary EXO 0748-676. *The Astrophysical Journal*, **308**, 199.
- Patel, S. K., et al. (2001). Chandra Observations of the Anomalous X-ray Pulsar 1E 2259+586. *The Astrophysical Journal*, **563**, L45.
- Patterson, J. (1998). Late Evolution of Cataclysmic Variables. *The Publications of the Astronomical Society of the Pacific*, **110**, 1132.
- Patterson, J. (2001). Accretion-Disk Precession and Substellar Secondaries in Cataclysmic Variables. *The Publications of the Astronomical Society of the Pacific*, **113**, 736.
- Paul, B., Kawasaki, M., Dotani, T., & Nagase, F. (2000). Study of the Long-Term Stability of Two Anomalous X-ray Pulsars, 4U 0142+61 and 1E 1048.1-5937, with ASCA. *The Astrophysical Journal*, **537**, 319.
- Pavlov, G. G., Zavlin, V. E., & Trümper, J. (1999). X-ray Pulsations from the Central Source in Puppis A. *The Astrophysical Journal*, **511**, L45.
- Pavlov, G. G., Sanwal, D., Kiziltan, B., & Garmire, G. P. (2001). The Compact Central Object in the RX J0852.0-4622 Supernova Remnant. *The Astrophysical Journal*, **531**, L131.
- Pavlov, G. G., Sanwal, D., Garmire, G. P., & Zavlin, V. E. (2002). Central Compact Objects in Supernova Remnants. In *Neutron Stars in Supernova Remnants*, Slane, P. O. & Gaensler B. M. editors. San Francisco: ASP, 247.

- Pavlov, G. G., Zavlin, V. E., Sanwal, D., & Trümper, J. (2002). 1E 1207.4-5209: The Puzzling Pulsar at the Center of the Supernova Remnant PKS 1209-51/52. *The Astrophysical Journal*, **569**, L95
- Paczynski, B. (1967). Gravitational Waves and the Evolution of Close Binaries. *Acta Astronomica*, **17**, 287.
- Paczynski, B. (1981). Evolution of cataclysmic binaries. *Acta Astronomica*, **31**, 1.
- Paczynski, B., & Sienkiewicz, R. (1981). Gravitational radiation and the evolution of cataclysmic binaries. *The Astrophysical Journal*, **248**, L27.
- Percival, W., Charles, P., Kuulkers, E., Miller, L., Shahbaz, T., McLure, R., & Dunlop, J. (1998). *International Astronomical Union Circular*, **6902**.
- Perna, R., Hernquist, L., & Narayan, R. (2000). Emission Spectra of Fallback Disks Around Young Neutron Stars. *The Astrophysical Journal*, **541**, 344.
- Persson, S. E., Murphy, D. C., Krzeminski, W., Roth, M., & Rieke, M. J. (1998). A New System of Faint Near-Infrared Standard Stars. *The Astronomical Journal*, **116**, 2475.
- Persson, S. E., Phillips, M., Roth, M., & Birk, C. (2001). "Classic Cam" Near-IR Camera. Users Manual, Las Campanas Observatory, La Serena, Chile.
- Persson, S. E., West, S. C., Carr, D. M., Sivaramakrishnan, A., & Murphy, D. C. (1992). A near-infrared camera for Las Campanas Observatory. *Publications of the Astronomical Society of the Pacific*, **104**, 204.
- Petre, R., Becker, C.M., & Winkler, P.F. (1996). A Central Stellar Remnant in Puppis A. *The Astrophysical Journal*, **465**, L43.
- Petre, R., Kriss, G. A., Winkler, P. F., & Canizares, C. R. (1982). A high-resolution X-ray image of Puppis A - Inhomogeneities in the interstellar medium. *The Astrophysical Journal*, **258**, 22.
- Podsiadlowski, P., Rappaport, S., & Pfahl, E.D. (2002). Evolutionary Sequences for Low- and Intermediate-Mass X-ray Binaries. *The Astrophysical Journal*, **565**, 1107.
- Podsiadlowski, P., Han, Z, & Rappaport, S. (2003). Cataclysmic variables with evolved secondaries and the progenitors of AM CVn stars. *Monthly Notices of the Royal Astronomical Society*, **340**, 1214.
- Priedhorsky, W., & Terrell, J. (1984). Discovery of a 176 day period in 4U 1820-30. *The Astrophysical Journal*, **284**, L17.
- Psaltis, D. & Chakrabarty, D. (1999). The Disk-Magnetosphere Interaction in the Accretion-powered Millisecond Pulsar SAX J1808.4-3658. *The Astrophysical Journal*, **521**, 332.

- Ransom, S. M., Eikenberry, S. S., & Middleditch, J. (2002). Fourier Techniques for Very Long Astrophysical Time-Series Analysis. *The Astronomical Journal*, **124**, 1788.
- Raymond, J. C. (1993). A model of an X-ray-illuminated accretion disk and corona. *The Astrophysical Journal*, **412**, 267.
- Rappaport, S., & Joss, P. C. (1997). The Nature and Evolutionary History of GRO J1744-28. *The Astrophysical Journal*, **486**, 435.
- Rappaport, S., Joss, P. C., & Webbink, R. F. (1982). The evolution of highly compact binary stellar systems. *The Astrophysical Journal*, **254**, 616.
- Rappaport, S., Verbunt, F., & Joss, P. C. (1983). A new technique for calculations of binary stellar evolution, with application to magnetic braking. *The Astrophysical Journal*, **275**, 713.
- Rappaport, S., Ma, C. P., Joss, P. C., & Nelson, L. A. (1987). The evolutionary status of 4U 1820-30. *The Astrophysical Journal*, **322**, 842.
- Rappaport, S., Markert, T., Li, F.K., Clark, G.K., Jernigan, J.G., & McClintock, J.E. (1977). Discovery of a 7.68 second X-ray periodicity in 3U 1626-67. *The Astrophysical Journal*, **217**, L29.
- Reynoso, E. M., Dubner, G. M., Goss, W. M., & Arnal, E. M. (1995). VLA Observations of Neutral Hydrogen in the Direction of Puppis A. *The Astronomical Journal*, **110**, 318.
- Retter, A., Chou, Y., Bedding, T. R., & Naylor, T. (2002). Detection of negative superhumps in a LMXRB – an end to the long debate on the nature of V1405 Aql (X 1916–053). *Monthly Notices of the Royal Astronomical Society*, **330**, L37.
- Rieke, G. H. & Lebofsky, M. J. (1985). The interstellar extinction law from 1 to 13 microns. *The Astrophysical Journal*, **288**, 618.
- Roche, P., Chakrabarty, D., Morales-Rueda, L., Hynes, R., Slivan, S. M., Simpson, C., & Hewett, P. (1998). *International Astronomical Union Circular*, **6885**.
- Sansom, A. E., et al. (1989). *Publication of the Astronomical Society of Japan*, **41**, 591.
- Sanwal, D., Pavlov G. G., Zavlin, V. E., & Teter, M. A. (2002). Discovery of Absorption Features in the X-ray Spectrum of an Isolated Neutron Star. *The Astrophysical Journal*, **574**, L61.
- Schachter, J., Filippenko, A. V., & Kahn, S. M. (1989). Bowen fluorescence in Scorpius X-1. *The Astrophysical Journal*, **340**, 1049.
- Schechter, P.L., Mateo, M., & Saha, A. (1993). DOPHOT, a CCD photometry program: Description and tests. *The Publications of the Astronomical Society of the Pacific*, **105**, 1342.

- Schechter, P. L., et al. (2003). Active optics on the Baade 6.5-m (Magellan I) Telescope. *Proceedings of SPIE*, **4837**, 910.
- Schlegel, D. J., Finkbeiner, D. P., & Davis, M. (1998). Maps of Dust Infrared Emission for Use in Estimation of Reddening and Cosmic Microwave Background Radiation Foregrounds. *The Astrophysical Journal*, **500**, 525
- Schmidtke, P. C. (1988). The optical light curve of 4U 1915-05. *The Astronomical Journal*, **95**, 1528.
- Schultz, J. (2003). X-ray properties of 4U 1543-624. *Astronomy and Astrophysics*, **397**, 249.
- Schulz, N.S., Chakrabarty, D., Marshall, H., Canizares, C.R., Lee, J.C., & Houck, J. (2001). Double-peaked X-ray Lines from the Oxygen/Neon-rich Accretion Disk in 4U 1626-67. *The Astrophysical Journal*, **563**, 941.
- Seward, F. D., Charles, P. A., & Smale, A. P. (1986). A 6 second periodic X-ray source in Carina. *The Astrophysical Journal*, **305**, 814.
- Seward, F. D. (1990). Einstein Observatory of Galactic supernova remnants. *Astrophysical Journal Supplement Series*. **73**, 781.
- Shakura, N. I. & Sunyaev, R. A. (1973). Black holes in binary systems. Observational appearance. *Astronomy and Astrophysics*, **24**, 337.
- Shectman, S. A. & Johns M. (2003). The Magellan Telescopes. *Proceedings of SPIE*, **4837**, 910.
- Shinoda, K., Kii, T., Mitsuda, K., Nagase, F., Tanaka, Y., Makishima, K., & Shibazaki, N. (1990). Discovery of the quasi-periodic oscillations from the X-ray pulsar X1627-673. *Publication of the Astronomical Society of Japan*, **42**, L27.
- Sigurdsson, S., Richer, H. B., Hansen, B. M., Stairs, I. H., & Thorsett, S. E. (2003). A Young White Dwarf Companion to Pulsar B1620-26: Evidence for Early Planet Formation. *Science*, **301**, 193.
- Slane, P., Hughes, J. P., Edgar, R. J., Plucinsky, P. P., Miyata, E., Tsunemi, H., & Aschenbach, B. (2001). *The Astrophysical Journal*, **548**, 814.
- Singh, K.P., Apparao, K.M.V., & Kraft, R.P. (1994). X-ray spectral study of two X-ray binaries: 4U 1957+11 and 2S 1543-624. *The Astrophysical Journal*, **421**, 753.
- Smale, A. P., & Lochner J. C. (1992). Long-term variability in low-mass X-ray binaries - A study using data from VELA 5B. *The Astrophysical Journal*, **395**, 582.
- Smale, A. P., Mason, K. O., & Mukai, K. (1987). The period of the globular cluster X-ray source X1820-303 Confirmation from Ariel V data. *Monthly Notices of the Royal Astronomical Society*, **225**, 7P.

- Smale, A. P., Mason, K. O., White, N. E., & Gottwald, M. (1988). X-ray observations of the 50-min dipping source XB1916-053. *Monthly Notices of the Royal Astronomical Society*, **232**, 647.
- Smith, J.A., et al. (2002). The u'g'r'i'z' Standard-Star System. *The Astronomical Journal*, **123**, 2121.
- Spruit, H. C. (1995). Accretion disks. In *The Lives of Neutron Stars*, Alpar, M. A., Kiziloglu, U., & van Paradijs, J., editors. Dordrecht: Kluwer, 355.
- Stella, L., Priedhorsky, W., & White, N.E. (1987). The discovery of a 685 second orbital period from the X-ray source 4U 1820-30 in the globular cluster NGC 6624. *The Astrophysical Journal*, **312**, L17.
- Sturmer, S. J., & Dermer, C. D. (1996). On the Nature of the Bursting X-Ray Pulsar GRO J1744-28. *The Astrophysical Journal*, **465**, L31.
- Sugizaki, M., et al. (1997). Discovery of an 11-s X-ray Pulsar in the Galactic-Plane Section of the Scorpius Constellation. *Publication of the Astronomical Society of Japan*, **49**, L25.
- Swank, J. & Markwardt, C. (2001). Populations of Transient Galactic Bulge X-ray Source. In *New Century of X-ray Astronomy*, Inoue, H. & Kunieda, H., Editors. San Francisco: ASP, 94.
- Tan, J., et al. (1991). Changes in the 11 minute period of 4U 1820 - 30. *The Astrophysical Journal*, **374**, 291.
- Tanaka, Y. & Shibazaki, N. (1996). X-ray Novae. *Annual Review of Astronomy and Astrophysics*, **34**, 607.
- Tiengo, A., Göhler, E., Staubert, R., & Mereghetti, S. (2002). The anomalous X-ray pulsar 1E 1048.1-5937: Phase resolved spectroscopy with the XMM-Newton satellite. *Astronomy and Astrophysics*, **383**, 182.
- Tuohy, I. & Garmire, G. P. (1980). Discovery of a compact X-ray source at the center of the supernova remnant RCW 103. *The Astrophysical Journal*, **239**, 107.
- Tuohy, I., Garmire, G. P., Manchester, R. N., & Dopita, M. A. (1983). The central X-ray source in RCW 103 - Evidence for blackbody emission. *The Astrophysical Journal*, **268**, 778.
- van der Klis, M., et al. (1993). Further ROSAT measurements of the period of 4U 1820-30. *Astronomy and Astrophysics*, **279**, L21.
- van Paradijs, J. & McClintock, J. E. (1994). Absolute visual magnitudes of low-mass X-ray binaries. *Astronomy and Astrophysics*, **290**, 133.
- van Paradijs, J. & McClintock, J. E. (1995). Optical and ultraviolet observations of X-ray binaries. In *X-ray Binaries*, Lewin, W. H. G., van Paradijs, J., and van den Heuvel, E. P. J., editors. Cambridge University Press, 59.

- van Paradijs, J., van Amerongen, S., Damen, E., & van der Woerd, H. (1986). Five-colour photometry of early-type stars in the direction of galactic X-ray sources. *Astronomy and Astrophysics Supplement Series*, **63**, 71.
- Vasisht, G. & Gotthelf, E. V. (1997). The Discovery of an Anomalous X-ray Pulsar in the Supernova Remnant Kes 73. *The Astrophysical Journal*, **486**, L129.
- Verbunt, F. & Zwaan, C. (1981). Magnetic braking in low-mass X-ray binaries. *Astronomy and Astrophysics*, **100**, L7.
- Vogt, N. (1974). Photometric study of the dwarf Nova VW Hydri. *Astronomy and Astrophysics*, **36**, 369.
- Vrtilek, S. D., Raymond, J. C., Garcia, M. R., Verbunt, F., & Hasinger, G. (1990). Observations of Cygnus X-2 with IUE - Ultraviolet results from a multiwavelength campaign. *Astronomy and Astrophysics*, **235**, 162
- Vrtilek, S. D., et al. (1990). Observations of Cygnus X-2 with IUE - Ultraviolet results from a multiwavelength campaign. *Astronomy and Astrophysics*, **235**, 162.
- Walter, F. M., Bowyer, S., Mason, K. O., Clarke, J. T., Henry, J. P., Halpern, J., & Grindlay, J. E. (1982). Discovery of a 50 minute binary and a likely 22 magnitude optical counterpart for the X-ray burster 4U 1915-05. *The Astrophysical Journal*, **253**, L67.
- Wang, Q. D., Gotthelf, E. V., & Lang, C. C. (2002). A faint discrete source origin for the highly ionized iron emission from the Galactic Centre region. *Nature*, **415**, 148.
- Warner, B. (1975). Observations of rapid blue variables- 15. *Monthly Notices of the Royal Astronomical Society*, **170**, 219.
- Warner, B. (1995). Catalysmic Variable Stars. Cambridge: Cambridge Univ. Press.
- Weisskopf, M. C., O'dell, S. L., van Speybroeck L. P. (1996). Advanced X-Ray Astrophysics Facility (AXAF). *Proceedings of SPIE*, **2805**, 2.
- White, N.H., & Swank, J.H. (1982). The discovery of 50 minute periodic absorption events from 4U 1916-05. *The Astrophysical Journal*, **253**, L61.
- White, N. E., Nagase, F., & Parmar, A. N. (1995). The properties of X-ray binaries. In *X-ray Binaries*, Lewin, W. H. G. and van Paradijs, J. and van den Heuvel, E. P. J., editors. Cambridge University Press, 1.
- Whitehurst, R. (1988). Numerical simulation of accretion discs. II - Design and implementation of a new numerical method. *Monthly Notices of the Royal Astronomical Society*, **233**, 529.
- Whitehurst, R., & King, A. (1991). Superhumps, resonances and accretion discs. *Monthly Notices of the Royal Astronomical Society*, **249**, 25.

- Wijnands, R. (2004). Observations of millisecond X-ray pulsars. In *X-ray Timing 2003: Rossi and Beyond*, Kaaret, P., Lamb, F. K., and Swank, J. H., editors. Melville, NY.
- Wijnands, R., & Wang, Q. D. (2002). A Chandra Observation of GRO J1744-28: The Bursting Pulsar in Quiescence. *The Astrophysical Journal*, **568**, L93.
- Wijnands, R., Kuiper, L., in 't Zand, J., Dotani, T., van der Klis, M., & Heise, J. (2001). Very Low Luminosities from the Accretion-driven Millisecond X-ray Pulsar SAX J1808.4-3658 during quiescence. *The Astrophysical Journal*, **570**, 69.
- Wijnands, R., & van der Klis, M. (1998). A millisecond pulsar in an X-ray binary system. *Nature*, **394**, 344.
- Winkler, P. F. Tuttle, J. H., Irwin, M. J. (1988). In *Supernova Remnants and the Interstellar Medium*. Roger, R. S. & Landecker, T. L., Editors. Cambridge: Cambridge Univ. Press, 65.
- Woodgate, B.E., et al. (1998). The Space Telescope Imaging Spectrograph Design. *The Publications of the Astronomical Society of the Pacific*, **110**, 1183.
- Yungelson, L.R., Nelemans, G., van der Heuvel, E.P.J. (2002). On the formation of neon-enriched donor stars in ultracompact X-ray binaries. *Astronomy and Astrophysics*, **388**, 546.
- Yusef-Zadeh, F., Law, C., Wardle, M., Wang, Q. D., Fruscione, A., Lang, C. C., & Cotera, A. (2002). Detection of X-Ray Emission from the Arches Cluster near the Galactic Center. *The Astrophysical Journal*, **570**, 665.
- Zavlin, V. E., Pavlov, G. G., Sanwal, D., & Trümper, J. (2000). Discovery of 424 Millisecond Pulsations from the Radio-quiet Neutron Star in the Supernova Remnant PKS 1209-51/52. *The Astrophysical Journal*, **540**, 25.
- Zombeck, M. V., Chappell, J. H., Kenter, A. T., Moore, R. W., Murray, S. S., Fraser, G. W., & Serio, S. (1995). High-resolution camera (HRC) on the Advanced X-Ray Astrophysics Facility (AXAF). *Proceedings of SPIE*, **2518**, 96.